Proceedings of the International Workshop on e^+e^- collisions from ϕ to ψ (PHIPSI15)

Hefei, September 23～26, 2015

International Advisory Committee

R. Baldini (INFN, Frascati)
K. T. Chao (PKU, Beijing)
G. Colangelo (University of Bern)
H. Czyz (University of Katowice)
M. Davier (LAL, Orsay)
A. Denig (University of Mainz)
S. Eidelman (Budker Institute, Novosibirsk)
P. Gauzzi (Universita' La Sapienza, Roma)
F. A. Harris (University of Hawaii)
G. Isidori (INFN, Frascati)
J. H. Kuehn (KIT, Karlsruhe)
A. Lusiani (Scuola Normale Superiore, Pisa)
J. P. Ma (ITP, Beijing)
M. Passera (INFN, Padova)
B. L. Roberts (University of Boston)
X. Y. Shen (IHEP, Beijing)
E. Solodov (Budker Institute, Novosibirsk)
E. Tomasi-Gustafsson (IRFU, Saclay)
L. Trentadue (University of Parma)
A. Vainshtein (University of Minnesota)
G. Venanzoni (INFN, Frascati)
Z. P. Zheng (IHEP, Beijing)

Local Organizing Committee (USTC, Hefei)

X. L. Wang
Q. Wang
H. P. Peng
W. B. Yan
J. B. Liu
Y. W. Liu
L. Yan
H. J. Xu
M. H. Liu
Z. B. Tang
Y. F. Zhang
H. Zeng
J. Dong
X. R. Zhou
Y. Liang
C. Z. Yuan (co-chair, IHEP, Beijing)
G. S. Huang (co-chair)
Z. G. Zhao (chair)

FORWARD

ZHAO Zhengguo
(for the PHIPSI15 Local Organizing Committee)
University of Science and Technology of China, Hefei 230026, China

The "International Workshop on e^+e^- collisions from ϕ to ψ" (PHIPSI15), was held at University of Science and Technology of China (USTC), Hefei, China, from Wednesday, September 23 to Saturday, September 26, 2015. This is the 10th workshop in a series, which started in Karlsruhe in 1996 and continued in Novosibirsk (1999), SLAC (2001), Pisa (2003), Novosibirsk (2006), Frascati (2008), Beijing (2009), Novosibirsk (2011) and Rome (2013), carrying now the name "from ϕ to ψ" first used at the Novosibirsk workshop in 1999. The aim of the workshop is to discuss in detail the state of art of various problems in hadronic physics at low energy e^+e^- colliders and the potential of existing and future facilities.

The subjects of the Workshop include: (1) R measurements; (2) Radiative corrections; (3) Form Factors and OZI rule violation; (4) Spectroscopy (Light and Heavy); (5) muon $g-2$, experimental measurements and theoretical calculations; (6) Flavor physics; (7) Proton radius puzzle; (8) Gamma-gamma physics; (9) Tau lepton physics; (10) Machines and detectors.

We thank all the participants and the international advisory committee for making a very successful Workshop.

The Workshop was sponsored by the Chinese Center for Advanced Science and Technology (CCAST), the National Natural Science Foundation of China (NSFC), the Ministry of Science and Technology of China, the Chinese Academy of Sciences (CAS), and the University of Science and Technology of China (USTC).

中国科学技术大学学报

第 46 卷　第 4 期(总第 276 期)　2016 年 4 月

目　　次

[**期刊基本参数**]　CN34-1054/N * 1965 * m * A4 * 88 * zh/en * P * ￥30.00 * 1200 * 13 * 2016-04

责任编辑　贺　伟　　**英文编辑**　崔海建　Federick Firstbrook

JOURNAL OF UNIVERSITY OF SCIENCE AND TECHNOLOGY OF CHINA

Vol. 46 No. 4(Serial No. 276) Apr. 2016

CONTENTS

第46卷第4期 中国科学技术大学学报 Vol. 46, No. 4
2016年4月 JOURNAL OF UNIVERSITY OF SCIENCE AND TECHNOLOGY OF CHINA Apr. 2016

Article ID:0253-2778(2016)04-0259-13

Overview of the CMD-3 results at the VEPP-2000 e^+e^- collider

FEDOTOVICH G. V.[1,2], AMIRKHANOV A. N.[1,2], ANISENKOV A. V.[1,2], AULCHENKO V. M.[1,2], BANZAROV V. S.[1], BASHTOVOY N. S.[1], BONDAR A. E.[1,2], BRAGIN A. V.[1], EIDELMAN S. I.[1,2], EPIFANOV D. A.[1], EPSHTEYN L. B.[1,2,3], EROFEEV A. L.[1,2], GAYAZOV S. E.[1,2], GREBENUK A. A.[1,2], GRIBANOV S. S.[1,2], GRIGORIEV D. N.[1,4], IGNATOV F. V.[1], IVANOV V. L.[1,2], KARPOV S. V.[1], KAZANIN V. F.[1,2], KOROBOV A. A.[1,2], KOVALENKO O. A.[1,2], KOZYREV A. N.[1,2], KOZYREV E. A.[1,2], KROKOVNY P. P.[1,2], KUZMENKO A. E.[1,2], KUZMIN A. S.[1,2], LOGASHENKO I. B.[1,2], LUKIN P. A.[1,2], MIKHAILOV K. Yu.[1,2], OKHAPKIN V. S.[1], PESTOV Yu. N.[1], POPOV A. S.[1,2], RAZUVAEV G. P.[1,2], RUBAN A. A.[1], RYSKULOV N. M.[1], RYZHENENKOV A. E.[1,2], SHEBALIN V. E.[1], SHEMYAKIN D. N.[1,2], SHWARTZ B. A.[1,2], SIBIDANOV A. L.[4], SHATUNOV Yu. M.[1], SOLODOV E. P.[1,2], TITOV V. M.[1], TALYSHEV A. A.[1,2], VOROBIOV A. I.[1], YUDIN Yu. V.[1,2]

(1. *Budker Institute of Nuclear Physics, Novosibirsk* 630090, *Russia*;
2. *Novosibirsk State University, Novosibirsk* 630090, *Russia*;
3. *Novosibirsk State Technical University, Novosibirsk* 630092, *Russia*;
4. *Falkiner High Energy Physics Department, School of Physics, The University of Sydney, New South Wales* 2006, *Australia*)

Abstract: The CMD-3 detector has been taking data since December 2010 at the VEPP-2000 electron-positron collider. The collected data sample corresponds to about 60 inverse picobarn of integrated luminosity in the c. m. energy range from 0.32 up to 2 GeV. Preliminary results of the analysis of various hadronic cross sections, in particular, $e^+e^-\to\pi^+\pi^-$, $\pi^+\pi^-\pi^0$, K_LK_S, K^+K^-, $\eta\gamma$, $3(\pi^+\pi^-)$, $2(\pi^+\pi^-\pi^0)$, $K^+K^-\pi^+\pi^-$, $K^+K^-\eta$, $K^+K^-\pi^0$, $\eta\pi^+\pi^-$, $\omega\pi^+\pi^-$ and $\omega\to\pi^0e^+e^-$ are presented. The processes with multihadron final states have several intermediate states which must be taken into account to correctly describe the angular and invariant mass distributions as well as cross section energy dependence.

Key words: hadrons; signal/background separation; cross section

CLC number: O572.3 **Document code**: A doi:10.3969/j.issn.0253-2778.2016.04.001

Citation: FEDOTOVICH G V, AMIRKHANOV A N, ANISENKOV A V, et al. Overview of the CMD-3 results at the VEPP-2000 e^+e^- collider[J]. Journal of University of Science and Technology of China, 2016, 46(4):259-271.

Received: 2015-11-30; **Revised**: 2016-04-20

Foundation item: Supported by Russian Fundation for Basic Research (10-02-00695-a, 10-02-00253-a, 11-02-00328-a, 11-02-00112-a, 12-02-31501-mol-a, 12-02-31499-mol-a, 12-02-31498-mol-a, 12-02-01032-a, 13-02-00215-a, 15-02-05674-a), Federal Target Program (14.B37.21.07777).

Biography: FEDOTOVICH G. V. (corresponding author), Prof. Research field: high energy physics. E-mail: fedotovich@inp.nsk.su

VEPP-2000正负电子对撞机上CMD-3物理结果综述

FEDOTOVICH G. V.[1,2], AMIRKHANOV A. N.[1,2], ANISENKOV A. V.[1,2], AULCHENKO V. M.[1,2], BANZAROV V. S.[1], BASHTOVOY N. S.[1], BONDAR A. E.[1,2], BRAGIN A. V.[1], EIDELMAN S. I.[1,2], EPIFANOV D. A.[1], EPSHTEYN L. B.[1,2,3], EROFEEV A. L.[1,2], GAYAZOV S. E.[1,2], GREBENUK A. A.[1,2], GRIBANOV S. S.[1,2], GRIGORIEV D. N.[1,4], IGNATOV F. V.[1], IVANOV V. L.[1,2], KARPOV S. V.[1], KAZANIN V. F.[1,2], KOROBOV A. A.[1,2], KOVALENKO O. A.[1,2], KOZYREV A. N.[1,2], KOZYREV E. A.[1,2], KROKOVNY P. P.[1,2], KUZMENKO A. E.[1,2], KUZMIN A. S.[1,2], LOGASHENKO I. B.[1,2], LUKIN P. A.[1,2], MIKHAILOV K. Yu.[1,2], OKHAPKIN V. S.[1], PESTOV Yu. N.[1], POPOV A. S.[1,2], RAZUVAEV G. P.[1,2], RUBAN A. A.[1], RYSKULOV N. M.[1], RYZHENENKOV A. E.[1,2], SHEBALIN V. E.[1], SHEMYAKIN D. N.[1,2], SHWARTZ B. A.[1,2], SIBIDANOV A. L.[4], SHATUNOV Yu. M.[1], SOLODOV E. P.[1,2], TITOV V. M.[1], TALYSHEV A. A.[1,2], VOROBIOV A. I.[1], YUDIN Yu. V.[1,2]

(1. 布德克尔核物理研究所,新西伯利亚 630090,俄罗斯;2. 新西伯利亚州立大学,新西伯利亚 630090,俄罗斯;3. 新西伯利亚州立理工大学,新西伯利亚 630092,俄罗斯;4. 悉尼大学物理学院福基纳高能物理系,新南威尔士州 2006,澳大利亚)

摘要:2010年12月VEPP-2000正负电子对撞机上的CMD-3探测器开始运行.在质心系能量区间0.32～2 GeV范围内,已经获取了积分亮度约为60 pb^{-1}的数据.目前已经得到多种强子末态截面的初步结果,尤其是$e^+e^-\to\pi^+\pi^-$, $\pi^+\pi^-\pi^0$, K_LK_S, K^+K^-, $\eta\gamma$, $3(\pi^+\pi^-)$, $2(\pi^+\pi^-\pi^0)$, $K^+K^-\pi^+\pi^-$, $K^+K^-\eta$, $K^+K^-\pi^0$, $\eta\pi^+\pi^-$, $\omega\pi^+\pi^-$和$\omega\to\pi^0e^+e^-$.为正确描述角分布和不变质量分布及截面分布,多强子末态过程必须考虑其中间共振态.

关键词:强子;信号/本底分离;截面

0 Introduction

The electron-positron collider VEPP-2000[1] has been operating at Budker Institute of Nuclear Physics since December 2010. The collider is designed to provide luminosity up to 10^{32} cm$^{-2}\cdot$s^{-1} at the maximum center-of-mass energy $\sqrt{s}=2$ GeV. Two detectors, CMD-3[2] and SND[3], are installed in the two interaction regions. The CMD-3 detector has high detection efficiency, good energy and angular resolutions for charged particles as well as for photons. The integrated luminosity collected by each detector is about 60 pb^{-1}.

The precision data on the hadronic cross sections are required, in particular, to evaluate the anomalous magnetic moment (AMM) of muon, $a_\mu=(g-2)_\mu/2$. The VEPP-2000 energy range gives the major hadronic contribution to AMM, both to the hadronic vacuum polarization itself (～92%) and to its uncertainty[4].

The precision of luminosity measurement is a key ingredient in many experiments which study the hadronic cross sections at e^+e^- colliders. It is very important to have several well-known QED processes such as $e^+e^-\to e^+e^-$, $\mu^+\mu^-$, $\gamma\gamma$ in order to perform cross checks and control the systematic uncertainty in luminosity determination. The CLEO collaboration was the first one to show in practice how a combined analysis of the processes $e^+e^-\to e^+e^-$, $\mu^+\mu^-$ and $\gamma\gamma$ helped to achieve a 1% accuracy for the luminosity[5]. The preliminary results on the luminosity determination and analysis of various hadronic cross sections for many

processes are presented.

1 CMD-3 detector

Cryogenic Magnetic Detector is a general-purpose detector shown in Fig. 1. Coordinates, angles and momenta of charged particles are measured by the cylindrical drift chamber (DC) which has a hexagonal cell. The coordinate resolution in the r-ϕ plane is $\sim 120\mu$. The coordinate along the beam axis is measured by charge division technique with resolution $\sim$2 mm. The momentum resolution goes like $\sigma_p/p \approx 1\% \sim 5\%$. The cylindrical multiwire double layer proportional Z-chamber is mounted directly behind DC and provides z-coordinate determination of the track by measuring the analogous information from cathode strips with an accuracy of $\sim$0.5 mm. The signals coming from anode sectors are used for the first level trigger and have time jitter $\sim$5 ns.

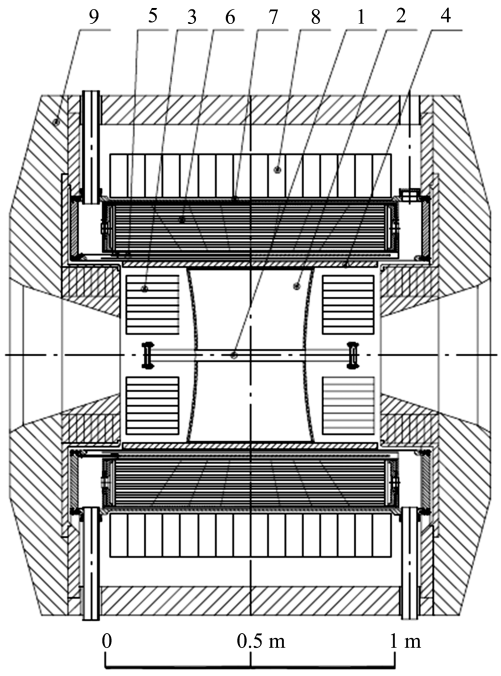

1 – beam pipe, 2 – drift chamber, 3 – BGO, calorimeter, 4 – Z-chamber, 5 – SC solenoid, 6 – LXe calorimeter, 7 – TOF system, 8 – CsI electromagnetic calorimeter, 9 – yoke, not shown the outer muon range system.

Fig. 1　CMD-3 detector

The calorimeter of the detector consists of three parts. The endcap BGO calorimeter consists of 640 crystals with a thickness 13.4 X_0 (radiation lengths). The barrel part is placed out-side of the 0.08 X_0 thin superconducting solenoid with 1.3 T magnetic field. The barrel calorimeter consists of two subsystems. The first one is based on Liquid Xenon calorimeter (5.4 X_0), the second one on the CsI crystals with a thickness 8.1 X_0 (1 152 crystals) which are arranged in 8 octants. The LXe calorimeter has a tower structure (264 channels) and seven cylindrical double layers with strip readout (1 286 channels). The strip information allows one to measure coordinates of the photon conversion point with precision of 1$\sim$2 mm. The energy resolution of the barrel calorimeter was measured using Bhabha events and was found to be: $\sigma_E/E \approx 4\% \sim 8\%$.

The muon range system is mounted outside of the magnetic yoke and consists of 36 scintillation counters in the barrel part and 8 counters at the endcap. This system serves as the cosmic veto and has time resolution $\sim$1 ns.

2 Energy scan and luminosity measurement

The energy range from 1 to 2 GeV was scanned twice up and down with the step of 50 MeV in 2011 and in 2012. At each energy point the integrated luminosity ~ 500 nb^{-1} was collected. The energy points during scan down (only in 2011) were shifted by 25 MeV with respect to the scan up. The beam energy was determined by measuring the momenta of Bhabha events with accuracy of 1 $\sim$ 3 MeV as well as using the Compton backscattering technique for several energy points near 2 GeV with accuracy $\sim$ 50 keV[6]. Two types of the first level triggers "CHARGED" and "NEUTRAL" were used while data taking. A special topological combination of signals from DC cells and Z-chamber, which roughly reproduce "track", start a special processor "TRACKFINDER" (TF). "CLUSTERFINDER" (CF) was started by signals coming from calorimeters. A positive decision of

any trigger generates a command for the data acquisition system. The average trigger counting rate was about 200～400 Hz while data taking.

The collected integrated luminosity is ～60 pb^{-1} with about 34.5 pb^{-1} above the ϕ energy range, 8.3 and 8.4 pb^{-1} at the ω and ϕ resonances, respectively, and 9.4 pb^{-1} at low energies. The peak luminosity ～2×10^{31} $cm^{-2}\cdot s^{-1}$ was reached and is currently limited by a positron injection rate. An upgrade of the injection facility will the gain of luminosity by a factor of ten is expected.

The sample of collinear Bhabha events e^+e^- were selected for luminosity determination as well as the events of process $e^+e^-\to\gamma\gamma$ as an independent tool for cross check. The relative difference of the luminosities determined with two processes versus energy is presented in Fig. 2, where only statistical errors are shown (scan 2012)[7]. The horizontal line is a fit for this ratio and in average is about (0.2±0.3)%. The main sources which contribute to systematic error are: interaction with material of the vacuum chamber wall about 0.2%～0.4%; the contribution due to the different angular resolution for Bhabha events and $\gamma\gamma$ is estimated as ～0.8%; a correction which takes into account inclination of the beam axis with respect to the detector ～0.4%, z-scale calibration accuracy of the DC wires contributes about 0.3%. Presently we estimate the systematic accuracy as ～1% for energies higher than 1 GeV.

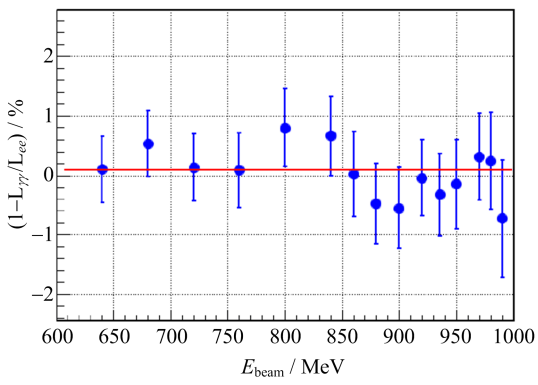

Fig. 2 The ratio of the relative difference of the luminosities vs beam energy (scan 2012)

3 Pion form factor measurement

One of the main goals of the CMD-3 experiment is to reduce a systematic uncertainty of the cross section of two-pion production to the level smaller than 0.5%. In this case the uncertainty of the hadronic contribution to the AMM value, coming from this channel, will be 0.3～0.4 ppm. The $\pi^+\pi^-$ events are separated either using the particle momenta or the energy deposition in the calorimeter. Two independent ways of event separation provide cross-check and allow to keep the systematic error under control.

Several features of the detector allow to reach the necessary level of systematic error. The fiducial volume is determined independently with the LXe calorimeter and the Z-chamber. The beam energy is measured with precision of $\sigma_E<50$ keV using Compton backscattering of the laser light. The radiative corrections are calculated according to Ref. [8] with the accuracy better than 0.2%.

The first energy scan below 1 GeV was performed in 2013[9]. The collected statistics is a few times higher than that in the previous CMD-2 measurements and it is at the level of ISR statistics collected by the BaBar and KLOE.

Preliminary results for the cross sections $\sigma(e^+e^-\to\pi^+\pi^-)$ measurements are shown in Fig. 3. The cross section of the process $e^+e^-\to$

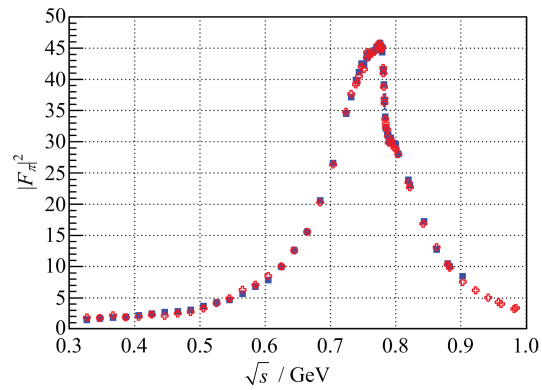

Squares-particle separation with momenta, points-particle separation with energy deposition in calorimeter

Fig. 3 Preliminary results of the pion form factor measurement

$\mu^+\mu^-$ was measured too. The results of the measurement are plotted in Fig. 4 with respect to the QED prediction and provide an important overall systematic test of the measurement. The horizontal line is a fit for the double ratio $(\sigma^{\rm exp}_{\ell\ell\gamma}/\sigma^{\rm QED}_{\ell\ell\gamma})/(\sigma^{\rm exp}_{ee}/\sigma^{\rm QED}_{ee})$ which was found to be $(99.5\pm0.5)\%$.

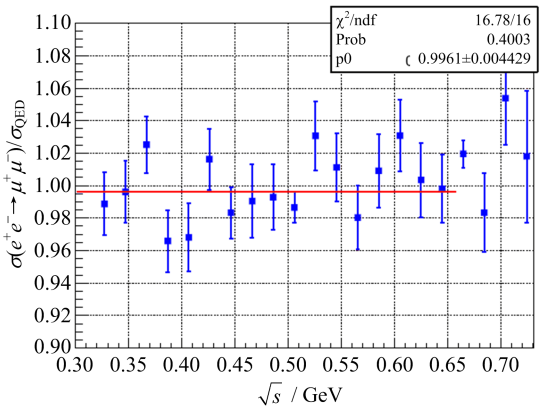

Fig. 4　Result of the measurement of muon pair production in comparison with the QED prediction

4　Study of the processes $e^+e^-\to K_SK_L$ and $e^+e^-\to K^+K^-$

The most precise previous study of the process has been performed by the CMD-2[10-13] and BaBar detectors. In this paper we present new measurement of the $e^+e^-\to K^0_SK^0_L$ and $e^+e^-\to K^+K^-$ cross sections. It is known the CMD-2 and BaBar results in the ϕ-peak region disagree at the level 5%, so new measurements are required. The $e^+e^-\to K^0_SK^0_L$ and $e^+e^-\to K^+K^-$ cross sections were measured in the c. m. energy range 1.004～1.060 GeV at 25 energy points. The detection of the neutral mode is based on the search for two tracks with a common vertex in DC from the $K^0_S\to\pi^+\pi^-$ decay. Each track has momentum, that corresponds to the kinematically allowed region and has ionization losses of relativistic pions. The number of events is determined by the fit of the two-pion invariant mass distribution with negligible background.

The detection of the charged mode is based on the search of two central collinear tracks of kaons with momentum known from DC. Each track has ionization losses significantly larger than m. i. p. due to relatively small velocity of kaons under study. After these requirements the level of remaining background is less than 0.5%. The detection efficiency of each kaon was determined with data as well as with MC simulation and delivers a deviation less than 1.5%.

The obtained cross sections for neutral and charged mode together with the fit are presented in Fig. 5 and Fig. 6, respectively. Currently the systematic accuracy for these cross sections is estimated as 2% and 3%, respectively.

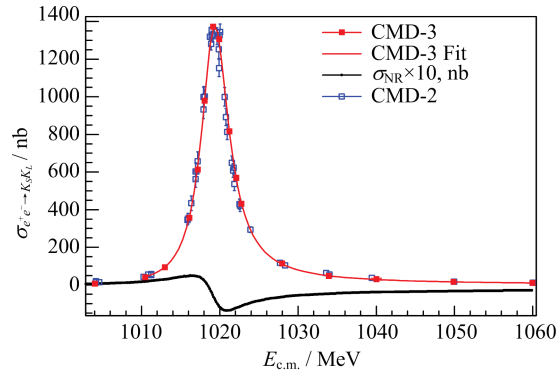

CMD-2, CMD-3 and BaBar data are presented. The black smooth curve (vertical scale increased by ten times) represents interference of the ϕ amplitude with ω, ρ and their excitations.

Fig. 5　The cross section of the process $e^+e^-\to K_LK_S$ around the ϕ-meson energy region

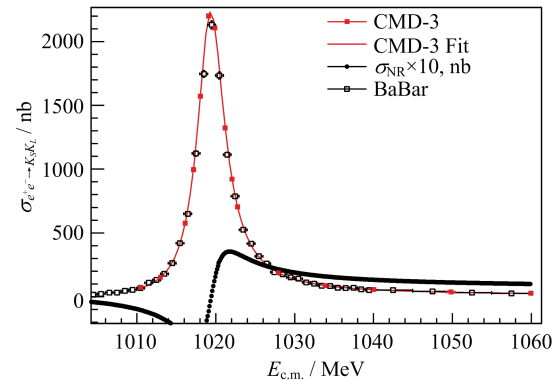

CMD-2, CMD-3 and BaBar data are presented. Black smooth curve (vertical scale increased by ten times) represents interference of the ϕ amplitude with ω, ρ and their excitations.

Fig. 6　The cross section of the process $e^+e^-\to K^+K^-$ around the ϕ-meson energy region

The measured cross section is approximated according to Vector Meson Dominance model as a sum of the ϕ, ω, ρ - like amplitudes and their excitations. The neutral and charged channels were approximated simultaneously, as a result the following values of the ϕ meson parameters have been obtained: $m_\phi = (1\,019.464 \pm 0.060)\,\mathrm{MeV}/c^2$, $\Gamma_\phi = (4.240 \pm 0.017)\,\mathrm{MeV}$, $\frac{B_{\phi\to K^+K^-}}{B_{\phi\to K_S^0K_L^0}} = 1.573 \pm 0.06$ and their accuracy is comparable or better than obtained in previous experiments. We plan to study these processes up to $E_{\mathrm{c.m.}} = 2\,000$ MeV, available with the VEPP-2000 collider.

5 Study of the process $e^+e^-\to K^+K^-\pi^0$

To select events under study the following requirements were applied: two central tracks in DC with two or more photons in the calorimeter. For each pair of photons the kinematics reconstruction was done under assumption that these photons are the product of the π^0 decay. If kinematics of these four particles satisfy energy-momentum conservation and ionization losses in DC correspond to kaons, the combination with the smallest χ^2 is chosen.

The main physical background comes from the processes $e^+e^-\to\pi^+\pi^-\pi^0$ and $e^+e^-\to\pi^+\pi^-\pi^0\pi^0$ which are significantly suppressed by using $\mathrm{d}E/\mathrm{d}x$ information. The events of the processes $e^+e^-\to K^+K^-2\pi^0$ and $e^+e^-\to K^+K^-\eta$ are rejected by the kinematics cuts. The detection efficiency was determined with MC simulation, including radiative corrections. Preliminary results of the cross section measurement are shown in Fig. 7 along with BaBar data[14].

6 Study of the process $e^+e^-\to K^+K^-\eta$

The $e^+e^-\to K^+K^-\eta$ process has been studied earlier by the BaBar in the c. m. energy range from 1.56 to 3.48 GeV in the $\eta\to 2\gamma$ decay channel[15], and in the energy range from 1.56 to 2.64 GeV when η decay to $\pi^+\pi^-\pi^0$[14]. It was found that the main intermediate mechanism is $e^+e^-\to\phi(1680)\to\phi(1020)\eta$, but the statistics was not enough to study the dynamics of the non-$\phi(1020)\eta$ contribution.

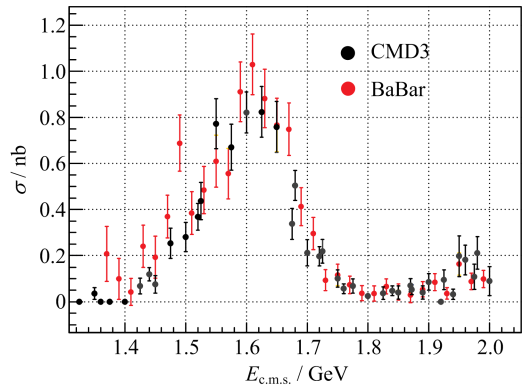

Black squares | this analysis, red dots — BaBar data.
Only statistical errors are shown.

Fig. 7 Preliminary results for $e^+e^-\to K^+K^-\pi^0$ cross section

The analysis of the $e^+e^-\to K^+K^-$ process is based on an integrated luminosity of 22 pb^{-1} collected in 2011～2012 at 30 c. m. energy points in the range from 1.59 up to 2.0 GeV. The η meson was treated as a recoil particle, and all the modes of η decay were used. To select events under study some cuts were applied: kaons are the product of the $\phi(1020)$ decay, two collinear tracks should be in DC with ionization losses $\mathrm{d}E/\mathrm{d}x$ which correspond to kaons. The latter condition allows significantly rejects the physical background.

The distributions in ΔE (defined below) of simulated signal and background events are fitted at every point of energy:

$$\Delta E = E_{K^+} + E_{K^-} + \sqrt{(-\boldsymbol{p}_{K^+} - \boldsymbol{p}_{K^-})^2 + m_\eta^2} - 2E_{\mathrm{beam}}.$$

For the signal events the fitting function is a sum of three Gaussian functions with the different mean values and widths. The simulated background events are fitted by a second-degree polynomial. The functions found are used to fit the distribution of experimental events in ΔE to determine the number of signal events and was found to be $N_{\mathrm{signal,total}} = 1\,454 \pm 48$. The preliminary results of the cross section of $e^+e^-\to\phi(1020)\eta$ process are shown in Fig. 8 along with BaBar data.

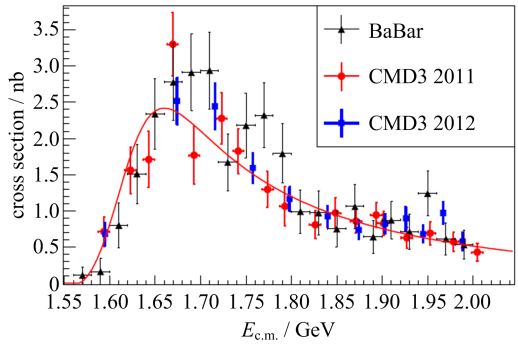

CMD-3 results, based on the data collected in 2011 (circular markers) and in 2012 (squared markers); BaBar results, measured in $\eta \to 2\gamma$ mode (triangle markers).

Fig. 8　The cross section of $e^+ e^- \to \phi(1020)\eta$ process

7　Study of the processes $e^+ e^- \to \eta\gamma$

This process with 3γ in the final state is under study in the whole VEPP-2000 energy range from 400 MeV up to 2 GeV. To select signal events, the following criteria are applied: three or more photons in the calorimeter and no tracks in DC. These three particles should satisfy energy-momentum conservation and the kinematic reconstruction was performed for them. The combination with the smallest χ^2 is used to choose the best group with more than three photons. The number of signal events is determined from a fit of the two-photon invariant mass spectrum. The QED process of e^+e^- annihilation to three photons is the main background and is rejected significantly by kinematics cuts.

The total cross section is calculated according to the formula

$$\sigma(e^+ e^- \to P\gamma) = N/[L\varepsilon_{\mathrm{NT}}\varepsilon_{det}(1+\delta_{\mathrm{rad}})B(P \to 2\gamma)],$$

where P stands for π^0 or η, N is the number of signal events, L is the integrated luminosity, δ_{rad} is the radiation correction, $\varepsilon_{\mathrm{det}}$ is the detection efficiency from Monte Carlo simulation, $B(P \to 2\gamma)$ is the branching ratio, and $\varepsilon_{\mathrm{NT}}$ is a neutral trigger efficiency studied with an $e^+ e^- \to e^+ e^- \gamma$ process. The preliminary results of the cross section measurement in the energy range around the ϕ meson are presented in Fig. 9 with the CMD-2 data[16].

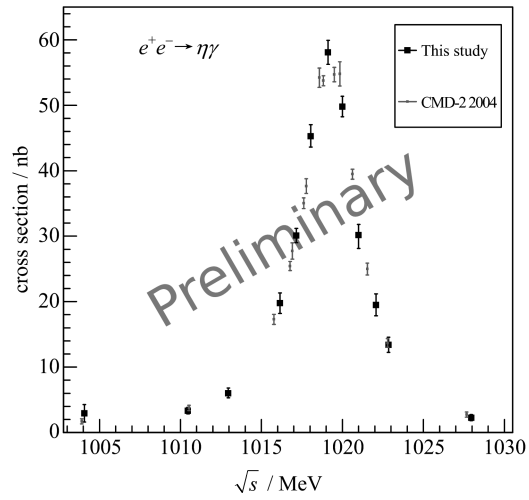

Black squares — this analysis, only statistical errors are shown; red dots — CMD-2

Fig. 9　$e^+ e^- \to \eta\gamma$ cross section

8　Study of the process $e^+ e^- \to \pi^+ \pi^- \pi^0$

The analysis of the process with three pions $\pi^+\pi^-\pi^0$ in the final state was performed using 23 pb^{-1} of data collected in the energy range 1.05～1.8 GeV. Events with two reconstructed tracks and at least two detected photons in the barrel calorimeter were selected and then underwent a kinematic reconstruction based on energy-momentum conservation. The combination of two photons which provides the best χ^2 value is selected for a further analysis. Additional cuts on tracks including their recoil mass, momentum, energy losses $\mathrm{d}E/\mathrm{d}x$ in DC and collinearity are used to suppress the physical background mainly coming from the process $e^+ e^- \to \pi^+ \pi^- \pi^0 \pi^0$. The number of 3π events is obtained by a fit to the two-photon invariant mass distribution using a sum of the signal and background functions. The total number of selected 3π events was found to be 6 269. The same procedure has been applied to the sample of Monte-Carlo events which were simulated with a primary generator using the GEANT4 package and then reconstructed with the same software as with the experimental data. The preliminary results for the Born cross section are shown in Fig. 10 in comparison with the BaBar and

SND.

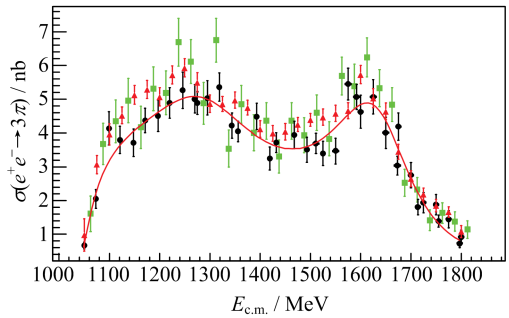

Black points- CMD3, squares - BaBar data, triangles - SND (2015)

Fig. 10 Born cross section of $e^+\ e^-\to\pi^+\ \pi^-\ \pi^0$ [17-18]

9 Study of the process $e^+\ e^-\to K^+\ K^-\ \pi^+\ \pi^-$

The cross section measurement of the process $e^+\ e^-\to K^+\ K^-\ \pi^+\ \pi^-$ is based on the integrated luminosity of 22 pb^{-1} in the c. m. energy range from 1.5 to 2.0 GeV and this process was studied before by the BaBar via ISR[14]. Nevertheless, the direct measurements are very important, since some contributions to a_μ are based on isospin relations of various $K\ \overline{K}\ n\pi$ final states. Any uncertainty of this approach will be crucial for a_μ accuracy.

The signal events should have three or four tracks in DC coming from the interaction region and obey the energy-momentum conservation. Two tracks corresponding to kaons should have the large ionization losses dE/dx in DC and this information was input to a likelihood function constructed for further K/π separation. Fig. 11 shows a scatter plot of the difference between the measured total energy and c. m. energy $\Delta E_4 = E_{\rm tot} - E_{\rm c.m.}$ vs the total momentum for all events with four tracks. The cluster of $\pi^+\ \pi^-\ \pi^+\ \pi^-$ events is located near the origin of coordinates. The cluster of signal events with a zero total momentum is shifted down along the vertical axis.

A similar procedure was used to select signal events with three tracks in DC. For these events energy deficit should correlate with the total (missing) momentum. For such events, the energy of a missing particle is calculated and added

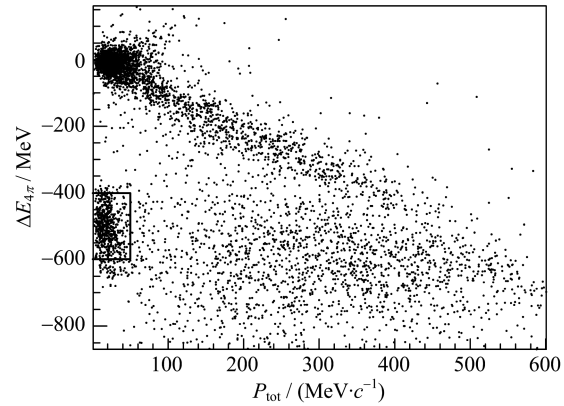

The upper cluster of dots represents $\pi^+\pi^-\pi^+\pi^-$ while the lower one - $K^+K^-\pi^+\pi^-$ events.

Fig. 11 Scatter plot of the difference between the total energy and c. m. energy (ΔE_4) versus the total momentum for four-track events

to the energy of three detected particles. The difference between the obtained energy ΔE_{3+1} and c. m. energy is shown in Fig. 12. The signal events are clearly seen. To obtain the number of $K^+K^-\pi^+\pi^-$ events the histogram was fitted with a sum of two Gaussian distributions for a signal peak and a quadratic polynomial for background. As a result, 13300 four-track events and 16000 three-track events were selected. To obtain a detection efficiency, the $K^+\ K^-\ \pi^+\ \pi^-$ events were simulated with a primary generator using the GEANT4 package and then reconstructed with the same software as with the experimental data.

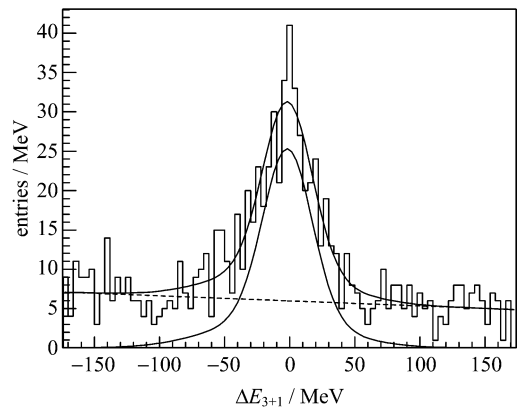

Upper smooth line - histogram fit, dotted line - background fit, lower smooth curve - fit simulated signal events.

Fig. 12 The histogram of the difference between the calculated total energy with energy of fourth particle ΔE_{3+1} and c. m. energy

Production mechanisms with the $K^+K^-\rho$, $K1(1270;1400)K\to K^*\pi K$, $\phi\pi^+\pi^-$ and K^*K^* intermediate states are required to correctly describe angular and invariant mass distributions of the experimental data and to determine the detection efficiency which was found to be about 50%～60%.

The cross section as a function of energy, shown in Fig. 13, are in good agreement with the previous BaBar measurement[19] presented by open circles. Systematic error is under study and currently is estimated as 6%. The main systematic uncertainty is due to the theoretical model, describing intermediate states and affecting the detection efficiency.

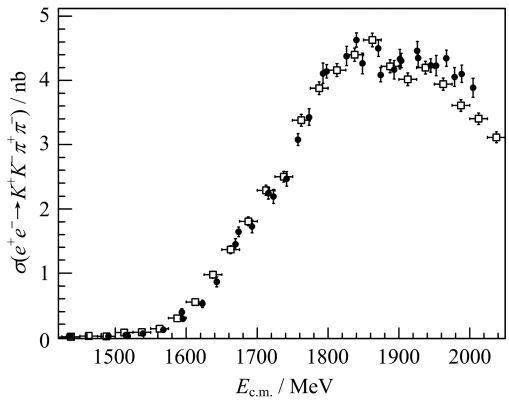

Dots-CMD-3, open circles-BaBar results

Fig. 13　Measurement of the $e^+e^-\to K^+K^-\pi^+\pi^-$ cross section

10　Production of six pions

Production of six pions in e^+e^- annihilation was studied at DM2[20-22] and BaBar[23]. The DM2 experiment observed a "dip" in the cross section of the process $3(\pi^+\pi^-)$ near 1.9 GeV, confirmed later by the BaBar. The origin of the "dip" remains unclear, but the most popular explanation is related to opening $p\bar{p}$ and $n\bar{n}$ channels as discussed in many theoretical papers[24].

The analysis is based on 22 pb^{-1} of integrated luminosity collected in the c. m. energy range from 1.5 to 2 GeV. Candidates for the process under study are required to have five or six tracks in DC. For six- or five-track candidates the total energy and total momentum are calculated, assuming all tracks to be pions:

$$E_{tot}=\sum_{i=1}^{5,6}\sqrt{p_i^2+m_\pi^2},\ P_{tot}=\left|\sum_{i=1}^{5,6}\bar{p}_i\right|.$$

Fig. 14 shows a scatter plot of the difference between the total energy and c. m. energy $\Delta E_6=E_{tot}-E_{c.m.}$ versus momentum for six-track candidates. A clear signal of six-pion events is seen as a cluster of dots near zero and "tail" which corresponds to events when initial electrons (positrons) radiate photons. The events with total momentum less than 150 MeV/c and with the difference ΔE_6, $-200<\Delta E_6<100$ MeV, are required to determine the number of six-pion events. To estimate the background MC simulation of the major processes $2(\pi^+\pi^-\pi^0)$ and $2(\pi^+\pi^-)\pi^0$ was performed and was found to be smaller than 1%.

To determine the number of events with one missing particle, a sample with five selected tracks is used. These events have energy deficit correlated with the total (missing) momentum. The energy of a missing particle is calculated and added to the energy of five detected pions. The difference of the obtained energy and c. m. energy ΔE_{5+1} is shown in the left part of the same graph by points together with the simulated background coming mainly from the processes $e^+e^-\to 2(\pi^+\pi^-\pi^0)$ and $e^+e^-\to 2(\pi^+\pi^-)\pi^0$ and shown by a solid line.

The polynomial fit parameters vary for the experimental and MC simulated background distributions as well as different cuts that lead to a ～3% uncertainty in the number of signal events. A more detailed analysis can be found in Ref. [25]. We have studied intermediate states in the final state with six charged pions and came to the following conclusion: the dynamics production changes versus energy and this phenomenon demands a further investigation. High statistics, which will be obtained at VEPP-2000, will allow to study dynamics with much better accuracy and reduce the models systematics. Calculation results

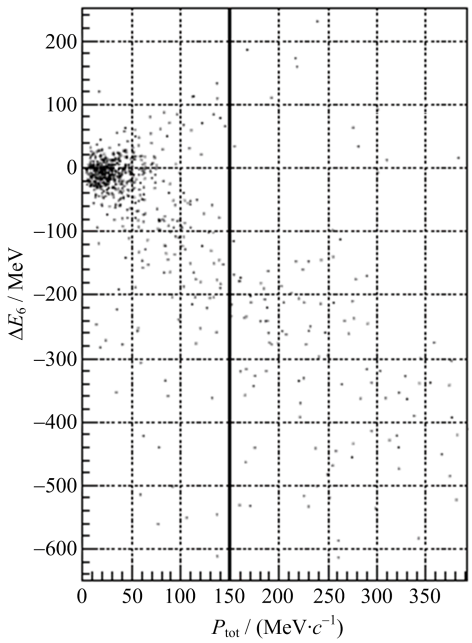

(a)

The vertical line shows the applied selection.

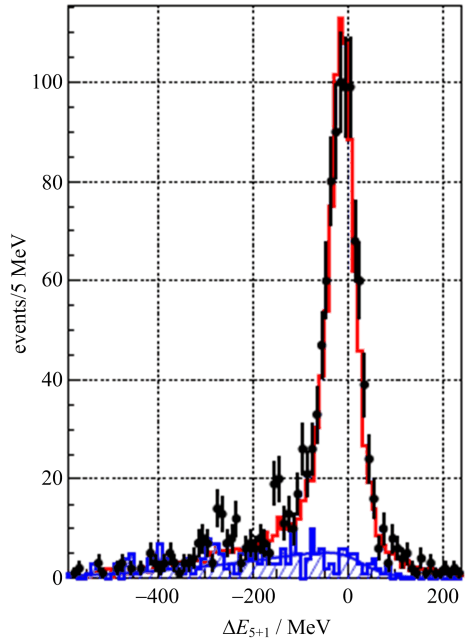

(b)

Points with errors are data and the histogram represents the MC simulated events. The shaded histogram shows an estimate of background events with a fit function used to subtract background.

Fig. 14 A scatter plot of the difference between the total energy and c. m. energy (ΔE_6) versus total momentum for six-track events (a) and the number of events (b)

for the cross section are presented in Fig. 15.

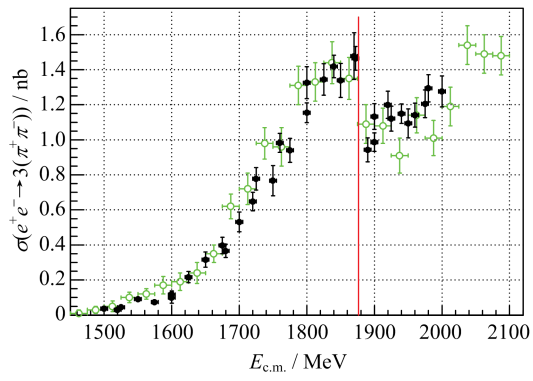

Black points-CMD-3, open circles-BaBar data

Fig. 15 Measurement of the $e^+e^-\to 3(\pi^+\pi^-)$ cross section

To measure the cross section of the process $e^+e^-\to 2(\pi^+\pi^-\pi^0)$, a sample of events with four charged and two neutral pions was selected. To select neutral pions, the spectrum of invariant mass of all two-photon combinations was studied inside the energy gap from 60 MeV/c^2 to 200 MeV/c^2 and a combination with the nearest to the pion mass is chosen.

The number of signal events at each energy point was determined by a fit of the ΔE distribution, which represents the difference between the total energy of event $e^+e^-\to 2(\pi^+\pi^-\pi^0)$ and c. m. energy: $\Delta E = E(2(\pi^+\pi^-\pi^0)) - E_{c.m.}$. A sum of three Gaussian functions for signal events and quadratic polynomial for back-ground were used to describe this distribution. The cross section is calculated according to the number of determined events and takes into account radiative corrections and detection efficiency. The results for the cross section are presented in Fig. 16. The

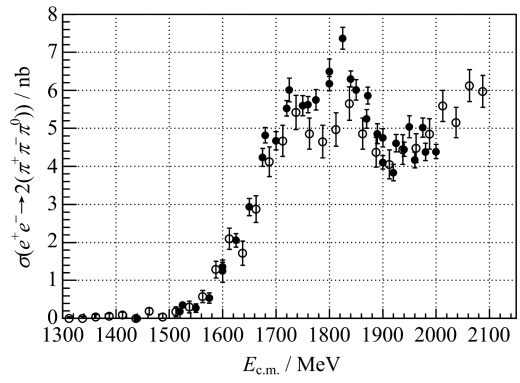

Black points-CMD-3, open circles-BaBar data

Fig. 16 Measurement of the $e^+e^-\to 2(\pi^+\pi^-\pi^0)$ cross section

analysis of the data is going on now.

11 Cross section measurement of the $e^+e^-\to\pi^+\pi^-$ and $e^+e^-\to\omega\pi^+\pi^-$ processes

11.1 $e^+e^-\to\eta\pi^+\pi^-$, $\eta\to\gamma\gamma$

The candidates for events under study with two tracks in DC and two or more photons were selected. A combination of two photons with the best χ^2 is chosen and events of $\gamma\gamma\pi^+\pi^-$ undergo a kinematic fit. To calculate the number of the $\eta\pi^+\pi^-$ events the invariant mass distribution is fitted and shown in Fig. 17, at the energy point 1 500 MeV.

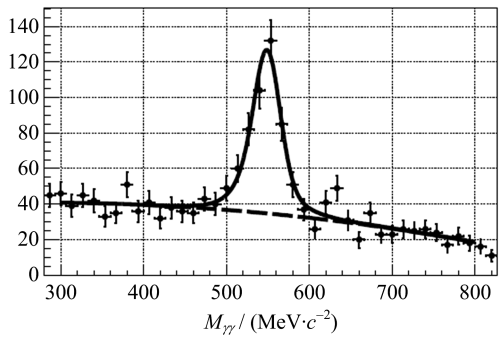

Fig. 17　The fit of two-photon invariant mass at the energy point of 1 500 MeV shown with a linear fit for the background

The preliminary results for the cross section of the $e^+e^-\to\eta\pi^+\pi^-$ process are plotted in Fig. 18 with SND results[14,17]. The systematic uncertainty for this process is about 5.2% and mainly due to the detection efficiency, which depends on the theoretical model describing the angular distribution of the final particles and is calculated using Monte Carlo simulation. Two different fits of the $e^+e^-\to\eta\pi^+\pi^-$ Born cross section under the VDM model are presented too with/without $\rho(1700)$. At the current statistics it is not possible to make a conclusion about presence of the $\rho(1700)$.

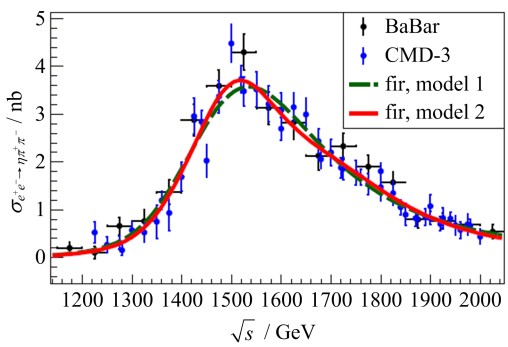

The results are presented together with BaBar data.

Fig. 18　The $e^+e^-\to\eta\pi^+\pi^-$ Born cross section measured in the $\eta\to\gamma\gamma$ channel

11.2 $e^+e^-\to\eta\pi^+\pi^-\to\pi^+\pi^-\pi^0\pi^+\pi^-$, $e^+e^-\to\omega\pi^+\pi^-\to\pi^+\pi^-\pi^0\pi^+\pi^-$

The form of the $\pi^+\pi^-\pi^0$ invariant mass distribution for the $e^+e^-\to\pi^+\pi^-\pi^+\pi^-\pi^0$ process has been determined with Monte Carlo simulation and was used to determine the numbers of the signal events under study. The preliminary results for the Born cross sections of the $e^+e^-\to\eta\pi^+\pi^-$ and $e^+e^-\to\omega\pi^+\pi^-$ processes are shown in Figs. 19 and 20.

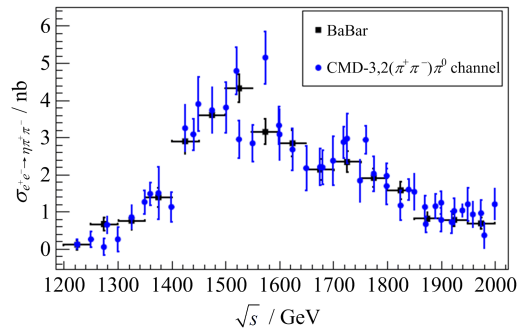

The results are presented together with BaBar data.

Fig. 19　The $e^+e^-\to\eta\pi^+\pi^-$ Born cross sections measured when η decay into three pions $\pi^+\pi^-\pi^0$

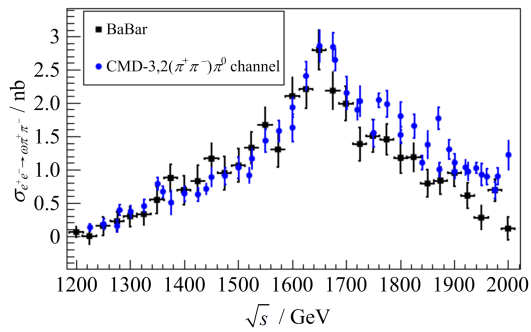

The results are presented together with BaBar data.

Fig. 20　The $e^+e^-\to\omega\pi^+\pi^-$ Born cross sections measured when ω decays into three pions $\pi^+\pi^-\pi^0$

The current systematic uncertainty for these channels is estimated as 15%.

12 Study of the process $\omega \to \pi^0 e^+ e^-$

This process was studied earlier with the CMD-2 detector[26]. The current analysis is based on an integrated luminosity of 10 pb^{-1} collected in the center-of-mass energy range $760 \div 840$ MeV. The ω decay to $\pi^0 e^+ e^-$ has been studied using the π^0 dominant decay mode: $\pi^0 \to \gamma\gamma$. The main background for this process comes from the decay ω to $\pi^+ \pi^- \pi^0$ and to $\pi^0\gamma$ followed by the Dalitz decay of the π^0 or γ conversion in the material in front of the drift chamber and QED processes. To select signal events under study, different cuts were applied. In particular, to suppress events from decay $\omega \to \pi^+ \pi^- \pi^0$ the following parameters were used: an opening angle between tracks should be $\Delta\psi \leqslant 1$ rad, the spectra of the recoil mass of photon pairs and some features of the kinematic decay. The separation method for $\pi^0 e^+ e^-$ and $\pi^0\gamma$ (with γ conversion on the material in front of DC) is based on the information about momentum of the track and vertex position which uses a neural network. The efficiency of suppression is: for $\pi^0\gamma$ ~84%, while we lose ~2% of signal events.

The detection efficiency $\varepsilon_{\pi^0 e^+ e^-} = 22\%$ was determined using MC simulation based on the GEANT4 package. The number of signal events has been obtained from a fit of the $\gamma\gamma$ invariant mass distribution at each energy point. These values were used to determine the visible cross section shown in Fig. 21.

The total number of selected $\omega \to \pi^0 e^+ e^-$ events is 1 228. The current value of $B(\omega \to \pi^0 e^+ e^-) = (7.15 \pm 0.38) \times 10^{-4}$, where the trigger efficiency, efficiency of reconstruction of close tracks and the contributions come from $\omega \to \pi^+ \pi^- \pi^0$; $\omega \to \pi^0\gamma$ were not taken into account. The analysis is still in progress.

13 Conclusion

VEPP-2000 successfully operates with a goal to get ~1 fb^{-1} in 5 ~ 10 years and provide new precise results on the hadron production. The current integrated luminosity was measured using two well-known QED processes $e^+ e^- \to e^+ e^-$, $\gamma\gamma$. Two types of the first level triggers "CHARGED" and "NEUTRAL" delivered the independent information that allowed to determine the detection efficiencies and to estimate their uncertainties. Data analysis is in progress, the already collected data sample delivers the same or better statistical precision for the hadronic cross sections than in previous experiments.

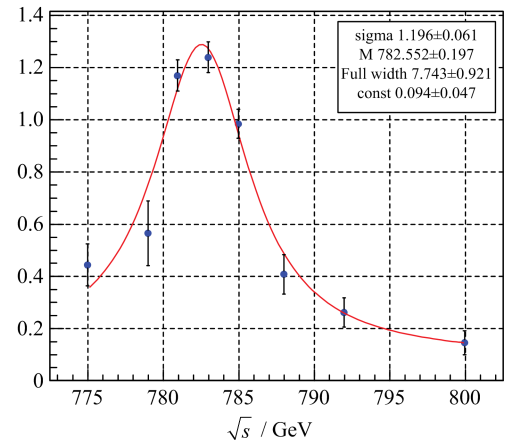

Fig. 21 The visible cross section for the process $\omega \to \pi^0 e^+ e^-$

Acknowledgements The authors are grateful to A. I. Milstein for the help with a theoretical interpretation and development of the models. We thank the VEPP-2000 team for excellent machine operation.

References

[1] KOOP I A. VEPP collider facilities in Novosibirsk: status and plan[J]. Nucl Phys B(Proc Suppl), 2008, 181-182: 371-375.

[2] KHAZIN B I. Physics and detectors for VEPP-2000 [J]. Nucl Phys B(Proc Suppl), 2008, 181-182: 376-380.

[3] ACHASOV M N, BERKAEV D E, BOGDANCHIKOV A G, et al. First experience with SND calorimeter at VEPP-2000 collider [J]. Nucl Instrum Meth A, 2009, 598(1): 31-32.

[4] DAVIER M, EIDELMAN S, HÖCKER A, et al. Updated estimate of the muon magnetic moment using revised results from $e^+ e^-$ annihilation [J]. Eur Phys J C, 2003, 31: 503-510.

[5] GRAWFORD G, DAUBENMIER C M, FULTON R,

et al. Luminosity measurement with the CLEO II detector[J]. Nucl Instrum Meth A, 1994, 345(3): 429-439.

[6] ABAKUMOVA E V, ACHASOV M N, BERKAEV D E, et al. Backscattering of laser radiation on ultrarelativisticelectrons in a transverse magnetic field: evidence of MeV-scale photon interference[J]. Phys Rev Lett, 2013, 110: 140402.

[7] AKHMETSHIN R R, ANISENKOVA A V, AULCHENKO V M, et al. Current status of luminosity measurement with the CMD-3 detector at the VEPP-2000 e^+e^- collider[J/OL]. JINST, 2014, 9: C09003[2015-11-30]. http://dx. doi. org/10. 1088/1748-0221/9/09/C09003.

[8] ARBUZOV A B, FEDOTOVICH G V, IGNATOV F V, et al. Monte-Carlo generator for e^+e^- annihilation into lepton and hadron pairs with precise radiative corrections[J]. Eur Phys J C, 2006, 46: 689-703.

[9] LOGASHENKO I B, AKHMETSHIN R R, ANISENKOV A V, et al. Measurement of $e^+e^-\to\pi^+\pi^-$ cross section at CMD-3[J/OL]. EPJ Web Conf, 2014, 72: 00013[2015-11-30]. http://dx. doi. org/10. 1051/epjconf/20147200013.

[10] KOZYREV E A, AKHMETSHIN RR, Anisenkov A V, et al. Investigation of the process $e^+e^-\to K^+K^-$ with the aid of the CMD-3 detector at the VEPP-2000 electron-positron collider[J]. Phys Atom Nucl, 2015, 78(3): 358-362.

[11] КОЗЫРЕВ Е А, АХМЕТШИН Р Р, АНИСЕНКОВ А В, et al. ИЗУЧЕНИЕ ПРОЦЕССА С ДЕТЕКТОРОМ КМД-3 НА -КОЛЛАЙДЕРЕ ВЭПП-2000[J]. Yad Fiz, 2015, 78(5): 388-392.

[12] AKHMETSHIN R R, AULCHENKO V M, BANZAROV V Sh, et al. Measurement of $\phi(1020)$ meson leptonic width with CMD-2 detector at VEPP-2M collider[J]. Phys Lett B, 2011, 695(5): 412-418.

[13] LEES J P, POIREAU V, TISSERAND V, et al. Precision measurement of the $e^+e^-\to K^+K^-(\gamma)$ cross section with the initial-state radiation method at BABAR[J]. Phys Rev D, 2013, 88: 032013.

[14] AUBERT B, BONA M, BOUTIGNY D, et al. Measurements of $e^+e^-\to K^+K^-\eta$, $K^+K^-\pi^0$, and $K^0_S K^\pm\pi^\mp$ cross sections using initial state radiation events[J]. Phys Rev D, 2008, 77: 092002.

[15] AUBERT B, BONA M, BOUTIGNY D, et al. The $e^+e^-\to 2(\pi^+\pi^-)\pi^0$, $2(\pi^+\pi^-)\eta$, $K^+K^-\pi^+\pi^-\pi^0$ and $K^+K^-\pi^+\pi^-\eta$ cross sections measured with initial-state radiation[J]. Phys Rev D, 2007, 76: 092005.

[16] AKHMETSHIN R R, AULCHENKO V M, BANZAROV V Sh, et al. Study of the processes $e^+e^-\to\eta\gamma$, $\pi^0\gamma\to 3\gamma$ in the c. m. energy range 600～1 380 MeV at CMD-2[J]. Phys Lett B, 2005, 605: 26-36.

[17] AULCHENKO V M, ACHASOV M N, BARNYAKOV A Yu, et al. Measurement of the $e^+e^-\to\eta\pi^+\pi^-$ cross section in the center-of-mass energy range 1.22～2.00 GeV with the SND detector at the VEPP-2000 collider[J]. Phys Rev D, 2015, 91: 052013.

[18] Aubert B, Barate R, Boutigny D, et al. Study of the $e^+e^-\to\pi^+\pi^-\pi^0$ process using initial state radiation with BABAR[J]. Phys Rev D, 2004, 70: 072004.

[19] AALTONEN T, A'LVAREZ GONZA'LEZ B, AMERIO S, et al. Search for high-mass resonances decaying into ZZ in $p\bar{p}$ collisions at $\sqrt{s}=1.96$ TeV[J]. Phys Rev D, 2012, 85: 012008.

[20] BALDINI R. Reported at the "Fenice" workshop, Frascati [R]. [S. l.: s. n.], 1988.

[21] CLEGG A B, DONNACHIE A. Rhoprimes in 6π states from material isation of photons [J]. Z Phys C, 1990, 45(4): 677-680.

[22] WHALLEY M R. A compilation of data on hadronic total cross sections in e^+e^- interactions[J/OL]. J Phys G: Nucl Part Phys, 2003, 29: A1[2015-11-30]. http://dx. doi. org/10. 1088/0954-3899/29/12A/R01.

[23] AUBERT B, BARATE R, BOUTIGNY D, et al. The $e^+e^-\to 3(\pi^+\pi^-)$, $2(\pi^+\pi^-\pi^0)$ and $K^+K^-2(\pi^+\pi^+)$ cross sections at center-of-mass energies from production threshold to 4.5 GeV measured with initial-state radiation[J]. Phys Rev D, 2006, 73: 052003.

[24] SIBIRTSEV A, HAIDENBAUER J, KREWALD S, et al. Near threshold enhancement of the $p\bar{p}$ mass spectrum in J/Ψ decay [J]. Phys Rev D, 2005, 71: 054010.

[25] AKHMETSHIN R R, ANISENKOV A V, ANOKHIN S A, et al. Study of the process $e^+e^-\to 3(\pi^+\pi^-)$ in the c. m. energy range 1.5～2.0 GeV with the CMD-3 detector[J]. Phys Lett B, 2013, 723: 82-89.

[26] AKHMETSHIN R R, AULCHENKO V M, BANZAROV V Sh, et al. Study of the ρ and ω meson decays into a pseudoscalar meson and e^+e^- pair with the CMD-2 detector[J]. Phys Lett B, 2005, 613: 29-38.

Article ID:0253-2778(2016)04-0272-07

Study of e^+e^- annihilation into hadrons below 2 GeV with SND

DIMOVA T. V.[1,2], ACHASOV M. N.[1,2], BARNYAKOV A. Yu.[1,2], BELOBORODOV K. I.[1,2], BERDYUGIN A. V.[1,2], BOGDANCHIKOV A. G.[1], BOTOV A. A.[1], DRUZHININ V. P.[1,2], GOLUBEV V. B.[1,2], KARDAPOLTSEV L. V.[1,2], KHARLAMOV A. G.[1,2], KOOP I. A.[1,2,3], KOROL A. A.[1,2], KOSHUBA S. V.[1,2], KOVRIZHIN D. P.[1,2], KUPICH A. S.[1,2], MARTIN K. A.[1], MUCHNOI N. Yu.[1,2], OBRAZOVSKY A. E.[1], PAKHTUSOVA E. V.[1], SEREDNYAKOV S. I.[1,2], SHATUNOV Yu. M.[1,2], SHTOL D. A.[1], SILAGADZE Z. K.[1,2], SURIN I. K.[1,2], VASILJIEV A. V.[1,2]

(1. *Budker Institute of Nuclear Physics*, *Novosibirsk* 630090, *Russia*;
2. *Novosibirsk State University*, *Novosibirsk* 630090, *Russia*;
3. *Novosibirsk State Technical University*, *Novosibirsk* 630092, *Russia*)

Abstract: Beginning from 2010 experiments with the SND detector were carried out at the e^+e^--collider VEPP-2000 in the energy range 0.3～2.0 GeV. New results on the study of the processes of e^+e^- annihilation into hadrons based on data collected in these experiments are presented.

Key words: universal detector; hadrons; cross section; data analysis
CLC number: O572.3 **Document code**: A doi:10.3969/j.issn.0253-2778.2016.04.002
2010 Mathematics Subject Classification:

Citation: DIMOVA T V, ACHASOV M N, BARNYAKOV A Yu, et al. Study of e^+e^- annihilation into hadrons below 2 GeV with SND[J]. Journal of University of Science and Technology of China, 2016,46(4):272-278.

SND上质心能量2 GeV以下正负电子淹没到强子过程的研究

DIMOVA T. V.[1,2], ACHASOV M. N.[1,2], BARNYAKOV A. Yu.[1,2], BELOBORODOV K. I.[1,2], BERDYUGIN A. V.[1,2], BOGDANCHIKOV A. G.[1], BOTOV A. A.[1], DRUZHININ V. P.[1,2], GOLUBEV V. B.[1,2], KARDAPOLTSEV L. V.[1,2], KHARLAMOV A. G.[1,2], KOOP I. A.[1,2,3], KOROL A. A.[1,2], KOSHUBA S. V.[1,2], KOVRIZHIN D. P.[1,2], KUPICH A. S.[1,2], MARTIN K. A.[1], MUCHNOI N. Yu.[1,2], OBRAZOVSKY A. E.[1], PAKHTUSOVA E. V.[1], SEREDNYAKOV S. I.[1,2], SHATUNOV Yu. M.[1,2], SHTOL D. A.[1], SILAGADZE Z. K.[1,2], SURIN I. K.[1,2], VASILJIEV A. V.[1,2]

Received: 2015-11-30; **Revised**: 2016-04-20
Foundation item: Supported by Russian Science Foundation (14-50-00080), Russian Foundation for Basic Research (15-02-01037, 15-02-03391).
Biography: DIMOVA T. V. (corresponding author), female, PhD/Senior. Research field: particle physics. E-mail: baiert@inp.nsk.su

(1. 布德克尔核物理研究所，新西伯利亚 630090，俄罗斯；
2. 新西伯利亚州立大学，新西伯利亚 630090，俄罗斯；
3. 新西伯利亚州立理工大学，新西伯利亚 630092，俄罗斯)

摘要：从 2010 年开始，VEPP-2000 正负电子对撞机上的 SND 探测器在质心能量区间 0.3～2.0 GeV 正式运行. 基于已获取数据，得到了正负电子淹没到强子过程研究的新结果.

关键词：通用探测器；强子；截面；数据分析

0 Introduction

The VEPP-2000 e^+ e^- collider[1] (Fig. 1) operates in the center-of-mass (c. m.) energy range from 0.3 to 2.0 GeV. Experiments at VEPP-2000 were carried out in 2010～2013. The maximal luminosity achieved during these experiments was 2×10^{31} cm$^{-2}\cdot$s^{-1}. The luminosity was limited by deficit of positrons. Currently the VEPP-2000 complex is being upgraded. This upgrade is expected to provide an increase of VEPP-2000 luminosity at 2 GeV up to 10^{32} cm$^{-2}\cdot$s^{-1} and should result in a more stable operation of the accelerator complex.

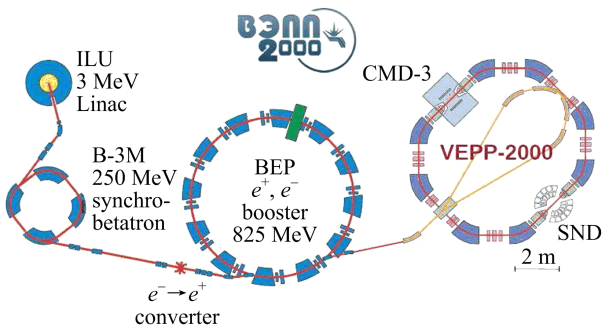

Fig. 1　The layout of the VEPP-2000 e^+ e^- collider

The Spherical Neutral Detector (SND)[2-3] (Fig. 2) is the universal nonmagnetic detector, which consists of a nine-layer drift chamber, an aerogel Cherenkov counter, a three-layer spherical electromagnetic calorimeter with 1640 NaI(Tl) crystals, and a muon system. During 2010～2013 a data sample with an integrated luminosity of about 69 pb^{-1} was recorded with the SND detector in the energy range from 0.32 to 2.00 GeV. Data accumulated in the energy region above the ϕ-meson resonance correspond to an integrated luminosity of 45 pb^{-1}.

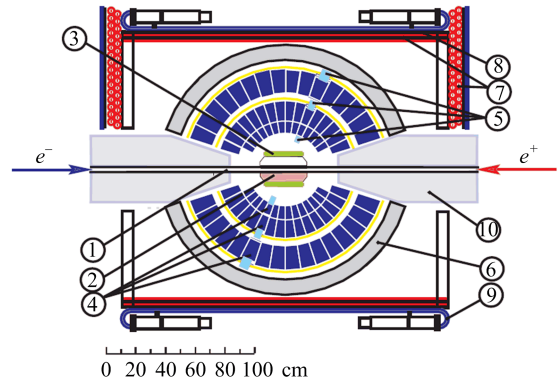

1 - beam pipe, 2 - tracking system, 3 - aerogel Cherenkov counters, 4 - NaI(Tl) crystals, 5 - phototriodes, 6 - iron muon absorber, 7～9 - muon detector, 10 - focusing superconducting solenoids.

Fig. 2　The SND detector

The physical program for VEPP-2000 includes precise measurements of all major channels of e^+e^- annihilation to hadrons from threshold up to 2 GeV. The main goal of these measurements is to improve the accuracy of $R=\sigma(e^+e^-\to\text{hadrons})/\sigma(e^+e^-\to\mu^+\mu^-)$, which is used for calculating the muon anomaly $(g-2)_\mu$ and the fine structure constant at Z-mass $\alpha_{em}(s=M_Z^2)$. Other items of the program are: study of the production, dynamics and decays of the excited vector states ρ', ρ'', ω', ω'', and ϕ', the comparison of the isovector cross sections with the corresponding spectral functions in τ decays, study of the nucleon pair production near threshold and some others.

1 Multihadron processes

1.1　$e^+e^-\to\pi^+\pi^-\pi^0$ [4]

The $e^+e^-\to\pi^+\pi^-\pi^0$ cross section measured by SND is shown in Fig. 3 in comparison with data of previous experiments. This is the most precise

measurement in the energy range 1.05 ~ 2.00 GeV. For energies below 1.8 GeV the cross section data are well described by the VMD model with the contributions of ω, ϕ, $\omega(1420)$ and $\omega(1650)$ resonances. Above 1.8 GeV, an extra resonance or a non-resonant contribution needs to be added to describe cross section energy dependence.

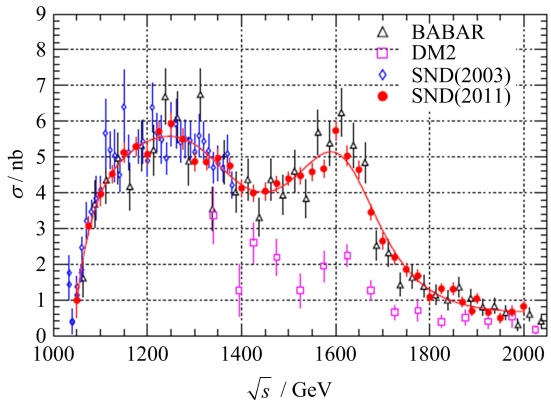

Fig. 3 The cross section for $e^+e^-\to\pi^+\pi^-\pi^0$ obtained by SND at VEPP-2000 in comparison with the previous SND[5] and BABAR[6] data

1.2 $e^+e^-\to\pi^+\pi^-\eta$[7]

It is usually assumed that the dominant mechanism for this reaction is the transition via the $\rho(770)\eta$ intermediate state. The measured $\pi^+\pi^-$ invariant mass spectrum is shown in Fig. 4. It can be seen that it differs from the spectrum calculated under the $\rho(770)\eta$ assumption. The observed deviation may be a result of a contribution of other intermediate state, e. g. $\rho(1450)\eta$.

The $e^+e^-\to\pi^+\pi^-\eta$ cross section measured by SND at VEPP-2000 in comparison with previous measurements is shown in Fig. 5. The fit to the cross section data was performed for two models: ① a sum of the $\rho(770)$, $\rho(1450)$ and $\rho(1700)$ resonance contributions and ② a sum of the $\rho(770)$ and $\rho(1450)$ contributions. The value of the $\rho(1700)$ amplitude obtained in the first model deviates from zero by 2σ. So, we cannot come to a definite conclusion that the $\rho(1700)$ contribution is needed for data description.

Using our data on the $e^+e^-\to\eta\pi^+\pi^-$ cross section under the CVC hypothesis, the branching fraction of the decay $\tau\to\eta\pi^-\pi^0\nu_\tau$ is calculated to be $(0.156\pm0.011)\%$. This value is in reasonable agreement with the PDG[8] value $B(\tau\to\eta\pi^-\pi^0\nu_\tau)=(0.139\pm0.01)\%$.

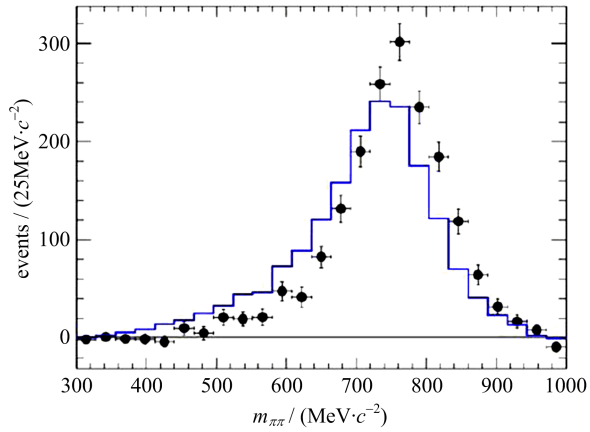

The histogram is the simulated spectrum for the $\rho\eta$ mechanism.

Fig. 4 The $\pi^+\pi^-$ invariant mass spectrum for $e^+e^-\to\pi^+\pi^-\eta$ data events (points with error bars)

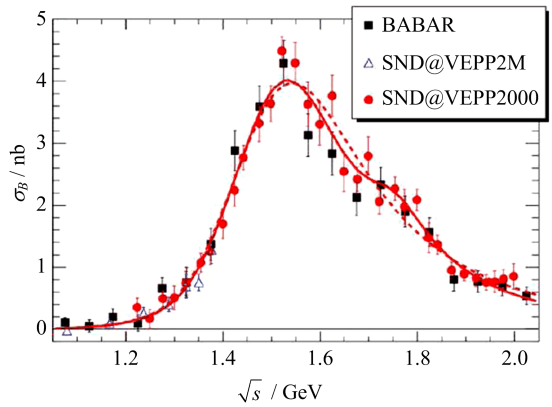

The solid curve is the result of the fit with ρ, $\rho(1450)$ and $\rho(1700)$ contributions. The dashed line is the result of the fit with ρ and $\rho(1450)$ contributions.

Fig. 5 The $e^+e^-\to\pi^+\pi^-\eta$ cross section obtained by SND at VEPP-2000 in comparison with the previous SND[9] and BABAR[10] measurements

1.3 $e^+e^-\to K^+K^-\eta$

This process is studied in the $\eta\to\gamma\gamma$ decay mode. The measured cross section in comparison with BABAR data is shown in Fig. 6. The fit to the cross section data is performed in the hypothesis that the main mechanism of this reaction is $e^+e^-\to\phi(1680)\to\phi(1020)\eta$. The result

of the fit is in agreement with the data.

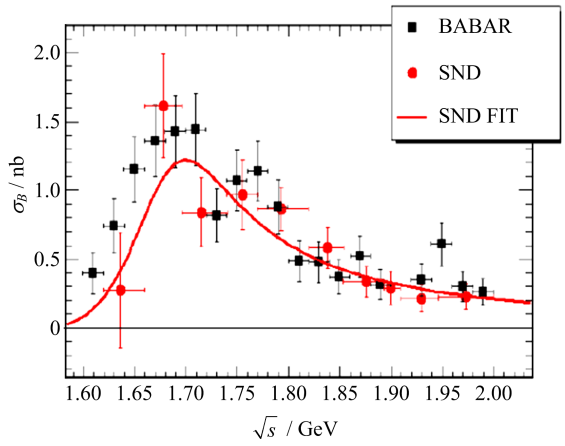

The solid curve is the result of the fit described in the text.

Fig. 6　The $e^+e^-\to K^+K^-\eta$ cross section obtained by SND in comparison with the BABAR measurement[11]

1.4　$e^+e^-\to\pi^+\pi^-\pi^0\eta$

This process runs through different intermediate states. The contributions of the $\omega\eta$ and $\phi\eta$ intermediate states are clearly seen in the spectrum of the $\pi^+\pi^-\pi^0$ invariant mass shown in Fig. 7. The contribution of $a\rho$ intermediate state is seen in the $\eta\pi$ invariant mass spectrum shown in Fig. 8. There is also a non-resonant contribution.

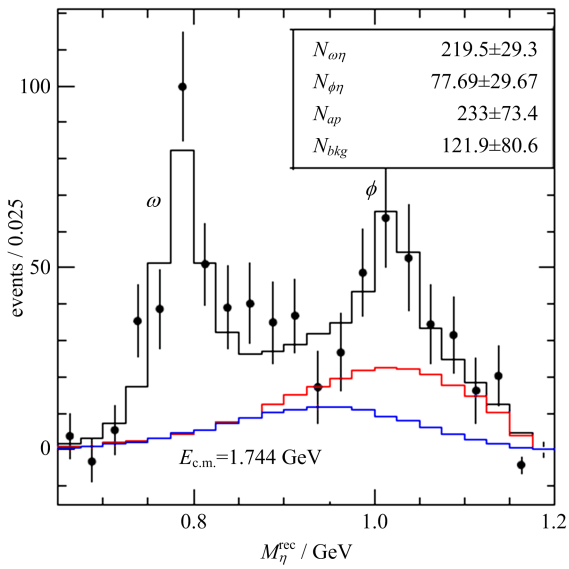

Fig. 7　The $\pi^+\pi^-\pi^0$ invariant mass spectrum for $e^+e^-\to\pi^+\pi^-\pi^0\eta$ data events (points with error bars) at $E_{cm}=1.794$ GeV

The measured $e^+e^-\to\pi^+\pi^-\pi^0\eta$ cross section is shown in Fig. 9. This is the first measurement of

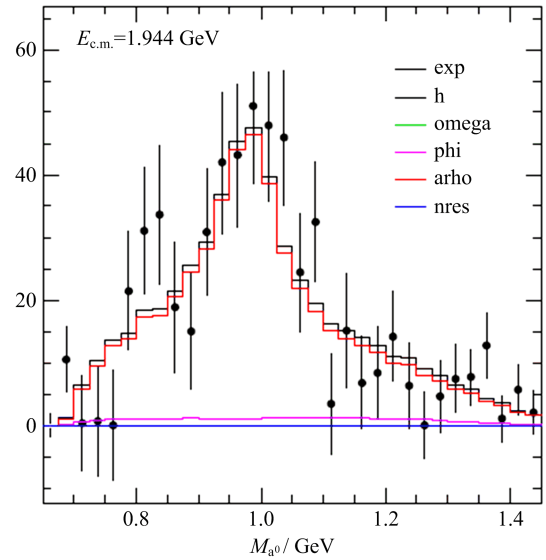

Fig. 8　The $\eta\pi$ invariant mass spectrum for $e^+e^-\to\pi^+\pi^-\pi^0\eta$ data events (points with error bars) at $E_{cm}=1.944$ GeV

the cross section. We suppose that the dominant contributions to the $e^+e^-\to\pi^+\pi^-\pi^0\eta$ cross section comes from the $\phi(1680)$ and $\omega(1650)$ resonances. The cross section for the $\omega\eta$ component is shown in Fig. 10 in comparison with BABAR data. The fit to cross section data takes into account contributions of the $\phi(1680)$ and $\omega(1420)$ resonances. The sharp decrease of the cross section to zero above $E_{cm}>1.8$ GeV is explained by destructive interference of the two resonance amplitudes.

1.5　$e^+e^-\to\omega\pi^0$

The update of our previous measurement of the $e^+e^-\to\omega\pi^0$ cross section[13] based on the full SND data set collected at VEPP-2000 is presented in Fig. 11 in comparison with the SND at VEPP-2M result (SND 2000) and CLEO data. The CLEO cross section is calculated under the CVC hypothesis from the spectral function in the $\tau\to\omega\pi\nu_\tau$ measured in Ref. [15]. The cross-section energy dependence is well described by contributions of the ρ, $\rho(1450)$ and $\rho(1700)$ resonances. The transition form factor $F_{\omega\pi\gamma}$ for $\gamma^*\to\omega\pi^0$ vertex $F_{\omega\pi\gamma}$ obtained from the measured cross section is shown in Fig. 12. Below 0.7 GeV the same form factor measured in the $\omega\to\pi^0\mu^+\mu^-$

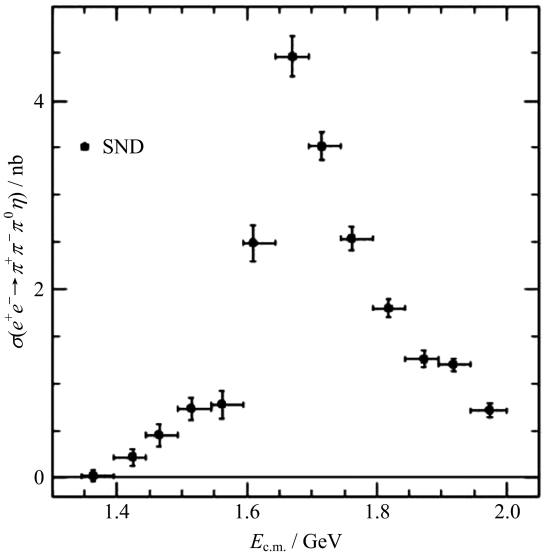

Fig. 9 The $e^+e^-\to\pi^+\pi^-\pi^0\eta$ cross section measured by SND

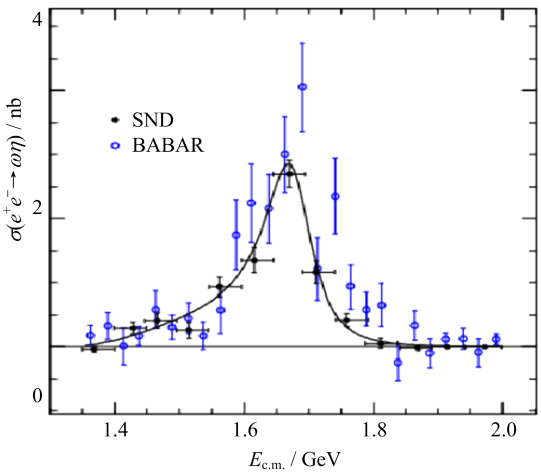

Fig. 10 The $e^+e^-\to\omega\eta$ cross section obtained by SND in comparison with BABAR data[12]

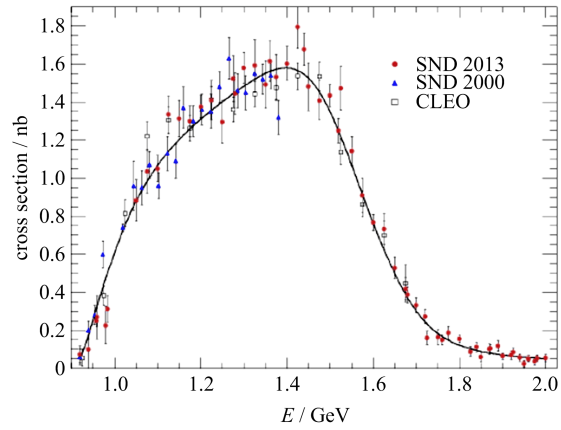

Fig. 11 The $e^+e^-\to\omega\pi^0$ cross section obtained by SND at VEPP-2000 in comparison with previous SND at VEPP-2M results[14] and CLEO data[15]

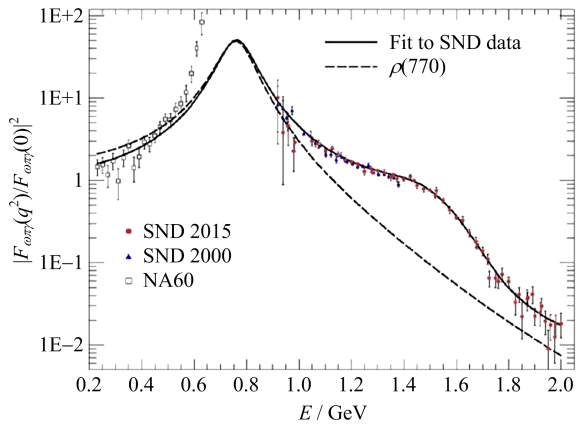

The circles represent SND at VEPP-2000 data, the triangles of previous SND and VEPP-2M data and squares data from the NA60 experiment[16]

Fig. 12 The transition form factor for the $\gamma^*\to\omega\pi^0$ vertex

decay[16] is shown. The solid curve represents the results of the VMD prediction with the parameters obtained from our cross section fit. The dashed curve shows the $\rho(770)$ contribution only. One can see that the data from e^+e^- annihilation and $\omega\to\pi^0\mu^+\mu^-$ decay cannot be described with the VMD model.

1.6 $e^+e^-\to K^+K^-$

In this measurement charged kaon identification is based on information from the aerogel threshold Cherenkov counters[17]. Our preliminary result on the $e^+e^-\to K^+K^-$ cross section in comparison with BABAR data is shown in Fig. 13. The complex energy dependence of the cross section is explained by interference of the amplitudes of all isoscalar and isovector resonances located in the energy region under study.

1.7 Production of nucleon-antinucleon pairs

The cross sections for the $e^+e^-\to p\bar{p}$ and $e^+e^-\to n\bar{n}$ processes measured by SND are shown in Figs. 14 and 15. Both cross sections are constant in the energy region under study. The values of the $p\bar{p}$ and $n\bar{n}$ cross sections coincide within errors.

2 Search for the rare decays $\eta',\eta\to e^+e^-$

In the Standard Model (SM) these decays proceed through the two-photon intermediate state and therefore are suppressed by a factor of α^2 compared with the two photon decays, where α is

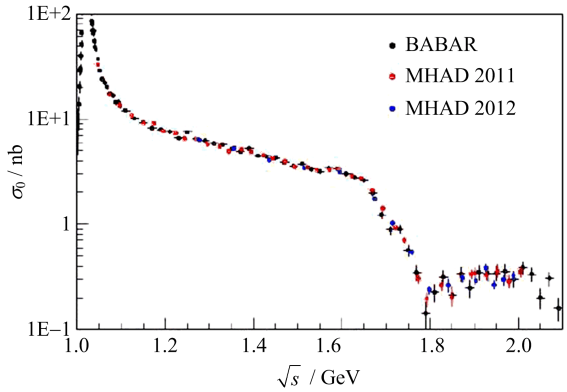

Fig. 13　The $e^+e^-\to K^+K^-$ cross section obtained by SND in comparison with BABAR data[18]

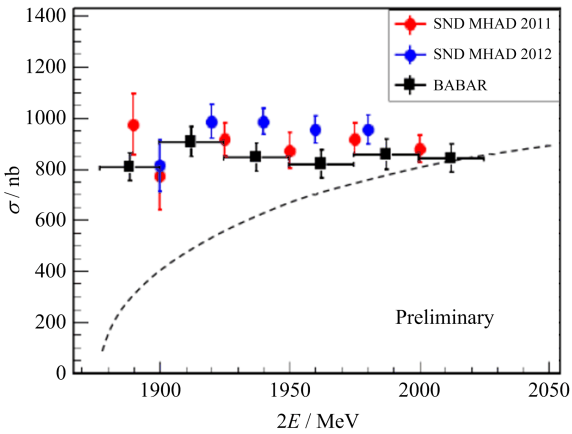

Fig. 14　The $e^+e^-\to p\bar{p}$ cross section obtained by SND in comparison with BABAR data[19]

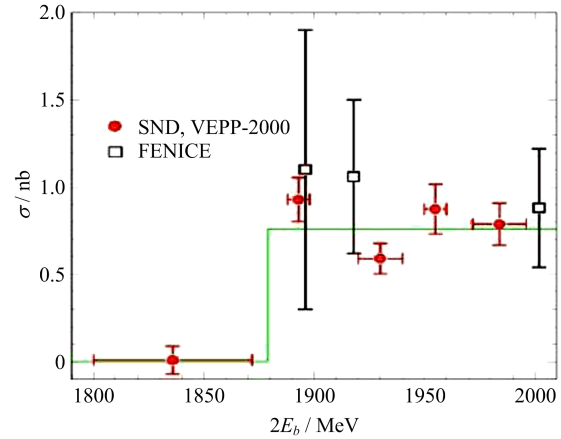

Fig. 15　The $e^+e^-\to n\bar{n}$ cross section obtained by SND in comparison with FENICE data[20]

the fine structure constant. An additional suppression of $(m_e/m_{\eta',\eta})^2$ arises from the approximate helicity conservation. So, the partial width of η', $\eta\to e^+e^-$ decays is less than the corresponding two-photon width by a factor of $\sim\alpha^2(m_e/m_{\eta',\eta})^2$. The low probability makes these decays sensitive to possible contributions of new physics beyond the SM. At the VEPP-2000 e^+e^- collider these decays can be searched for using the inverse reaction $e^+e^-\to\eta',\eta$. The strictest upper limit on the branching fraction $\mathcal{B}(\eta'\to e^+e^-)<1.2\times10^{-8}$ at the 90% confidence level (CL) was set in the experiment with the CMD-3 detector at VEPP-2000[21]. The upper limit on the η-decay $\mathcal{B}(\eta\to e^+e^-)<2.3\times10^{-6}$ was recently set in the HADES experiment[22].

Search for the $\eta'\to e^+e^-$ decay is based on the data set with an integrated luminosity of about 2.9 pb^{-1} collected by SND at c.m. energy close to $m_{\eta'}=(957.78\pm0.06)$ MeV. Five decay chains with a total branching fraction of 51.5% are used to reconstruct η'. No data events satisfying η' selection criteria process have been found. As a result the upper limit has been obtained $\mathcal{B}(\eta'\to e^+e^-)<1.0\times10^{-8}$ at 90% CL. The combined SND and CMD-3 limit is $\mathcal{B}(\eta'\to e^+e^-)<5.6\times10^{-9}$.

During the 2010～2013 experiments the SND detector didn't collect data at $m_\eta=(548.862\pm0.018)$ MeV. So, we study the possibility to perform $\eta\to e^+e^-$ search after VEPP-2000 upgrade. To do this, data with an integrated luminosity of 108 nb^{-1} collected in the c.m. energy range 520～580 MeV are used. No background events for the reaction $e^+e^-\to\eta$ in the decay mode $\eta\to\pi^0\pi^0\pi^0$ have been found. This means that data with an integrated luminosity of 324 nb^{-1} will provide a sensitivity of 10^{-6} for $\mathcal{B}(\eta\to e^+e^-)$. Such data may be accumulated in two weeks of VEPP-2000 operation.

3　Conclusion

During 2010 ～ 2013, experiments at the VEPP-2000 e^+e^- collider with the SND detector were carried in the c.m. energy range from 320 to 2 000 MeV. Data with an integrated luminosity of about of 69 pb^{-1} were collected. Analysis of these data is in progress. Obtained results on hadronic cross sections have the same or better statistical precision than previous measurements. After

VEPP-2000 upgrade, data taking will be resumed with the goal to collect 1 fb^{-1}.

References

[1] SHATUNOV YU M , EVSTIGNEEV A V; GANYUSHIN D I, et al. Project of a new electron positron collider VEPP-2000[C/OL]//Proceedings of the 7th European Particle Accelerator Conference. 2000:439[2015-11-30]. http://accelconf. web. cern. ch/AccelConf/e00/PAPERS/MOP4A08. pdf

[2] ACHASOV M N, BERKAEV D E, BOGDANCHIKOV A G, et al. First experience with SND calorimeter at VEPP-2000 collider[J]. Nucl Instrum Meth A,2009,598(1): 31-32.

[3] AULCHENKO V M, BOGDANCHIKOV A G, BOTOV A A, et al. SND tracking system — Tests with cosmic muons[J]. Nucl Instrum Meth A,2009,598(1): 102-104.

[4] AUL'CHENKO V M, ACHASOV M N, BARNYAKOV A Yu, et al. Study of the $e^+e^-\to\pi^+\pi^-\pi^0$ process in the energy range 1.05～2.00 GeV [J]. JETP, 2015, 121(1): 27-34.

[5] ACHASOV M N, AULCHENKO V M, BELOBORODOV K I, et al. Study of the process $e^+e^-\to\pi^+\pi^-\pi^0$ in the energy region $\sqrt{s}$ from 0.98 to 1.38 GeV[J]. Phys Rev D,2002, 66: 032001.

[6] AUBERT B, BARATE R, BOUTIGNY D, et al. Study of the $e^+e^-\to\pi^+\pi^-\pi^0$ process using initial state radiation with BABAR[J]. Phys Rev D, 2004, 70:072004.

[7] AULCHENKO V M, ACHASOV M N, BARNYAKOV A Yu, et al. Measurement of the $e^+e^-\to\eta\pi^+\pi^-$ cross section in the center-of-mass energy range 1.22～2.00 GeV with the SND detector at the VEPP-2000 collider[J]. Phys Rev D, 2015, 91: 052013.

[8] OLIVE K A, AGASHE K, AMSLER C, et al. Review of particle physics [J]. Chin Phys C, 2014, 38(09): 090001.

[9] ACHASOV M N, BELOBORODOV K I, BERDYUGIN A V,et al. Measurement of the $e^+e^-\to\eta\pi^+\pi^-$ cross section in the $\sqrt{s}$=1.04～1.38 GeV energy range with a spherical neutral detector at the VEPP-2M collider[J]. JETP Lett, 2010, 92(2): 80-84.

[10] AUBERT B, BONA M, BOUTIGNY D, et al. The $e^+e^-\to2(\pi^+\pi^-)\pi^0$, $2(\pi^+\pi^-)\eta$, $K^+K^-\pi^+\pi^-\pi^0$ and $K^+K^-\pi^+\pi^-\eta$ cross sections measured with initial-state radiation[J]. Phys Rev D, 2007, 76:092005.

[11] AUBERT B, BONA M, BOUTIGNY D, et al. Measurements of $e^+e^-\to K^+K^-\eta$, $K^+K^-\pi^0$ and $K^0_SK^\pm\pi^\mp$ cross sections using initial state radiation events[J]. Phys Rev D, 2008, 77: 092002.

[12] AUBERT B, BARATE R, BOUTIGNY D, et al. The $e^+e^-\to3(\pi^+\pi^-)$, $2(\pi^+\pi^-\pi^0)$ and $K^+K^-2(\pi^+\pi^-)$ cross sections at center-of-mass energies from production threshold to 4.5 GeV measured with initial-state radiation[J]. Phys Rev D, 2006, 73: 052003.

[13] ACHASOV M N, AULCHENKO V M, BARNYAKOV A Yu, et al. Study of $e^+e^-\to\omega\pi^0\to\pi^0\pi^0\gamma$ in the energy range 1.05～2.00 GeV with the SND detector[J]. Phys Rev D, 2013, 88: 054013.

[14] ACHASOV M N ,BELOBORODOV K I, BERDYUGIN A V,et al. The process $e^+e^-\to\omega\pi^0\to\pi^0\pi^0\gamma$ up to1.4 GeV[J]. Phys Lett B, 2010, 486:29-34.

[15] EDWARDS KW, JANICEK R, PATEL P M, et al. Resonant structure of $\tau\to3\pi\pi^0\nu_\tau$ and $\tau\to\omega\pi\nu_\tau$ decays[J]. Phys Rev D, 2000, 61: 072003.

[16] ARNALDI R, BANICZ K, CASTOR J, et al. Study of the electromagnetic transition form-factors in $\eta\to\mu^+\mu^-\gamma$ and $\omega\to\mu^+\mu^-\pi^0$ decays with NA60[J]. Phys Lett B,2009, 677: 260-266.

[17] BARNYAKOV A Yu, BARNYAKOV M Yu, BELOBORODOV K I, et al. Particle identification system based on dense aerogel for SND detector at VEPP-2000 collider[J]. JINST ,2014, 9(09):C09023.

[18] LEES J P, POIREAU V, TISSERAND V, et al. Precision measurement of the $e^+e^-\to K^+K^-(\gamma)$ cross section with the initial-state radiation method at BABAR[J]. Phys Rev D, 2013, 88:032013.

[19] AUBERT B, BARATE R, BOUTIGNY D, et al. Study of $e^+e^-\to p\bar{p}$ using initial state radiation with BABAR[J]. Phys Rev D, 2006, 73: 012005.

[20] ANTONELLI A, BALDINI R, BERTANI M, et al. First measurement of the neutron electro-magnetic form factor in the time-like region[J]. Phys Lett B, 1993, 313: 283-287.

[21] AKHMETSHIN R R, ANISENKOV A V, AULCHENKO V M, et al. Search for the process $e^+e^-\to\eta'(958)$ with the CMD-3 detector[J]. Phys Lett B, 2015, 740: 273-277.

[22] AGAKISHIEV G, BALANDA A, BELVER D, et al. Searching a dark photon with HADES[J]. Phys Lett B, 2014, 731: 265-271.

第46卷第4期 中国科学技术大学学报 Vol. 46, No. 4
2016年4月 JOURNAL OF UNIVERSITY OF SCIENCE AND TECHNOLOGY OF CHINA Apr. 2016

Article ID:0253-2778(2016)04-0279-03

Experimental study of the $e^+ e^- \to K^+ K^-$ process cross section with the SND detector at the VEPP-2000 $e^+ e^-$ collider

BELOBORODOV K. I. (for the SND Collaboration)

(*Budker Institute of Nuclear Physics, Novosibirsk State University, Novosibirsk* 630090, *Russia*)

Abstract: In experiments at the VEPP-2000 $e^+ e^-$ collider with the SND detector the $e^+ e^- \to K^+ K^-$ process cross section has been measured in the energy range 1.05～2.0 GeV. Its value was found to be consistent with previous measurements.

Key words: collider; experiment; calorimeter; mesons

CLC number: O572.3 **Document code**: A doi:10.3969/j.issn.0253-2778.2016.04.003

2010 Mathematics Subject Classification:

Citation: BELOBORODOV K I. Experimental study of the $e^+ e^- \to K^+ K^-$ process cross section with the SND detector at the VEPP-2000 $e^+ e^-$ collider[J]. Journal of University of Science and Technology of China, 2016, 46(4): 279-281.

VEPP-2000 对撞机上 SND 探测器对于 $e^+ e^- \to K^+ K^-$ 过程的研究

BELOBORODOV K. I. (SND 合作组)

(布德克尔核物理研究所,新西伯利亚 630090,俄罗斯)

摘要:在 VEPP-2000 对撞机上的 SND 探测器进行的实验中,测量了质心能量区间为 1.05～2.0 GeV 下的 $e^+ e^- \to K^+ K^-$ 过程的截面.测得的截面值与之前的测量值相吻合.

关键词:对撞机;实验;量能器;介子

0 Introduction

Experimental study of the $e^+ e^- \to K^+ K^-$ process is of interest because of its considerable contribution to the total $e^+ e^- \to$ hadrons cross section, which is important for $(g-2)_\mu$ factor and α_{em} constant at Z-mass. The isovector part of this cross section is related to the $\tau \to K^+ K^0 \nu_\tau$ decay mass spectrum. In addition, the $e^+ e^- \to K^+ K^-$ cross section can be used to specify the excited vector meson parameters.

This process has been studied in many experiments, the latest are experiments at VEPP-2M[1-2] and BABAR[3].

In this talk the $e^+ e^- \to K^+ K^-$ cross section was measured at VEPP-2000 collider[4] with the

Received: 2015-11-30; **Revised**: 2016-04-20

Foundation item: Supported by Russian Science Foundation (14-50-00080), Russian Foundation for Basic Research (15-02-01037, 14-02-00129-a).

Biography: BELOBORODOV K. I., male, born in 1973. Research field: high energy physics. E-mail: K. I. Beloborodov@inp.nsk.su

SND detector[5-8]. The important feature of the SND detector is the aerogel Cherenkov detector with $n=1.13$ index of refraction[9], used in our study to separate pions and kaons.

The data were collected during 2011 and 2012 runs, the integrated luminosity in the energy range 1.05～2.0 GeV is about 35 pb^{-1}.

1 Data analysis

In our analysis the events were selected with two collinear tracks coming from the interaction region. Besides the K^+K^- events, the similar collinear processes $e^+e^-\to e^+e^-$, $\mu^+\mu^-$, $\pi^+\pi^-$, $p\bar{p}$ and cosmic muon events contribute to this class. To suppress the $\mu^+\mu^-$ and $\pi^+\pi^-$ background we require that one of the tracks hit the Cherenkov counter, which produces the veto signal from these events. The K^+K^- events don't produce the Cherenkov signal in our momentum range. To suppress the background from $p\bar{p}$ events, the dE/dx cut was imposed for one of two tracks: $dE/dx_K<1.5\cdot dE/dx_e$, where indices K and e correspond to kaons and electrons. The $e^+e^-\to e^+e^-$ background was subtracted using the total energy deposition in calorimeter (shown as a peak 1 in Fig. 1). The background from the multihadron processes like $e^+e^-\to\pi^+\pi^-\pi^0$, $\pi^+\pi^-\pi^0\pi^0$, $K^+K^-\pi^0$, etc. was subtracted by the sideband method in the $\Delta\phi-\Delta\theta$ plane, where $\Delta\phi$ and $\Delta\theta$ are noncolinearity angles in ϕ and θ planes for the pair of tracks.

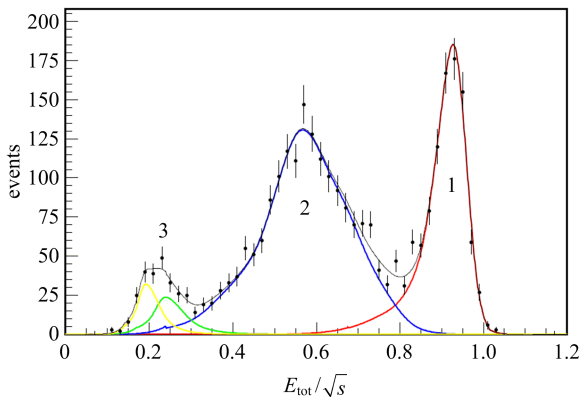

The lines are the approximation curves for the signal and background processes.

Fig. 1 The distribution of the normalized energy deposition in calorimeter at $E=1.425$ GeV

The detection efficiency of the $e^+e^-\to K^+K^-$ process versus beam energy is shown in Fig. 2. The dependence of the detection efficiency on the radiative photon energy in Fig. 3 is taken into account. The correction coefficient from the kinematic cut is estimated to be $c_{kin}=1.0076\pm0.0022$, the correction from Cherenkov counter is $c_{ch}=1.0035\pm0.0012$, and the geometry correction is $c_{geom}=1.0025\pm0.0013$.

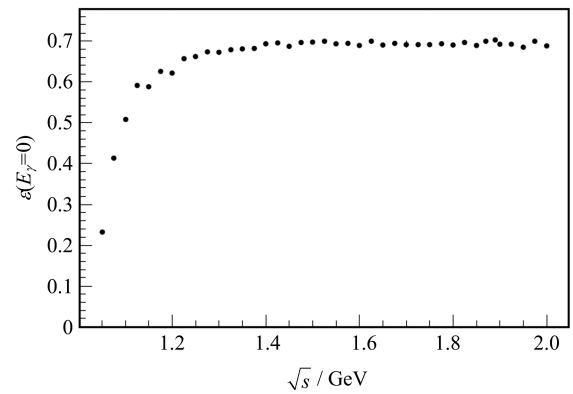

Fig. 2 The detection efficiency of the process $e^+e^-\to K^+K^-$ versus energy

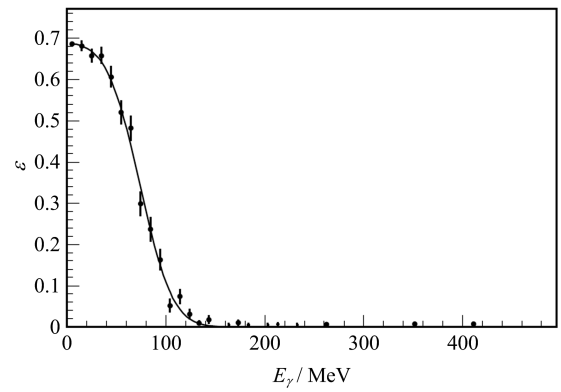

Fig. 3 The detection efficiency of the process $e^+e^-\to K^+K^-$ versus radiative photon energy at $E=1.6$ GeV

2 The total cross section

The visible cross section σ_{vis} of the process under study is related to the total cross section σ_0:

$$\sigma_{vis}(\sqrt{s})=\int_0^1 dz\cdot\sigma_0(\sqrt{s}(1-z))\cdot F(z,s)\cdot\varepsilon(\sqrt{s},z) \quad (1)$$

where $s=E^2$, $F(z,s)$ is the probability for the initial particles to emit the photon carrying the

fraction of energy $\sqrt{s}$, $\varepsilon(\sqrt{s}, z)$ is a detection efficiency as a function of $\sqrt{s}$ and z.

The total cross section σ_0 is determined using the following procedure. The measured visible cross section at each energy point as a function of energy $\sigma_{vis}=N/IL$ (here N is a number of selected events, IL is an integrated luminosity) is approximated by a function calculated using Eq. (1) with some model for the total cross section. As a result of the approximation the parameters of this model are calculated together with the function $R(s)=\sigma_{vis}(s)/\sigma_0(s)$. Experimental values for the total cross section are determined, and then according to the following equation:

$$\sigma_0 = \frac{\sigma_{vis}}{R(s)} \qquad (2)$$

Model dependence of the result is estimated by varying the total cross section models.

In Fig. 4 the obtained values of the cross section versus energy are presented together with the previously measured BABAR result. The good agreement between both measurements is seen. The rise of the cross section at ~1 GeV is due to the $\phi(1020)$ state, and the structure at ~1.7 GeV comes from the contribution of the $\phi(1680)$ resonance.

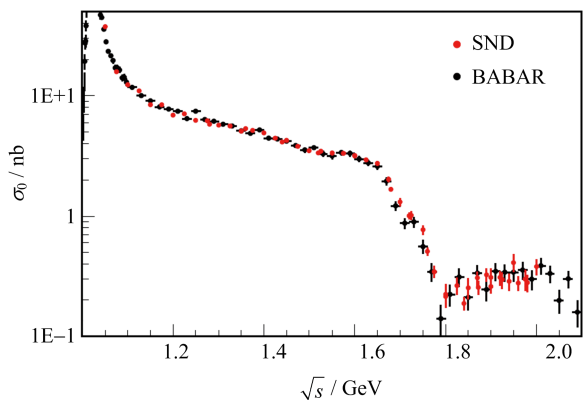

Fig. 4 The total cross section of the $e^+e^-\to K^+K^-$ process from this work and BABAR[3]

The systematic uncertainty in the measured cross section is defined by the luminosity accuracy 1%, the detection efficiency error 1.3%, radiative correction error 0.1%. Total uncertainty is about 1.7%.

3 Conclusion

The cross section of the $e^+e^-\to K^+K^-$ process in the energy range 1.05~2.0 GeV was measured at the VEPP-2000 e^+e^- collider with the SND detector. The measured cross section well agrees with existing data.

References

[1] ACHASOV M N, BELOBORODOV K I, BERDYUGIN A V, et al. Measurement of the $e^+e^-\to K^+K^-$ cross section in the energy range $\sqrt{s}=1.04\sim1.38$ GeV with the SND detector at the VEPP-2M e^+e^- collider[J]. Phys Rev D, 2007,76: 072012.

[2] AKHMETSHIN R R, AULCHENKO V M, BANZAROV V Sh, et al. Measurement of $e^+e^-\to\varphi\to K^+K^-$ cross section with CMD-2 detector at VEPP-2M collider[J]. Phys Lett B,2008, 669:217-222.

[3] Lees J P, Poireau V, Tisserand V, et al. Precision measurement of the $e^+e^-\to K^+K^-(\gamma)$ cross section with the initial-state radiation method at BABAR[J]. Phys Rev D, 2013,88:032013.

[4] SHATUNOV YU M, EVSTIGNEEV A V, GANYUSHIN D I, et al. Project of a new electron positron collider VEPP-2000[C/OL]//Proceedings of the 7th European Particle Accelerator Conference. 2000:439[2015-11-30]. http://accelconf.web.cern.ch/AccelConf/e00/PAPERS/MOP4A08.pdf

[5] ACHASOV M N, BERKAEV D E, BOGDANCHIKOV A G, et al. First experience with SND calorimeter at VEPP-2000 collider[J]. Nucl Instrum Meth A, 2009,598: 31-32.

[6] AULCHENKO V M, BOGDANCHIKOV A G, BOTOV A A, et al. SND tracking system — Tests with cosmic muons[J]. Nucl Instrum Meth A, 2009, 598: 102-104.

[7] BARNYAKOV A Yu, BARNYAKOV M Yu, BELOBORODOV K I, et al. High density aerogel for ASHIPH SND — test results[J]. Nucl Instrum Meth A, 2009, 598:163-165.

[8] AULCHENKOET V M, BOGDANCHIKOV A G, BOTOV A A, et al. DAQ and electronics for SND at VEPP-2000 — First test results[J]. Nucl Instrum Meth A, 2009,598: 340-341.

[9] BARNYAKOV A Yu, BARNYAKOV M Yu, BELOBORODOV K I, et al. Particle identification system based on dense aerogel for SND detector at VEPP-2000 collider[J]. JINST, 2014, 9(09):C09023.

第46卷第4期 中国科学技术大学学报 Vol. 46, No. 4
2016年4月 JOURNAL OF UNIVERSITY OF SCIENCE AND TECHNOLOGY OF CHINA Apr. 2016

Article ID:0253-2778(2016)04-0282-04

Recent results from the KEDR detector at the VEPP-4M

TODYSHEV K. Yu.[1,2] (for the KEDR collaboration)

(1. *Budker Institute of Nuclear Physics*, *Novosibirsk* 630090, *Russia*;
2. *Novosibirsk State University*, *Novosibirsk* 630090, *Russia*)

Abstract: The result is presented of precise measurement the values of R_{uds} and R at seven points of the center-of-mass energy between 3.12 and 3.72 GeV based on the data collected with the KEDR detector at the VEPP-4M e^+e^- collider in Novosibirsk. Also present is the preliminary result of determination of the product of the electron partial width by the branching fraction into hadrons of J/ψ resonance.

Key words: R measurement; J/ψ resonance; charmonium

CLC number: O572.3 **Document code**: A doi:10.3969/j.issn.0253-2778.2016.04.004

Citation: TODYSHEV K Yu. Recent results from the KEDR detector at the VEPP-4M[J]. Journal of University of Science and Technology of China, 2016,46(4):282-285,315.

VEPP-4M 对撞机上 KEDR 探测器的最新结果

TODYSHEV K. Yu.[1,2] (KEDR 合作组)

(1. 布德克尔核物理研究所,新西伯利亚 630090,俄罗斯;2. 新西伯利亚州立大学,新西伯利亚 630090,俄罗斯)

摘要:基于新西伯利亚 VEPP-4M 正负电子对撞机的 KEDR 探测器采集的数据,报道了质心能量在 3.12～3.72 GeV 之间 7 个能量点的 R_{uds} 和 R 值的精确测量结果.同时报道了 J/ψ 共振态衰变的电子和强子的联合分宽度.

关键词:R 值测量;J/ψ 共振态;粲偶素

0 Introduction

One of the most important quantities measured in e^+e^- annihilation is R, defined as the ratio of the radiatively corrected total hadronic cross section in electron-positron annihilation to the lowest-order QED cross section of the muon pair production. The precise $R(s)$ measurements are crucial to testing QCD predictions and allow one to determine the value of the strong coupling constant $\alpha_s(s)$, the anomalous magnetic moment of the muon $(g-2)_\mu$ and the value of the electromagnetic fine structure constant at the Z^0 peak $\alpha(M_Z^2)$. Note that the systematic errors dominate in all experiments to measure the R value in the energy region between the J/ψ and $\psi(2S)$. That is a good motivation for new experiments on the precise measurement of R in this energy range.

The knowledge of the narrow resonance parameters allows us to calculate analytically their

Received: 2015-11-30; **Revised**: 2016-04-20

Foundation item: Supported by Russian Science Foundation (14-50-00080), Presidential Scholarship (SP5889:2013:2).

Biography: TODYSHEV K. Yu., male, born in 1977, PhD. Research field: high energy physics. E-mail: todyshev@inp.nsk.su

contribution in R. The product of the dielectronic width of the J/ψ resonance and the branching fraction for its decay to hadrons, $\Gamma_{ee}\boldsymbol{B}_{\rm hadr}$ was measured in the KEDR experiment, and the preliminary result is reported in the present article.

1 R measurement

1.1 Analysis

The following principles are used in our analysis. We subtract tails of the J/ψ and $\psi(2S)$ resonances from the observed cross section taking into account contributions from physical processes. The vacuum polarization is calculated without the contribution of narrow resonances.

The R value was calculated as follows:

$$R=\frac{\sigma_{\rm obs}(s)-\sum\varepsilon_{\rm bg}(s)\sigma_{\rm bg}(s)-\sum\varepsilon_{\psi}(s)\sigma_{\psi}(s)}{\varepsilon(s)(1+\delta(s))\sigma^{0}_{\mu\mu}(s)} \tag{1}$$

where $\sigma_{\rm obs}(s)=\dfrac{N_{\rm mh}-N_{\rm res.\,bg.}}{\int\boldsymbol{L}{\rm d}t}$ is observed hadronic annihilation cross section, $N_{\rm mh}$ represents all events that pass hadronic selection criteria, $N_{\rm res.\,bg.}$ represents the residual machine background. $\sigma^{0}_{\mu\mu}(s)$ is the Born cross section for $e^+e^-\to\mu^+\mu^-$ and $\varepsilon(s)$ is the detection efficiency for the single photon annihilation to hadrons. The second term in the numerator corresponds to the physical background from e^+e^-, $\mu^+\mu^-$ production, $\tau^+\tau^-$ production above threshold and two-photon processes. The third term represents a contribution of the J/ψ and $\psi(2S)$.

The detection efficiencies ε and $\varepsilon_{\rm bg}$ were determined from simulation. The efficiencies ε_{ψ} were found by fitting the resonance regions. The resonances were fitted separately in each scan, the free parameters were the detection efficiency at the world average values of the leptonic width Γ_{ee} and its product by the hadronic branching fraction $\boldsymbol{B}_{\rm hadr}$, the machine energy spread and the observed continuum cross section magnitude in the reference point below the resonance. The procedures of a narrow resonance cross section calculation and fitting are described in more detail in Refs. [1-2].

In our approach the radiative correction factor can be written as

$$1+\delta(s)=\int\frac{{\rm d}x}{1-x}\frac{\boldsymbol{F}(s,x)}{|1-\widetilde{\Pi}((1-x)s)|^2}\cdot\frac{\widetilde{R}((1-x)s)\varepsilon((1-x)s)}{R(s)\varepsilon(s)} \tag{2}$$

where $\boldsymbol{F}(s,x)$ is the radiative correction kernel[3]. The vacuum polarizations $\widetilde{\Pi}$ and $\widetilde{R}$ do not include the J/ψ and $\psi(2S)$ resonances.

It should be mentioned that, using the way described above we get the $R_{\rm uds}$ value. To obtain the quantity R, it is necessary to take into account the contribution of narrow resonances.

1.2 Experiment description and results

In 2011 the region of the J/ψ and $\psi(2S)$ resonances was scanned in the KEDR experiment with an integrated luminosity of about 1 pb^{-1} at seven energy points. To determine the relative contributions of the J/ψ and $\psi(2S)$ in the observed cross section without external data, the additional data samples of about 0.4 pb^{-1} were collected at ten points in the peak regions. The data points and the resonance fits are shown in Fig. 1.

The following sources of systematic uncertainty have been considered for the R measurement at each energy point: luminosity, radiative correction, systematic uncertainties related to the detection efficiency of hadronic events, detector response, background from physical processes and residual machine background from the accelerator.

The major sources of the systematic uncertainty on the $R_{\rm uds}$ value are listed in Tab. 1. The uncertainties vary depending on the energy points.

During data collection at a given energy point the relative beam energy variation was less than 10^{-3} allowing us to neglect this source of uncertainty.

The obtained $R_{\rm uds}$ and R values and luminosity-weighted average center-of-mass energies are presented in Tab. 2. The results and analysis

presented above are discussed in more detail in Ref. [4].

Tab. 1 R_{uds} systematic uncertainties

Source	Uncertainty/%
Continuum simulation	1.4～2.1
Luminosity measurement	1.1
Radiative correction	0.4～0.6
J/ψ and $\psi(2S)$ contribution	0.1～2.8
e^+e^-X contribution	0.1～0.2
l^+l^- contribution	0.1～0.2
Trigger efficiency	0.2
Nuclear interaction	0.2
Cuts variation	0.6
Machine background	0.5～1.1
Sum in quadrature	2.1～3.6

Tab. 2 Measured values of $R_{uds}(s)$ and $R(s)$ with statistical and systematic uncertainties

$\sqrt{s}$/MeV	$R_{uds}(s)\{R(s)\}$
3119.9±0.2	2.215{2.237}±0.089±0.066
3223.0±0.6	2.172{2.173}±0.057±0.045
3314.7±0.7	2.200{2.200}±0.056±0.043
3418.2±0.2	2.168{2.168}±0.050±0.042
3520.8±0.4	2.200{2.201}±0.050±0.044
3618.2±1.0	2.201{2.207}±0.059±0.044
3719.4±0.7	2.187{2.211}±0.068±0.060

2 $\Gamma_{e^+e^-}(J/\psi)\cdot B(J/\psi\to\text{hadrons})$ analysis

The product of the dielectronic width of the J/ψ resonance and branching fraction for its decay to hadrons, $\Gamma_{e^+e^-}\times B_{hadr}$, was measured in experiment with KEDR detector performed during energy scan at the VEPP-4M e^+e^- collider in 2005. In that experiment, the integrated luminosity 230 nb^{-1} was collected, which corresponds to about 250 thousand J/ψ mesons.

Analytical expression for the e^+e^- annihilation cross section near a narrow resonance in the soft photon approximation was first obtained in Ref. [5] forty years ago. With up-to-date modifications the procedures of a narrow resonance cross section calculation can be found in Refs. [1-2]. The hadronic cross section includes a resonant part and interference which are proportional to leptonic and hadronic widths. The observed multihadron and e^+e^- production cross sections as a function of the center of mass energy near J/ψ resonance are presented in Fig. 2.

The fitting of the resonance cross section allows us to determine the product dielectronic

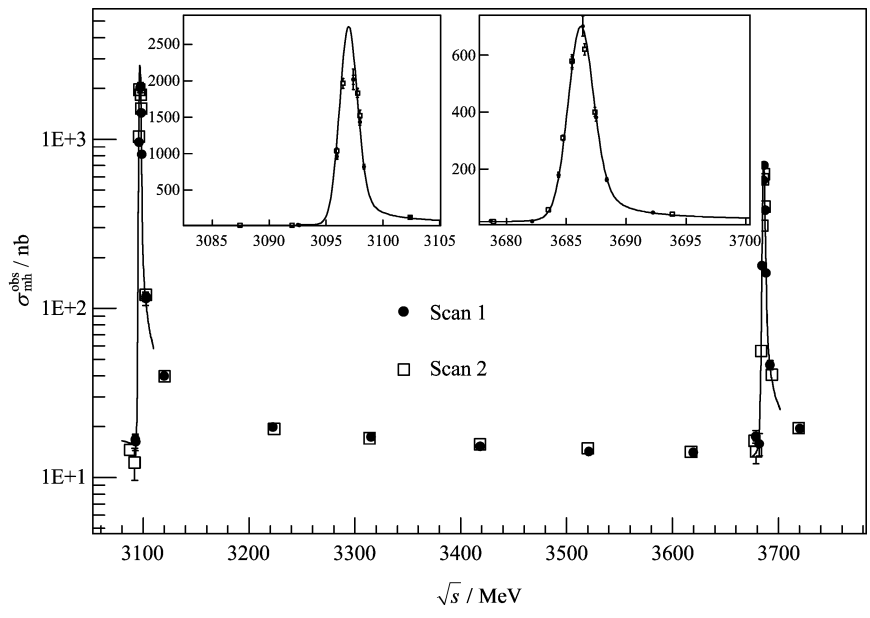

The curves are the result of the fits of the narrow resonances. The inserts show the closeup of the J/ψ and $\psi(2S)$ regions.

Fig. 1 The observed multihadronic cross section as a function of the c. m. energy for the two scans

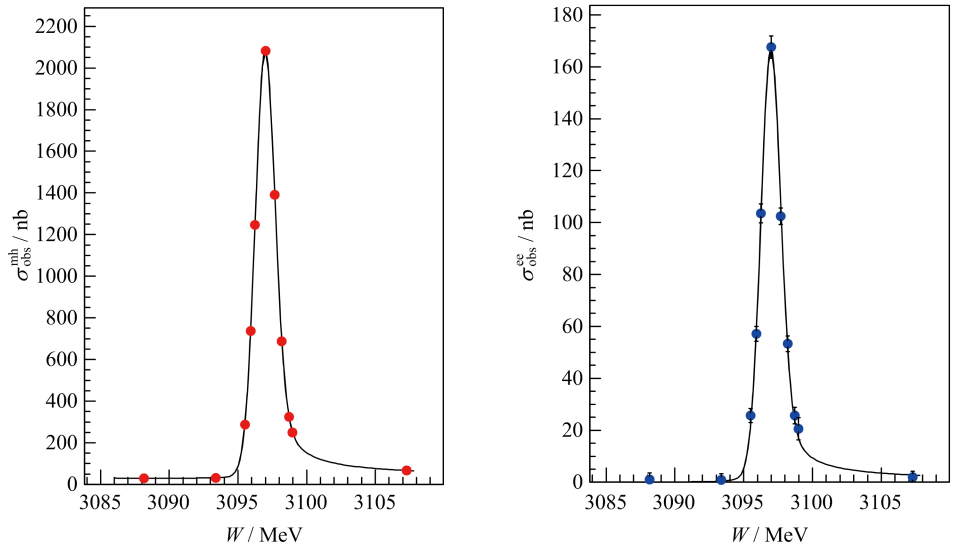

The curves are the result of the combined fit. All data are corrected for the efficiency.

Fig. 2　The observed multihadron cross section as a function of the c. m. energy (left figure) and cross section of the process $J/\psi \to e^+ e^-$ (right figure)

width and hadronic branching fraction. The preliminary result is $\Gamma_{ee} \times \boldsymbol{B}_{\mathrm{hadr}} = (4.88 \pm 0.07 \pm 0.15)$ keV. The main sources of systematic uncertainties are listed in Tab. 3.

Tab. 3　Main systematic uncertainties in the measurements $\Gamma_{ee} \times \boldsymbol{B}_{\mathrm{hadr}}$ of J/ψ

Source	Uncertainty/%
J/ψ decay simulation	2.0
Luminosity measurement	1.5
Detector response	1.5
Energy determination	0.5
Other	0.5
Sum in quadrature	3.0

Our preliminary result agrees with those of other measurements and has a better precision, as shown in Fig. 3.

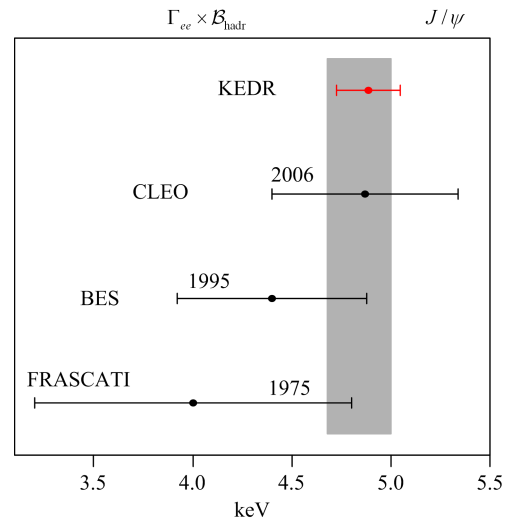

The gray band corresponds to the world-average value[6] with allowance for the uncertainty in it.

Fig. 3　Results of experiments aimed at measuring the product of the dielectronic-decay width of the J/ψ meson and the branching ratio for its decay to hadrons

3　Conclusion

We have measured the R ratio at seven points with the center-of-mass energy between 3.12 and 3.72 GeV. The achieved accuracy is about or better than 3.3% at most of energy points at the systematic uncertainty of about 2.1%.

The products of the dielectron width of the J/ψ meson and the branching fraction of its decays to the hadrons were preliminarily measured with an accuracy of 3.4%.

Acknowledgments　We greatly appreciate the permanent support of the staff of the experimental, accelerator and electronics laboratories while preparing and performing this experiment.

(下转第 315 页)

第46卷第4期 中国科学技术大学学报 Vol. 46, No. 4
2016年4月 JOURNAL OF UNIVERSITY OF SCIENCE AND TECHNOLOGY OF CHINA Apr. 2016

Article ID:0253-2778(2016)04-0286-06

Results on hadronic cross sections at KLOE

DE LEO V. (on behalf of the KLOE and KLOE-2 Collaborations)

(*INFN Sezione di Roma Tre, Roma* 00146, *Italy*)

Abstract: The precise determination of the $e^+e^-\to\pi^+\pi^-(\gamma)$ cross section is particularly important to evaluate the hadronic loop contribution to the SM calculation of the muon $(g-2)$, where a long-standing 3σ discrepancy with the direct experimental determination is observed. The KLOE experiment studied the production of $\pi^+\pi^-$ in the ISR channel and published three measurements (in 2005, 2008 and 2012) of the $\pi^+\pi^-$ cross section with the ISR photon emitted at small angles and an independent measurement (in 2010) with the ISR photon emitted at large angles and using data at a collision energy of 1 GeV. The combination of the last analysis (KLOE12) with two previously published (KLOE08, KLOE10) together with the preliminary fit by using the Gounaris-Sakurai model is presented.

Key words: Muon anomaly; Initial state radiation; pion form factor

CLC number: O572.3 **Document code**: A doi:10.3969/j.issn.0253-2778.2016.04.005

Citation: DE LEO V. Results on hadronic cross sections at KLOE[J]. Journal of University of Science and Technology of China, 2016,46(4):286-291.

KLOE 谱仪强子截面结果

DE LEO V.(KLOE 和 KLOE-2 合作组)

(意大利国家核物理研究所,罗马 00146,意大利)

摘要:长期以来 μ 子反常磁矩$(g-2)$的理论计算与实验观测相差 3 倍标准偏差,而 $e^+e^-\to\pi^+\pi^-(\gamma)$截面的精确数值对于标准模型计算中强子的圈图贡献起到了相当重要的作用.基于在 1 GeV 获取的数据,通过对含有初态辐射的 $\pi^+\pi^-$ 过程的研究,KLOE 实验已经报道了在 2005,2008 和 2012 年对初态辐射光子在小角度发射进行的 3 次测量,以及在 2010 年对初态辐射光子在大角度发射进行的测量.本文介绍对最近的 KLOE12 和之前的 KLOE08,KLOE10 所做的联合分析,以及用 Gounaris-Sakurai 模型进行初步拟合的结果.

关键词:缪子反常磁矩;初态辐射;pion 形状因子

0 Introduction

The theoretical evaluations of the muon anomaly, $a_\mu=(g_\mu-2)/2$, find a discrepancy of about 3 standard deviations from the measurements performed at the Brookhaven Laboratory that have reached an accuracy of 0.54 ppm: $a_\mu=(11\ 659\ 208.9\pm6.3)\times10^{-10}$[1]. A large part of the uncertainty on the theoretical estimates comes

Received: 2015-11-30; **Revised**: 2016-04-20

Biography: DE LEO V., female, born in 1986, PhD. Research field: particle physics. E-mail: veronica.deleo@roma3.infn.it

from the leading-order hadronic contribution $a_\mu^{had,lo}$, which at low energies is not calculable by perturbative QCD, but has to be evaluated with a dispersion integral using the measured hadronic cross sections:

$$a_\mu^{Had}[LO] = \frac{1}{3}\left(\frac{\alpha}{\pi}\right)^2 \int_{m_\pi^2}^{\infty} \mathrm{d}s \, \frac{K(s)}{s} R(s) \qquad (1)$$

where $K(s)$ is a QED kernel function[2] and $R(s)$ is referred to as the ratio of the cross section for e^+e^- annihilation into hadrons to the pointlike muon-pair cross section at center of mass energy $\sqrt{s}$. The region below 1 GeV is dominated by the $\pi^+\pi^-$ final state and contributes with $\sim 70\%$ to $a_\mu^{had,lo}$, and $\sim 60\%$ to its uncertainty. Therefore, improved precision in the dipion cross section would result in a reduction of the uncertainty on the LO hadronic contribution to a_μ, and in turn to the SM prediction for a_μ. This energy region is accessible with the KLOE experiment in Frascati by exploiting the ISR process.

1 KLOE detector

The KLOE detector operates at *DAΦNE*, the Frascati ϕ-factory, an e^+e^- collider running at fixed energy, $W=\sqrt{s}\approx 1\,020$ MeV, the ϕ meson mass. It consists of a cylindrical drift chamber (DC)[3] and a calorimeter (EMC)[4]. The DC has a momentum resolution of $\sigma_{p_\perp}/p_\perp \sim 0.4\%$ for tracks with polar angle $\theta > 45°$. Track points are measured in the DC with a resolution in $r-\phi$ of ~ 0.15 mm and ~ 2 mm in z. The EMC has an energy resolution of $\sigma_E/E \sim 5.7\%/\sqrt{E}$(GeV) and an excellent time resolution of $\sigma_t \sim 54$ ps$/\sqrt{E}$(GeV) $\oplus$ 100 ps.

Calorimeter clusters are reconstructed grouping together energy deposits close in space and time. A superconducting coil provides an axial magnetic field of 0.52 T along the colliding beam direction, which is taken as the z axis of our coordinate system. The x axis is horizontal, the y axis is vertical, directed upwards. A cross section of the detector in the y, z plane is shown in Fig. 1.

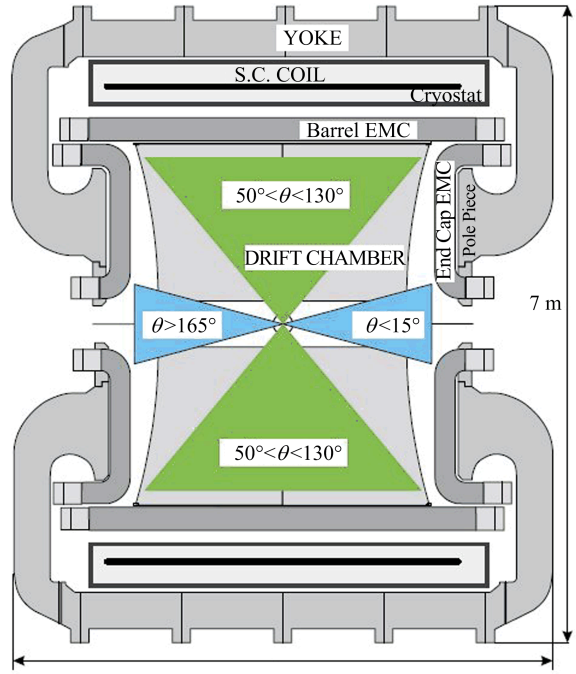

Fig. 1 Vertical cross section of the KLOE detector, showing the small and large angle regions where photons and pions (or muons) are accepted

2 Measurement of the $e^+e^- \to \pi^+\pi^-$ cross section at KLOE

The differential cross section measured at KLOE is evaluated using the following relation:

$$s \left.\frac{\mathrm{d}\sigma(\pi^+\pi^-\gamma)}{\mathrm{d}s_\pi}\right|_{\mathrm{ISR}} = \sigma_{\pi\pi}(s_\pi)\, H(s_\pi, s) \qquad (2)$$

where s_π is the $\pi^+\pi^-$ invariant mass squared. The radiator function H is computed from QED with complete NLO corrections[5] and depends on the e^+e^- center of mass energy squared s. $\sigma_{\pi\pi}$ obtained from Eq. (2) requires accounting for final state radiation (FSR).

In the 2008 and 2012 KLOE measurements a data sample of integrated luminosity of 240 pb^{-1} collected in 2002 was used[6-8]. In both analyses the "small angle photon" selection is chosen. Such selection requires two tracks of opposite sign with $50° < \theta_\pi < 130°$ (wide cones in Fig. 1) and a missing photon emitted within a cone of $\theta_\gamma < 15°$ around the beamline (narrow cones in Fig. 1). Since the photon is not explicitly detected, its momentum has to be reconstructed from kinematics: $\boldsymbol{p}_\gamma \backsimeq \boldsymbol{p}_{\mathrm{miss}} =$

$-(\boldsymbol{p}_+ + \boldsymbol{p}_-)$. However, although these cuts guarantee a high statistics for ISR signal events, and a reduced contamination both from the resonant process $e^+e^- \to \pi^+\pi^-\pi^0$ in which the π^0 mimics the missing momentum of the photon(s) and from the final state radiation process $e^+e^- \to \pi^+\pi^-\gamma_{FSR}$, a highly energetic photon emitted at small angle forces the pions also to be at small angles (and thus outside the selection cuts), resulting in a kinematical suppression of events with $M^2_{\pi\pi} < 0.35$ GeV^2. From the bare cross section, $\sigma^0_{\pi\pi(\gamma)}$, (related to the pion form factor in the following Eq. (4)), i. e. corrected for the running of α_{em} and inclusive of FSR, the dipion contribution to the muon anomaly $\Delta^{\pi\pi} a_\mu$ is measured. The dispersion integral for $\Delta^{\pi\pi} a_\mu$ is computed as the sum of the values for $\sigma^0_{\pi\pi(\gamma)}$ times the kernel $K(s)$:

$$\Delta^{\pi\pi} a_\mu = \frac{1}{4\pi^3}\int_{s_{\min}}^{s_{\max}} \mathrm{d}s\sigma^0_{\pi\pi(\gamma)}(s)K(s) \qquad (3)$$

where the kernel is given in Ref. [9] and it gives:

$$\Delta^{\pi\pi} a_\mu(0.35\ \text{GeV}^2 < M^2_{\pi\pi} < 0.95\ \text{GeV}^2) = (387.2 \pm 0.5_{\text{stat}} \pm 2.4_{\text{sys}} \pm 2.3_{\text{th}}) \times 10^{-10}.$$

To access the two pion threshold, in 2010 the KLOE collaboration performed an analysis requiring events that were selected to have a photon at large polar angles between $50° < \theta_\gamma < 130°$ (wide cones in Fig. 1, left), in the same angular region as the pions[9]. The 140 pb^{-1} data sample has been collected at CM energy $\sqrt{s} = 1$ GeV in order to significantly reduce the contamination from the $f_0\gamma$ and $\rho\pi$ decays of the ϕ-meson. On the other hand, this selection results in a reduction in statistics and an increase of the background from the process $\phi \to \pi^+\pi^-\pi^0$. The following value for the dipion contribution to the muon anomaly $\Delta^{\pi\pi} a_\mu$ was found:

$$\Delta^{\pi\pi} a_\mu(0.1 \sim 0.85\ \text{GeV}^2) = (478.5 \pm 2.0_{\text{stat}} \pm 5.0_{\text{sys}} \pm 4.5_{\text{th}}) \times 10^{-10}.$$

In the last KLOE measurement (KLOE12) the $\pi^+\pi^-\gamma/\mu^+\mu^-\gamma$ ratio is used to extract the dipion cross section. Eq. (2) in fact, is also valid for $e^+e^- \to \mu^+\mu^-\gamma$ and $e^+e^- \to \mu^+\mu^-$ with the same radiator function H. The pion form factor is calculated by:

$$|F_\pi(s')|^2 = \frac{3}{\pi}\frac{s'}{\alpha^2\beta^3_\pi}\sigma^0_{\pi\pi(\gamma)}(s')(1+\delta_{VP})(1-\eta_\pi(s')) \qquad (4)$$

where δ_{VP} is the Vacuum Polarization (VP) correction, η_π accounts for FSR radiation assuming point-like pions and $\sigma^0_{\pi\pi}(\gamma)$ is the bare cross section defined as[5]

$$\sigma^0(\pi^+\pi^-, s') = \frac{\mathrm{d}\sigma(\pi^+\pi^-(\gamma), \text{ISR})/\mathrm{d}s'}{\mathrm{d}\sigma(\mu^+\mu^-(\gamma), \text{ISR})/\mathrm{d}s'} \times \sigma^0(e^+e^- \to \mu^+\mu^-(\gamma), s') \qquad (5)$$

where $s' = s_\pi = s_\mu$. As said before, the data sample used is the same as in the 2008 analysis. However, while the analysis for $\pi\pi\gamma$ is essentially the same as for KLOE08, some new elements have been introduced in the $\mu\mu\gamma$ analysis. First of all the separation between the $\pi\pi\gamma$ and $\mu\mu\gamma$ events is obtained by using the track mass variable (M_{TRK}), calculated from the energy and momentum conservation laws, with the following conditions: $M_{\text{TRK}} < 115$ MeV for the muons and $M_{\text{TRK}} > 130$ MeV for the pions (see Fig. 2).

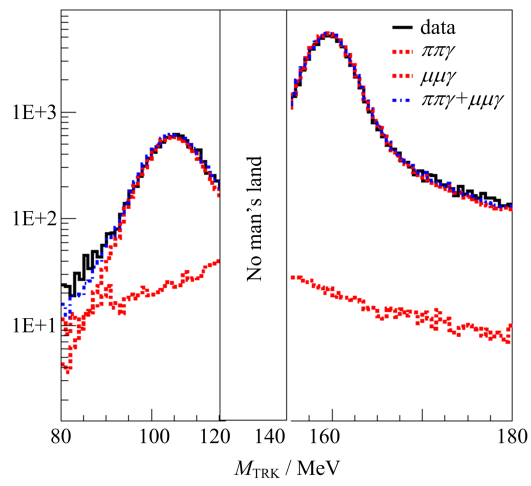

The vertical lines shows the selection cut ($M_{\text{TRK}} < 115$ MeV) for muons and ($M_{\text{TRK}} > 130$ MeV) for pions.

Fig. 2 $\mu\mu\gamma$ **and** $\pi\pi\gamma$ M_{TRK} **distributions**

This selection has been cross checked using a kinematic fit or applying a quality cut on the helix fit for both $\pi - \mu$ tracks. Consistent results have been obtained with all methods.

The differential $\mu\mu\gamma$ cross section is obtained

from the observed number of events $N_{\rm obs}$, after subtracting the residual background $N_{\rm bkg}$ and dividing for the selection efficiency ($\varepsilon(s_\mu)$) and luminosity (L), as:

$$\frac{{\rm d}\sigma_{\mu\mu\gamma}}{{\rm d}s_\mu}=\frac{N_{\rm obs}-N_{\rm bkg}}{\Delta s_\mu}\frac{1}{\varepsilon(s_\mu)L} \quad (6)$$

The result of the measured $\mu\mu\gamma$ cross section was compared with the QED calculations to NLO made by the MC code Phokhara[5] and a very good agreement was found within the quoted systematic uncertainties[7-8].

Then, the bare cross section $\sigma^0_{\pi\pi(\gamma)}$ (inclusive of FSR, with VP effects removed) is obtained from the bin-by-bin ratio of the $\pi\pi\gamma$ and $\mu\mu\gamma$ differential cross sections described above. This cross section is used in the dispersion integral to compute $\Delta^{\pi\pi}a_\mu$. The pion form factor $|F_\pi|^2$ is then calculated using Eq. (4).

Eq. (3) gives $\Delta^{\pi\pi}a_\mu=(385.1\pm1.1_{\rm stat}\pm2.6_{\rm sys}\pm0.8_{\rm th})\times10^{-10}$ in the interval $0.35\ {\rm GeV}^2<M^2_{\pi\pi}<0.95\ {\rm GeV}^2$. For each bin contributing to the integral, statistical errors are combined in quadrature and systematic errors are added linearly.

3 Comparison between the KLOE measurements and the results from other experiments

Comparing the results of the KLOE12 and KLOE08 analyses it is possible to see that they are in good agreement, in particular, in the ρ mass region (see Fig. 3). Since the KLOE12 result on the pion form factor was determined using the ratio of the dipion and dimuon cross sections, measured with the same data set, the radiator H function is not used, the luminosity of the sample cancels out and the acceptance corrections compensate, resulting in an almost negligible systematic error[7-8]. Fig. 4 shows the comparison between the $|F_\pi|^2$ distribution obtained in the KLOE12 and KLOE10 measurements, requiring the ISR photon to be reconstructed at an large angle, inside the EMC barrel. They are obtained from independent data sets under different running conditions ($W=M_\phi$ KLOE12, $W=1$ GeV KLOE10), and also with a different selection method, which implies independent systematic uncertainties. The two measurements are in very good agreement.

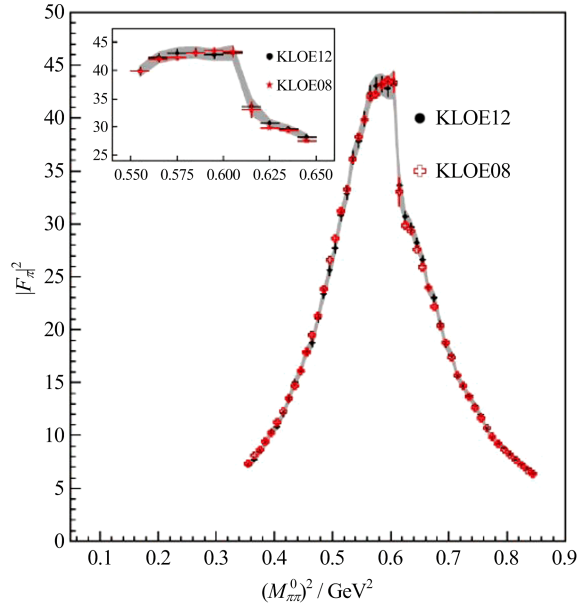

Fig. 3 Comparison of the KLOE12 measurement with the KLOE8 measurement

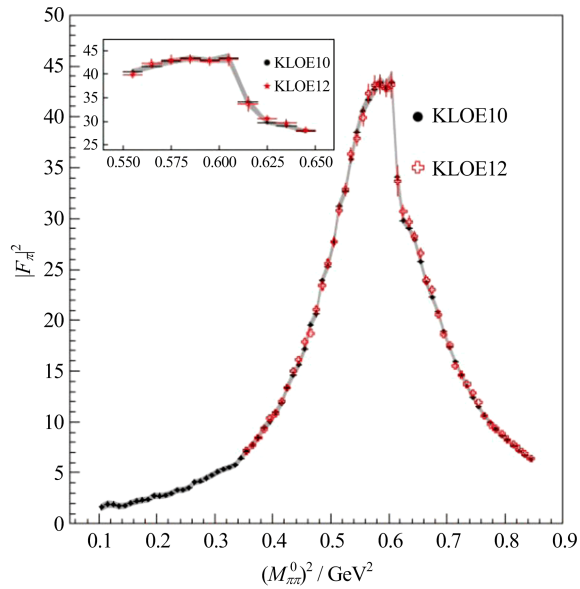

Fig. 4 Comparison of the KLOE12 measurement with the KLOE10 measurement

In Figs. 5 and 6, the KLOE12 result is compared, respectively, with the result from the BaBar experiment at SLAC[10] which uses the ISR method and the results obtained from the energy

scan experiments CMD-2[11-12] and SND[13] in Novosibirsk. Whenever several data points fall in one KLOE bin of 0.01 GeV^2, the values are statistically averaged.

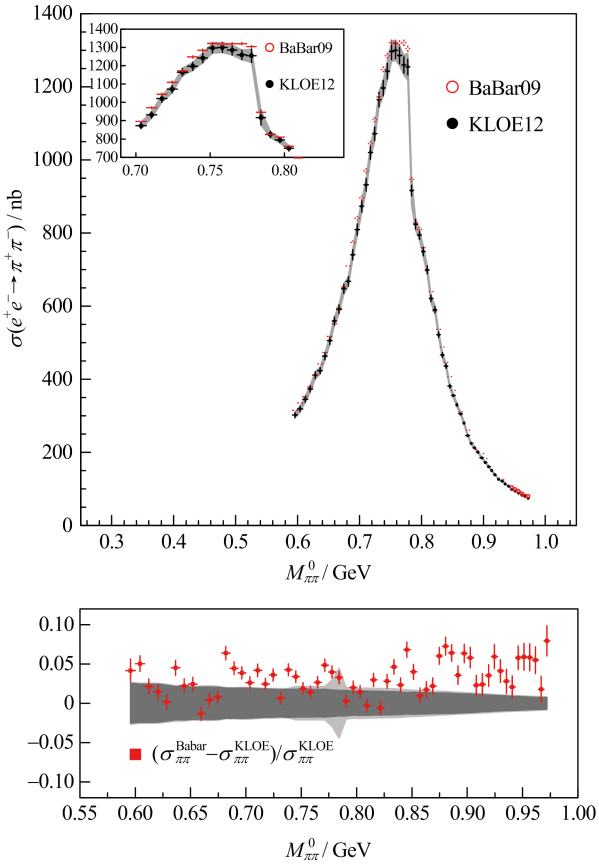

Fig. 5 $|F_\pi|^2$ **from the BaBar experiment**[10] **compared with the KLOE12 result**

The preliminary combination of the last three KLOE results (KLOE08, KLOE10, KLOE12)[14] is obtained using the Best Linear Unbiased Estimate (BLUE) method[15-16]. The following $a^\mu_{\pi\pi}$ values are found:

$a^\mu_{\pi\pi}(0.1\sim0.95\ \text{GeV}^2)=(487.8\pm5.7)\times10^{-10}$,

$a^\mu_{\pi\pi}(0.1\sim0.85\ \text{GeV}^2)=(378.1\pm2.8)\times10^{-10}$.

The combined measurement of the $|F_\pi|^2$ has also been fitted using the Gounaris-Sakurai (GS) model[17] (see Fig. 7). In the table of Fig. 7 preliminary fit results are reported. Only the statistical error is reported in the fit. The determination of the ω-meson mass parameter is very close to the current PDG value ($M_\omega^{\rm KLOE}=782.7\pm0.2_{\rm stat}$; PDG $M_\omega^{\rm PDG}=782.65\pm0.12$),

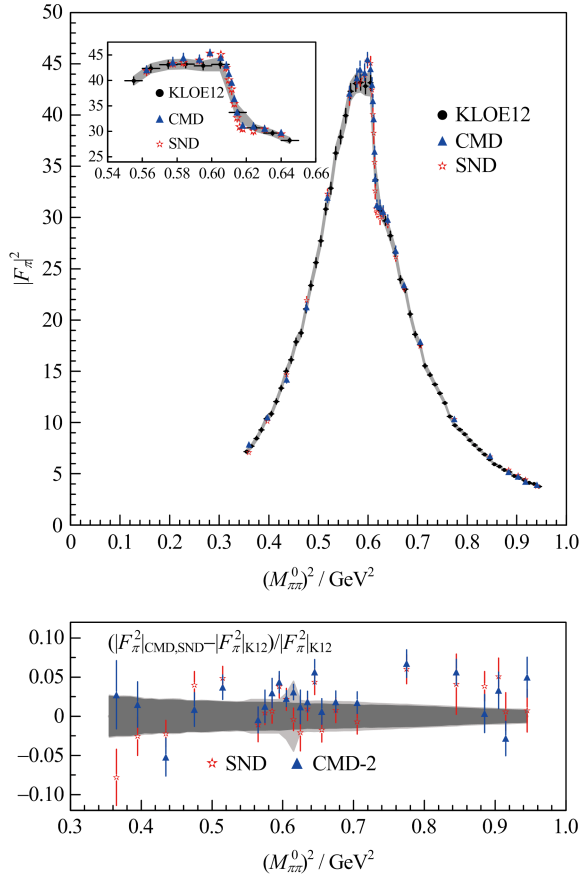

Fig. 6 $|F_\pi|^2$ **from CMD-2**[11-12]**, SND**[13] **experiments compared with the KLOE12 result**

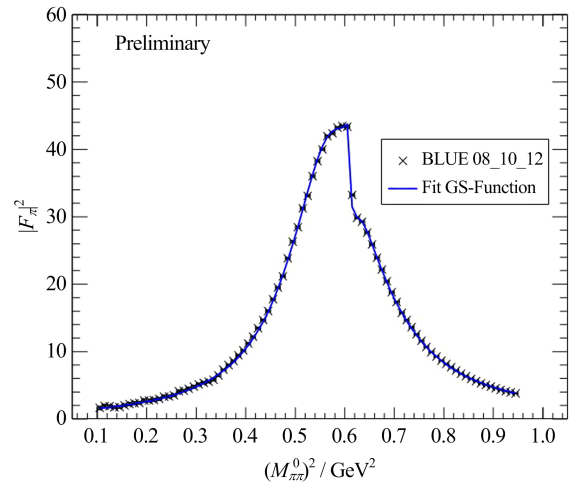

Fig. 7 Preliminary fit to the combination of the last three KLOE results (KLOE08, KLOE10, KLOE12) on the $|F_\pi|^2$

demonstrating the accuracy of the track momentum reconstruction of the KLOE detector. We expect that including also the systematic error in the fit the discrepancy with the PDG should reduce.

Tab. 1 Parameters obtained from the fit

Parameters(G-S)	KLOE(PDG)
M_ρ/MeV	774.3±0.1$_{stat}$(775.49±0.34)
Γ_ρ/MeV	146.9±0.2$_{stat}$(149.1±0.8)
M_ω/MeV	782.7±0.2$_{stat}$(782.65±0.12)
Γ_ω/MeV	7.0±0.4$_{stat}$(8.49±0.08)
$\alpha/10^{-3}$	1.45±0.04$_{stat}$
$\beta/10^{-3}$	−83.1±0.6$_{stat}$
δ/(°)	10.2±1.7$_{stat}$
χ^2/n.d.f	221.4/82(2.7)

4 Conclusion

During the last 10 years KLOE has performed a series of precision measurements using the Initial State Radiation process. The preliminary combined measurement of the last analysis (KLOE12) with two previously published results (KLOE08, KLOE10), with the corresponding fit using the GS parametrization, has been presented. The result confirms the current discrepancy ($\sim 3\sigma$) between the Standard Model (SM) calculation and the experimental value of the muon anomaly a_μ.

References

[1] JEGERLEHNER F, NYFFELER A. The muon $g-2$ [J]. Phys Rep, 2009,477(1/2/3):1-110.

[2] BRODSKY S J, DE RAFAEL E. Suggested boson-lepton pair couplings and the anomalous magnetic moment of the muon[J]. Phys Rev, 1968, 168(5): 1 620-1 622.

[3] ADINOLFI M, AMBROSINO F, ANDRYAKOV A, et al. The tracking detector of the KLOE experiment [J]. Nucl Instrum Meth A, 2002, 488(1/2):51-73.

[4] ADINOL M, AMBROSINO F, ANTONELLI A, et al. The KLOE electromagnetic calorimeter[J]. Nucl Instrum Meth A,2002,482(1/2):364-386.

[5] CZYŻ H, GRZELIŃSKA A, KÜHN J H, et al. Radiative return at Φ- and B-factories: FSR for muon pair production at next-to-leading order[J]. Eur Phys J C,2005,39:411-420.

[6] AMBROSINO F, ANTONELLI A, ANTONELLI M, et al. Measurement of $\sigma(e^+e^-\to\pi^+\pi^-\gamma(\gamma))$ and the dipion contribution to the muon anomaly with the KLOE detector[J]. Phys Lett B, 2009, 670(4/5): 285-291.

[7] BABUSCI D, BADONI D, BALWIERZ-PYTKO I, et al. Precision measurement of $\sigma(e^+e^-\to\pi^+\pi^-\gamma)/\sigma(e^+e^-\to\mu^+\mu^-\gamma)$ and determination of the $\pi^+\pi^-$ contribution to the muon anomaly with the KLOE detector[J]. Physics Letters B, 2013, 720(4/5): 336-343.

[8] AMBROSINO F, ARCHILLI F, BELTRAME P, et al. Measurement of $\sigma(e^+e^-\to\pi^+\pi^-)$ from threshold to 0.85 GeV^2 using initial state radiation with the KLOE detector[J]. Physics Letters B, 2011, 700(2): 102-110.

[9] LAUTRUP B E, PETERMAN A, DE RAFAEL E. On sixth-order radiative corrections to $a_\mu - a_e$[J]. Nuovo Cim A,1971,1(2):238-242.

[10] AUBERT B, KARYOTAKIS Y, LEES J P, et al. Precise Measurement of the $e^+e^-\to\pi^+\pi^-(\gamma)$ cross section with the initial state radiation method at BABAR[J]. Phys Rev Lett,2009,103:231801.

[11] AKHMETSHIN R R, AULCHENKO V M, BANZAROV V Sh, et al. High-statistics measurement of the pion form factor in the ρ-meson energy range with the CMD-2 detector[J]. Phys Lett B, 2007, 648(1):28-38.

[12] AUL'CHENKO V M, AKHMETSHIN R R, BANZAROV V Sh, et al. Measurement of the $e^+e^-\to\pi^+\pi^-$ cross section with the CMD-2 detector in the 370 ~520 MeV energy range[J]. JETP Lett,2006, 84(8): 413-417.

[13] ACHASOV M N, BELOBORODOV K I, BERDYUGIN A V, et al. Update of the $e^+e^-\to\pi^+\pi^-$ cross section measured by the spherical neutral detector in the energy region $400<\sqrt{s}<1\,000$ MeV[J]. J Exp Theor Phys, 2006,103(3):380-384.

[14] VAN DER BIJ J J, CZYŻ H, EIDELMAN S, et al. Mini-Proceedings of the 15th meeting of the Working Group on Rad. Corrections and MC Generators for Low Energies[EB/OL]. (2014-06-18)[2015-11-30]. http://arxiv.org/abs/1406.4639.

[15] VALASSI A. Combining correlated measurements of several different physical quantities [J]. Nucl Instrum Meth A, 2003,500:391-405.

[16] D'AGOSTINI G. On the use of the covariance matrix to fit correlated data [J]. Nucl Instrum Meth A,1994, 346:306-311.

[17] SAKURAI G J, SAKURAI J J. Finite-width corrections to the vector-meson-dominance prediction for $\rho\to e^+e^-$[J]. Phys Rev Lett, 1968,21:244.

第46卷第4期 中国科学技术大学学报 Vol. 46, No. 4
2016年4月 JOURNAL OF UNIVERSITY OF SCIENCE AND TECHNOLOGY OF CHINA Apr. 2016

Article ID:0253-2778(2016)04-0292-09

Status of R Scan at BESIII

LI Yingtian[1,2], HU Haiming[2] (for the BESIII Collaboration)

(1. *Soochow University*, *Suzhou* 215006, *China*; 2. *Institute of High Energy Physics*, *CAS*, *Beijing* 100049, *China*)

Abstract: The data samples for the measurement of R values, hadron form factors, the line-shape scan of the high mass charmonium family and new states have been taken in the full energy region that BEPCII can reach, namely between 2.0 and 4.6 GeV. The present status of R value measurement is briefly reviewed.

Key words: R value measurement; the Standard Model; data analysis; Monte Carlo simulation

CLC number: O572.3 **Document code**: A doi:10.3969/j.issn.0253-2778.2016.04.006

Citation: LI Yingtian, HU Haiming. Status of R Scan at BESIII[J]. Journal of University of Science and Technology of China, 2016, 46(4): 292-300, 307.

BESIII R 值扫描测量进展

李应天[1,2], 胡海明[2] (BESIII 合作组)

(1. 苏州大学, 江苏苏州 215006; 2. 中国科学院高能物理研究所, 北京 100049)

摘要: BESIII 在 BEPCII 所能达到的能量范围(2.0～4.6 GeV)获取了 3 批实验数据, 用于 R 值、强子形状因子、重粲偶素共振结构及新粒子态的测量. 本文对目前 R 值测量的主要工作及进展作了简要评述.

关键词: R 值测量; 标准模型; 数据分析; 蒙特卡罗模拟

0 Introduction

R value is defined as the ratio of the hadronic production cross section via the electron and positron annihilation to that of the theoretical cross section of $\mu^+\mu^-$ at the Born level,

$$R=\frac{\sigma^0(e^+e^-\to\gamma^*\to\text{hadrons})}{\sigma^0(e^+e^-\to\gamma^*\to\mu^+\mu^-)} \quad (1)$$

The R value is an important input parameter for testing the Standard Model (SM). The precision of R values has a significant influence on the uncertainties of calculations of QED running electromagnetic coupling constant $\alpha(s)$, muon anomalous magnetic moment $(g-2)$, global fit of the Higgs mass in SM[1-3]. In the calculations, R values adopt experimental results below 5 GeV, and the pQCD prediction was used in the higher energy region.

When we look over the PDG published in different years, we may find that R values have been measured by many groups from the hadronic threshold to Z^0 scale. With the increase of the luminosity of the e^+e^- colliders, more data samples with larger statistics have been

Received: 2015-11-30; **Revised**: 2016-04-20

Foundation item: Supported by National Natural Science Foundation of China (11335008, 10979095, 11275211).

Biography: LI Yingtian, male, born in 1988, master. Research field: experimental high energy physics. E-mail: liyt@ihep.ac.cn

Corresponding author: HU Haiming, PhD/Prof. E-mail: huhm@ihep.ac.cn

accumulated, and in pace with the improvement of experimental methods, the precision of the R values has been evidently improved. Fig. 1 shows the current world data of R values from $2m_\pi$ to 110 GeV in PDG2014[4].

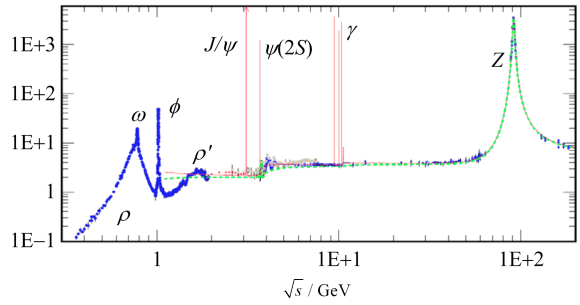

Fig. 1 The R values from $2m_\pi$ to Z^0 scale in PDG2014

BES Collaboration has performed three rounds of R value measurements using the data samples taken with BESII at BEPC[5-7], the results were shown in Fig. 2. The first and second rounds of measurements performed the R value scan at about 100 energy ponits between 2 ~ 5 GeV and took small data samples (only about 1 000 hadronic events collected at per energy point), and the relative precision of R values was reduced from over 15% in earlier experiments[8-14] to 7%. The third round of measurement of R values used larger data samples at three energy points (E_{cm} = 2.65, 3.07 and 3.65 GeV, the numbers of hadronic events were about 24 000, 34 000 and 84 000, respectively), and the results reached a better precision of about 3.5%. Theorists used R values measured with BESII data in the calculation of $\Delta\alpha^{(5)}_{\rm had}$ in the running electromagnetic coupling constant $\alpha(s) = 1/[1 - \Delta\alpha(s)]$, the relative uncertainty contribution resulting from the errors of R values between 2~5 GeV decreased to 35% from earlier 55%, and the relative uncertainty of $a_\mu^{\rm had}$ in $(g-2)$ was reduced to about 15% from an earlier 25%[1-3].

In the energy region above the open charm threshold, there exist several high-mass ψ-family charmonium resonances ($\psi(3770)$, $\psi(4040)$, $\psi(4190)$, $\psi(4415)$) with quantum number $J^{PC} = 1^{--}$ which were well confirmed in earlier

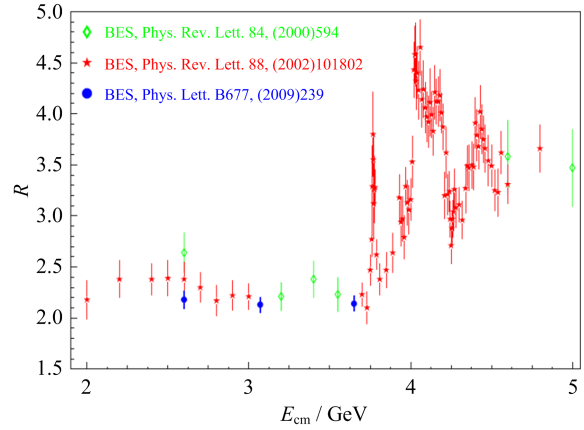

Fig. 2 The summarization R value scan with BEPC/BESII

experiments (see the references cited in Ref. [15] for details) and the newly discovered states $X(4260)$ and $X(4360)$, which can be produced directly in the $e^\pm$ annihilation. Based on the work presented in Ref. [6], the line shape and resonant parameters of $\psi(3770)$, $\psi(4040)$, $\psi(4190)$ and $\psi(4415)$ were measured[15]. Fig. 3 shows the measured R values and the fitted line-shape of these resonances. But because the small statistics and larger scan step, the broad structure in the $\pi^+\pi^- J/\psi$, called $Y(4260)$, discovered by BABAR[16], was missed in BESII scan.

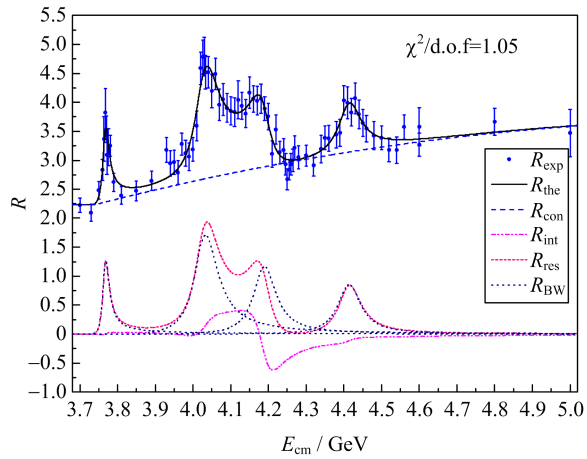

Fig. 3 The R scan of the high mass charmonium line-shape at BEPC/BESII

In the measurement of resonance parameters with BESII scan data, the fitting method was improved compared with earlier measurements (see the references cited in Ref. [15]) in the following aspects: ① intrinsic/effective initial phase angle in

Breit-Wigner amplitude was kept; ② interference terms between final states decayed from heavy ψ-family resonances were considered; ③ energy dependence of the total widths were calculated; ④ as the measurements of R values and resonant parameters are closely related and affected, they were measured using the iterative method, so that the R values and resonant parameters were updated simultaneously[15]. But due to the very small data statistics, some important information (such as, the selected numbers of various DD final states in $\psi(3770)$, $\psi(4040)$, $\psi(4160)$ and $\psi(4415)$ decay) are very limited, and so the accurate expression of the interference terms can not be obtained from the data analysis, and some approximations on model describing energy dependent widthes had to be taken.

BEPCII is a double-ring e^+e^- collider running at center-of-mass energies between 2.0 and 4.6 GeV and reaches a peak luminosity of 0.85×10^{33} $cm^{-2}\cdot s^{-1}$ at center-of-mass energy of 3770 MeV. The BESIII detector is located at the BEPCII[17], designed to fulfill the requirement of the τ-charm physics experiments[18]. Since the luminosity of BEPCII is about 100 times of that of BEPC, and BESIII performs much better than BESII, one may expect that R value measurement with data taken with BESIII may reach a better precision than that of BESII, and then the calculations of $\Delta\alpha(s)$ and $a_\mu^{\rm had}$ will have less uncertainties, and the SM prediction can get more better test.

1 Data samples of R scan

BESIII Collaboration made a comprehensive plan for R value measurement and QCD experimental study, and the main objects are as follows: the measurement of R values reaches a precision about 3%; the fit of the line-shape of high mass charmonium and resonance parameters, form factors of mesons and baryons get significant improvement. The whole data taking plan was divided into three phases.

1.1 Phase Ⅰ

The purpose of this phase is for machine study and prestudy of data analysis. The data samples were taken at 2.232 4, 2.4, 2.8 and 3.4 GeV with a total luminosity of about 12 pb^{-1} in 2012. Based on the obtained information, the next R scan plan was optimized and the time needed for the following data taking was estimated. These data can be used for the parameter tuning of the hadronic generator LUARLW[19], and the measurement of R values and the form factors of some hadronic channels with large production cross section.

1.2 Phase Ⅱ

It is a fine scan between 3.85 and 4.59 GeV for the measurement of R values and high mass charmonium line-shape and resonant parameters. Drawing on the experience of R scans at BESII[6], the data samples collected at 104 energy points with more reasonable energy arrangement and relative smaller step-size (2～5 MeV), the total luminosity is about 800 pb^{-1}, while 4 times of J/ψ fast scan was done for the beam energy calibration. The data samples at each energy point at least contains 10^5 hadronic events, so that the cross section of all $\overline{DD}$ final sates can be measured and the shortcoming in the BESII measurement can be overcome. Fig. 4 shows the online cross section at scan energy points.

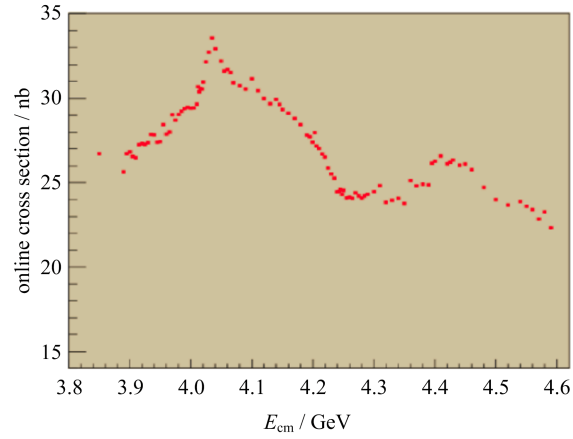

Fig. 4 The online cross section of the R scan with BESIII

1.3 Phase Ⅲ

BESIII collected the data samples at 22 energy points between 2.0 and 3.08 GeV with the total luminosity being about 500 pb^{-1}. Moreover, J/ψ fast scan was done three times for beam energy calibration, and separated beam samples were collected for the study of beam associated backgrounds. These data samples are used for the measurement of R values, meson and baryon and hyperon form factors, and the study of threshold effects of Λ, Σ, Ξ, etc.

2 Status of R value measurement

In the experiment, R value is measured with the following expression

$$R_{\rm exp}=\frac{N_{\rm had}^{\rm obs}-N_{\rm bg}}{\sigma_{l^+l^-}^0 L\varepsilon_{\rm trg}\bar{\varepsilon}_{\rm had}(1+\delta)} \qquad (2)$$

the meanings of all these quantities in above formula having been explained in Refs. [5-7]. So the work of R value measurement is, in fact, to determine these quantities from data analysis and Mont Carlo simulations and give their errors.

2.1 Data analysis

The tree level Feynman diagrams of the physical processes produced in e^+e^- collision in BEPCII energy region can be summarized into 5 types as shown in Fig. 5. Data analysis is the most basic work for R value measurement, consisting of luminosity measurement, background subtraction and selection of hadronic events.

The luminosity of the data samples can be measured by the processes of $e^+e^-\to e^+e^-$ or $\gamma\gamma$. These two QED processes are well understood in physics, and the precision of the corresponding BABAYAGA reaches 0.5%. The signal events of e^+e^- and $\gamma\gamma$ have very clear characteristics in the detector and can be well selected, and the remaining backgrounds are very limited. The error of luminosity measurements is about 1%[21].

The scheme of hadronic events selection is similar to that used in works[5-7] but optimized[22]. The hadronic event selection can be classified into track level and event level, which use the information of MDC, EMC, and TOF. The combined error of event selection and MC is estimated by the ratio $\Delta(N_{\rm had}^{\rm obs}/\bar{\varepsilon}_{\rm had})$ as in Ref. [7], the relative errors are preliminarily estimated as about 2.5%~3.0% dependent on energies.

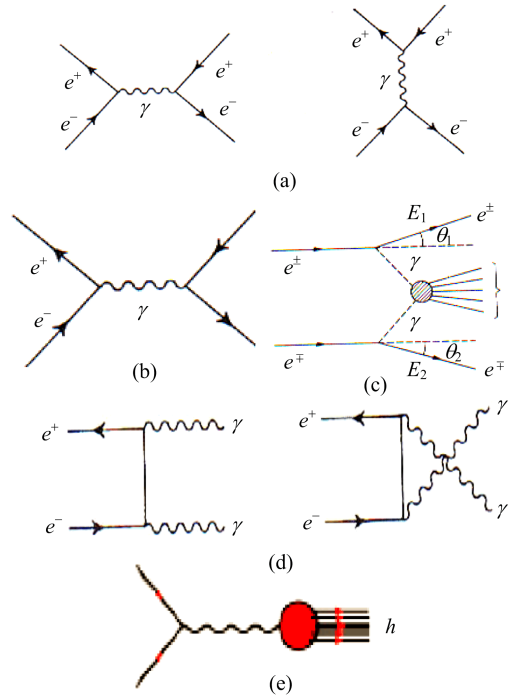

Fig. 5 The physics processes in e^+e^- collision: (a) Bhabha; (b) $\mu^+\mu^-$ and $\tau^+\tau^-$; (c) two photons; (d) $\gamma\gamma$; (e) hadrons.

The numbers of the residual QED background events, $N_{\rm bg}$ in Eq. (2), are determined employing the MC method,

$$N_{\rm bg}=L[\varepsilon_{ee}\sigma_{ee}+\varepsilon_{l^+l^-}\sigma_{l^+l^-}+\varepsilon_{\tau\tau}\sigma_{\tau\tau}+\varepsilon_{\gamma\gamma}\sigma_{\gamma\gamma}] \qquad (3)$$

where L is the integrated luminosity of data, σ_{ee} the cross section of Bhabha process, ε_{ee} the efficiency for Bhabha events that pass the hadronic event selection criteria, other symbols have corresponding meanings. The values of ε_{ee} and $\varepsilon_{l^+l^-}$ are about 5×10^{-4}, and $\varepsilon_{\tau\tau}$ smaller than 5% depending on the difference between energy point and threshold of $\tau^+\tau^-$. The amount of background from $e^+e^-\to e^+e^-X$ is smaller than 1% of $N_{\rm bg}$.

2.2 Generator LUARLW

The general picture of electron-positron annihilation and hadrons production are shown in Fig. 6. The nonperturbative hadronization can be

described by the phenomenological model. In R value measurement the Lund area law generator LUARLW[26] is used for determining the hadronic efficiency. LUARLW contains the following constitutes: initial state radiation (ISR), string fragmentation, multiplicity and momentum-energy distributions, decay of unstable hadrons.

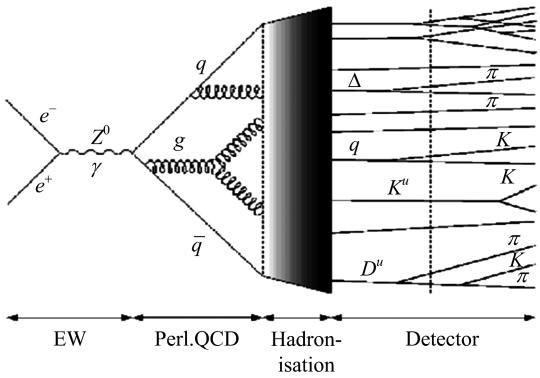

Fig. 6 The picture of e^+ e^- annihilation into hadrons

In the simulation of ISR return processes, the sampling of the effective center-of-mass energy E'_{cm} for a hadronic event can be obtained by the differential cross section[23-25], or the equivalent accumulative cross section, which are shown in Fig. 7.

There are some phenomenological parameters in LUARLW. In the BEPC energy, the main parameters are those which determine the ratios of mesons and baryons with different quantum numbers (s, L, J) in the string fragmentation process. In LUARLW these parameters are stored in array PARJ(1－20) as in JETSET[28], their default values were set with the values from fitting the data measured with DELPHI at LEP[20]. Fig. 8 shows the mesons (M) and baryons (B and $\bar{B}$) produced at the vertex of the light-cone area in the string fragmentation. The values of PARJ(1－20) are tuned to make the MC agree with the experimental data taken with BESIII.

Starting from the Lund area law, one may obtain an approximation expression of a poisson-like multiplicity distribution for the preliminary fragmentation hadrons[26]

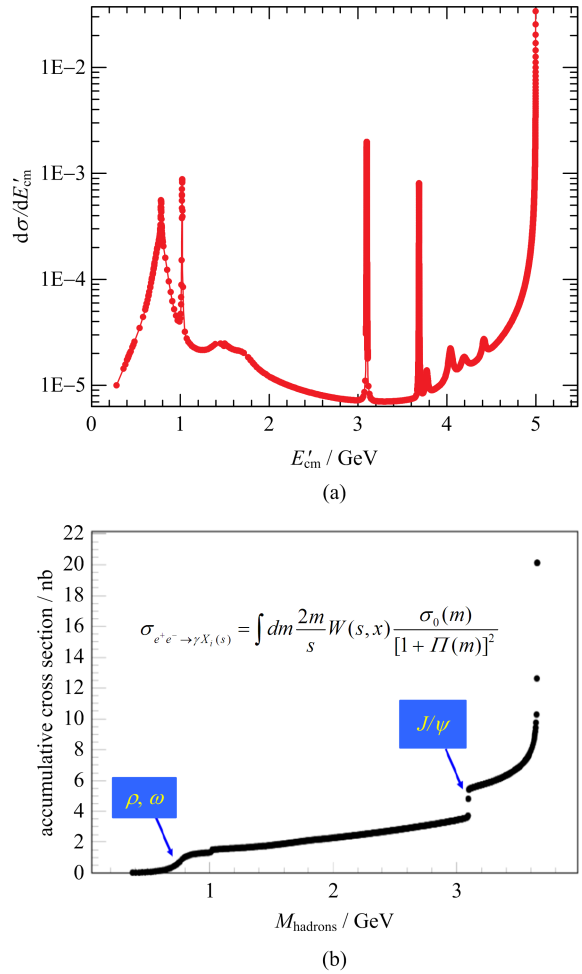

Fig. 7 (a) The differential cross section of ISR return process at E_{cm} =5 GeV (in any scale); (b) the accumulative cross section at E_{cm} =3.65 GeV

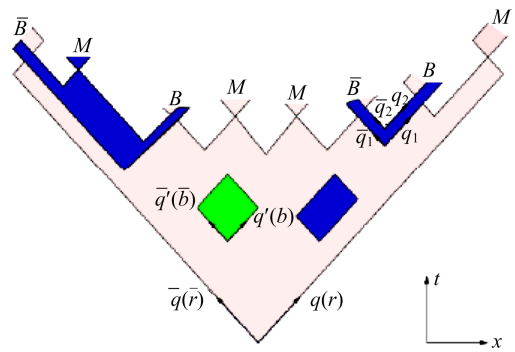

Fig. 8 The mesons and baryons production in the string fragmentation. M means meson, and B means baryon

$$P_n(s) = \frac{\mu^n}{n!}\exp[c_0 + c_1(n-\mu) + c_2(n-\mu)^2] \quad (4)$$

where n is the number of the fragmentation

hadrons, μ can be understood as the average multiplicity. The energy dependence of μ can approximately quote the QCD prediction

$$\mu = \alpha + \beta\exp(\gamma\sqrt{s}) \tag{5}$$

where c_1, c_2, c_3, α, β and γ are free parameters and need to be tuned.

The simulations of the continuum states include lowest and leading order QCD correction

$$e^+e^- \to \gamma^* \to \begin{cases} q\bar{q} \to \text{string} \to \text{hadrons} \\ gq\bar{q} \to 2\text{strings} \to \text{hadrons} \end{cases}$$

The vector mesons whose masses are smaller than 2 GeV and with $J^{PC}=1^{--}$ can directly couple to the virtual photon in the ISR return process

$$e^+e^- \to \gamma^* \to \rho(770), \omega(782), \phi(1020) \cdots \rho(1700) \tag{6}$$

The production and decay of the charmonium adopt the standard pictures[27]. For example, the simulation of J/ψ contain following channels

$$e^+e^- \to \gamma^* \to J/\psi \to \begin{cases} \gamma^* \to e^+e^-, \mu^+\mu^- \\ \gamma^* \to q\bar{q} \to \text{string} \to \text{hadrons} \\ ggg \to 3\text{strings} \to \text{hadrons} \\ \gamma gg \to 2\text{strings} \to \text{hadrons} \\ \gamma\eta_c \to gg \to 2\text{strings} \to \text{hadrons} \\ \gamma + \text{radiative decay channels.} \end{cases}$$

The simulations for $\psi(3686)$, $\psi(3770)$, $\psi(4040)$, $\psi(4190)$ and $\psi(4415)$ are similar.

The cross section for a chosen exclusive process $e^+e^- \to q\bar{q}(g) \to \text{string(s)} \to m_1 + m_2 \cdots + m_n$ can be factorized as

$$\mathrm{d}\sigma(s) = \mathrm{d}\sigma(e^+e^- \to q\bar{q}) \cdot \mathrm{d}\mathscr{P}(q\bar{q} \to m_1, m_2 \cdots m_n; s) \tag{7}$$

The $\mathrm{d}\sigma(e^+e^- \to q\bar{q})$ is the QED cross section, $d\mathscr{P}$ is the probability for string fragmentation into n hadrons and the energy-momentum distributions of the fragmentation hadrons are determined by Lund area law[26].

2.3 Parameter tuning of LUARLW

Two schemes used for parameter tuning and optimization will be described below.

2.3.1 Scheme A: ConExc+LUARLW

The red points in Fig. 9 show the sum of cross sections of the measured exclusive processes, and the black points the total cross sections measured inclusively. The differences between them show that only parts of the exclusive processes were measured above 2 GeV.

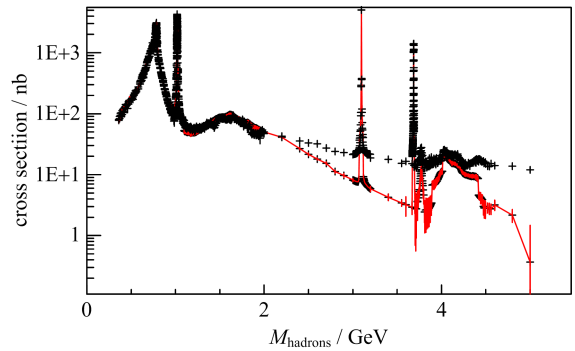

The black points are the total cross section measured in inclusive method, and the red points are the sum of the measured exclusive cross sections.

Fig. 9 The Born cross section of $e^+e^-\to$ hadrons below 5 GeV

We have a hadronic generator ConExc + LUARLW. The simulations for the measured processes adopt the exclusive way, the weights of events are proportional to the corresponding cross sections, and the momentums of the hadrons are determined by the phase-space method for multi-hadrons states and the specific angular distributions for two-hadrons states. But the remaining unmeasured or unknown processes will be generated via LUARLW in an inclusive way.

Choose m important parameters to be tuned, assume that their optimal values can be obtained by fitting the distributions of the final state observables x. In order to make the fit effective, the distributions of x should be sensitive to those chosen parameters. Parameter tuning is an iterative process. At the beginning, the default values are used as the initial values. Let $\boldsymbol{p}$ denote the parameters vector with m components, and change the chosen parameters around the initial value $\boldsymbol{p}_0$ by $\delta\boldsymbol{p}$, then the final state distributions for each bin of each distribution can be expressed as the functions of the parameters[20]

$$f(\boldsymbol{p}_0+\delta\boldsymbol{p},x)=$$

$$a_0^{(0)}(x)+\sum_{i=1}^{m}a_i^{(1)}(x)\delta p_i+\sum_{i,j=1}^{m}a_{ij}^{(2)}\delta p_i\delta p_j \quad (8)$$

$$\approx M(\boldsymbol{p}_0+\delta\boldsymbol{p},x) \quad (9)$$

The fit is equivalent to solving a system of linear equations

$$F\cdot\boldsymbol{a}(x)=\boldsymbol{M}(x) \quad (10)$$

where $\boldsymbol{M}(x)$ is the vector of model predictions corresponding to the vector of parameters $\boldsymbol{p}_0+\delta\boldsymbol{p}$, $\boldsymbol{a}(x)$ the vector of coefficients $a_{i(j)}^{(k)}(x)$, F the matrix containing parameter variations. The effective tuning should choose those parameters which are sensitive to the distributions of $\boldsymbol{M}(x)$. The sensitivity can be quantified as

$$S_i(x)=\frac{\delta M(x)}{M(x)}\Big/\frac{\delta p_i}{p_i},\ i=1,\cdots,m) \quad (11)$$

For the purpose of R value measurement, sensitive distributions may be charged and photon multiplicities, momentum of charged particles, polar angle cos θ, meson and baryon ratio, momentum, etc.

2.3.2 Scheme B: Pure LUARLW

In scheme A, the generated number of MC samples increases rapidly with the number of the chosen parameters to be tuned. In practice, an acceptable number of parameters to be tuned is around 10. In the model, every parameter has a specific function and can not be replaced by others. Therefore the number of parameters in need of tuning is much larger than 10. In fact, any number of parameters can be tuned manually, as long as its tuning can improve the MC simulations. At last, the fit method in scheme A was used to optimize them further.

2.3.3. Comparisons between data and MC

If the event generator is correct and the detector simulation is real, a good parameter set should make MC agree well with data for most of the distributions, especially for those which are sensitive to hadronic efficiency, such as charged and neutral multiplicities, cos θ, momentum. Fig. 10 and Fig. 11 show the comparisons between data and MC for some selected distributions. The differences mean further tuning is needed.

3 Conclusion

The three-phase data collection plan has been

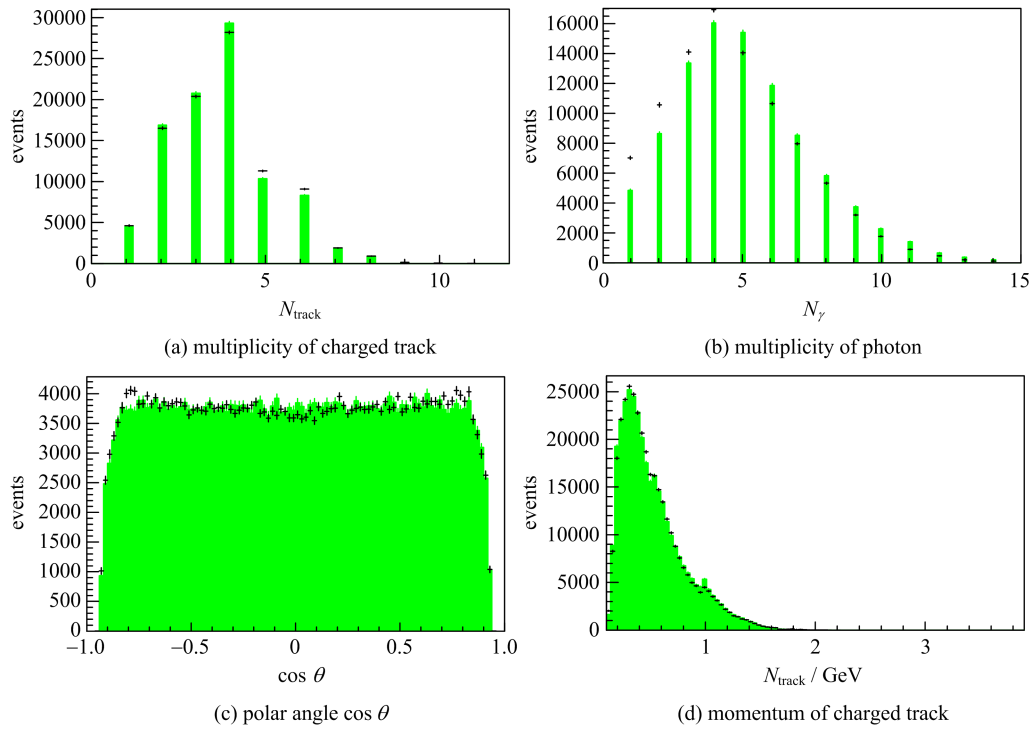

(a) multiplicity of charged track

(b) multiplicity of photon

(c) polar angle cos θ

(d) momentum of charged track

Fig. 10 Comparison between data and MC in scheme A at 3.65 GeV

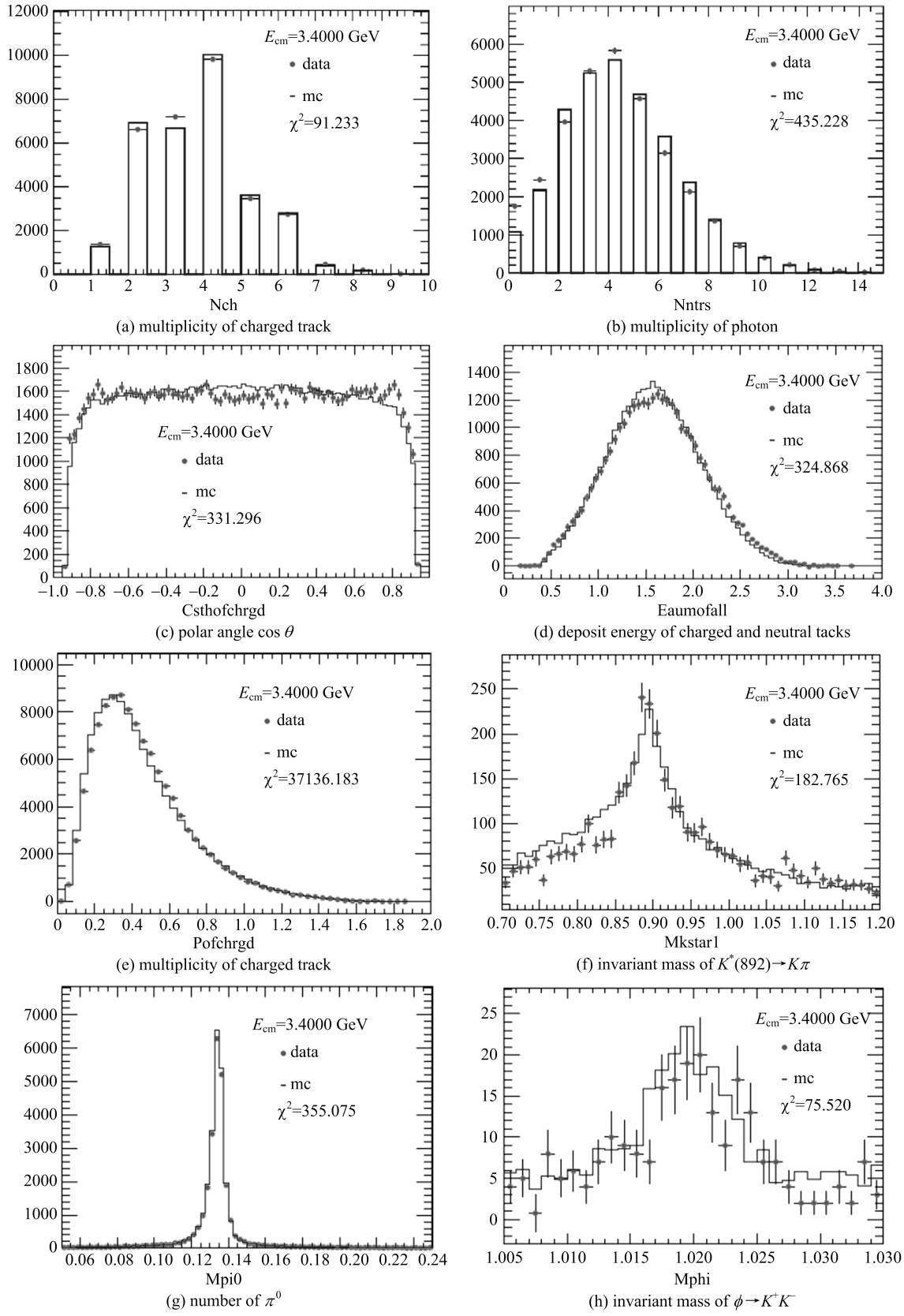

Fig. 11 Comparison between data and MC in scheme B at 3.400 GeV

carried out, and the data analysis is almost finished. Parameter tuning still remains a challenging task, which will continue to be done till the MC agrees well with data and the errors of hadronic efficiency reaches an acceptable level, for example, 2%, and the total error of R values is reduced to 3%.

References

[1] PIETRZYK B. Tests of the standard model and $\alpha(m_Z^2)$ [J]. Nucl Phys B (Proc Suppl), 2006, 162: 18-21.

[2] JEGERLEHNER F. Precision measurements of σ_{hadronic} for $\alpha_{\text{eff}}(E)$ at ILC energies and $(g-2)_\mu$[J]. Nucl Phys B (Proc Suppl), 2006, 162: 22-32.

[3] JEGERLEHNER F. Hadronic contributions to the photon vacuum polarization and their role in precision physics[EB/OL]. (2002-12-09)[2015-11-30]. http://arxiv.org/abs/hep-ph/0104304.

[4] OLIVE K A, AGASHE K, AMSLER C, et al. Review of particle physics [J]. Chin Phys C, 2014, 38(09): 090001.

[5] BAI J Z, BAN Y, BIAN J G, el al. Measurement of the total cross section for hadronic production by e^+e^- annihilation at energies between 2.6～5 GeV[J]. Phys Rev Lett, 2000, 84: 594-597.

[6] BAI J Z, BAN Y, BIAN J G, el al. Measurements of the cross section for $e^+e^-\rightarrow$hadrons at center-of-mass energies from 2 to 5 GeV[J]. Phys Rev Lett, 2002, 88: 101802.

[7] ABLIKIM M, BAI J Z, BAI Y, el al. R value measurements for e^+e^- annihilation at 2.60, 3.07 and 3.65 GeV[J]. Phys Lett B, 2009, 677: 239-245.

[8] CERADINI F, CONVERSI M, D'ANGELO S, et al. Multihadron production in e^+e^- collisions up to 3 GeV total C. M. energy[J]. Phys Lett B, 1973, 47: 80-84.

[9] BACCI C, PENSO G, SALVINI G, et al. Multihadronic cross sections from e^+e^- annihilation up to 3 GeV c. m. energy[J]. Phys Lett B, 1973, 44: 533-536.

[10] BATOLI B, FELICETTI F, OGREN H, et al. Electron-positron interactions at high energies [J]. Phys Rev D, 1972, 6: 2 374-2 404.

[11] BERNADINI M, BOLLINI D, BRUNINI P L, et al. The energy dependence of $\sigma(e^+e^-\rightarrow$hadrons) in the total centre-of-mass energy range 1.2 to 3.0 GeV[J]. Phys Lett B, 1974, 51: 200-204.

[12] COSME G, JEAN-MARIE B, JULLIAN S, et al. Hadronic production by e^+e^- collisions at the energy 990 MeV with the Orsay storage ring[J]. Phys Lett B, 1972, 40: 685-688.

[13] KURDADZE L M, ONUCHIN A P, SEREDNYAKOV S I, et al. Observation of multihadronic events in e^+e^- collisions at the energy of 1.18～1.34 GeV[J]. Phys Lett B, 1972, 42: 515-518.

[14] LITKE A, HANSON G, HOFMANN A, et al. Hadron production by electron-positron annihilation at 4 GeV center-of-mass energy [J]. Phys Rev Lett, 1973, 30: 1 189-1 192;1 349.

[15] ABLIKIM M, BAI J Z, BAN Y, et al. Determination of the $\psi(3770)$, $\psi(4040)$, $\psi(4160)$ *and* $\psi(4415)$ resonance parameters[J]. Phys Lett B, 2008, 660: 315-319.

[16] AUBERT B, BARATE R, BOUTIGNY D, et al. Observation of a broad structure in the $\pi^+\pi^- J/\psi$ mass spectrum around 4.26 GeV/c^2[EB/OL]. (2005-09-12)[2015-11-30]. http://arxiv.org/abs/hep-ex/0506081.

[17] ABLIKIM M, AN Z H, BAI J Z, et al. Design and construction of the BESIII detector[J]. Nucl Instrum Meth A, 2010,614: 345-399.

[18] CHAO K, WANG Y. Physics at BES-III [J/OL]. Int J Mod Phys A, 2009, 24 (supp01) [2015-11-30]. http://www.worldscientific.com/toc/ijmpa/24/supp01.

[19] GRANDPIERRE A. A Dynamic Solar Core Model: On the Activity-Related Changes of the Neutrino Fluxes [EB/OL]. (1998-10-08)[2015-11-30]. http://arxiv.org/abs/hep-ph/9810285.

[20] ABREU P, ADAM W, ADYE T , et al. Tuning and test of fragmentation models based on identified particles and precision event shape data[J]. Z Phys C, 1996, 73:11-60.

[21] ZHANG Bingxin. Luminosity measurement for the new R-QCD data: inner report at BESIII Annual [R]. [S. l. : s. n.], 2015.

[22] GAO Zhen. Data quality check for R-QCD run in 2～3 GeV: inner report at BESIII Annual [R]. [S. l. : s. n.], 2015.

[23] OSTERHELD A, HOFSTADTER R, HORISBERGER R, et al. Measurements of total hadronic and inclusive D^* cross-sections in e^+e^- annihilations between 3.87 and 4.5 GeV [R/OL]. 1986: SLAC-PUB-4160. (2014-12-15)[2015-11-30]. http://cds.cern.ch/record/176521? ln=zh_CN.

[24] EDWARD C, PARTRIDGE R, PECKEL C, et al. Hadron production in e^+e^- annihilation from $\sqrt{s}=5.0$ to 7.4 GeV[R/OL]. 1990: SLAC-PUB-5160 [2015-11-30]. http://www.slac.stanford.edu/cgi-wrap/getdoc/slac-pub-5160.pdf.

(下转第 307 页)

第46卷第4期 中国科学技术大学学报 Vol. 46, No. 4
2016年4月 JOURNAL OF UNIVERSITY OF SCIENCE AND TECHNOLOGY OF CHINA Apr. 2016

Article ID:0253-2778(2016)04-0301-07

BESIII $\pi^+\pi^-$ form factor measurement and perspective of $\pi^+\pi^-\pi^0$

WANG Yaqian (for the BESIII Collaboration)

(*Johannes-Gutenberg University, Mainz* 55128, *Germany*)

Abstract: The cross section is measured of $e^+e^-\to\pi^+\pi^-$ in the energy range between 600 and 900 MeV/c^2 with a 2.93 fb^{-1} data set taken at the center-of-mass energy 3.773 GeV at BESIII. The initial state radiation technique is used, and the total systematic uncertainty is estimated to be 0.9%. The squared form factor $|F_\pi|^2$ is extracted, and comparisons are made with results from both KLOE and BaBar. The two-pion contribution to the hadronic vacuum polarization contribution to $(g-2)_\mu$ is calculated to be $a_\mu^{\pi\pi,\mathrm{LO}}(600\sim900\ \mathrm{MeV}/c^2)=(368.2\pm2.5_{\mathrm{stat}}\pm3.3_{\mathrm{sys}})\times10^{-10}$.

Key words: muon anomalous magnetic moment $g-2$; vacuum polarization; initial state radiation (ISR)

CLC number: O572.3 **Document code**: A doi:10.3969/j.issn.0253-2778.2016.04.007

Citation: WANG Yaqian. BESIII $\pi^+\pi^-$ form factor measurement and perspective of $\pi^+\pi^-\pi^0$[J]. Journal of University of Science and Technology of China, 2016,46(4):301-307.

BESIII $\pi^+\pi^-$ 形状因子测量以及 $\pi^+\pi^-\pi^0$ 展望

王亚乾(BESIII 合作组)

(美因茨大学, 美因茨 55128,德国)

摘要:利用 BESIII 在 3.773 GeV 获取的 2.93 fb^{-1}数据,测量了 600～900 MeV/c^2 区间 $e^+e^-\to\pi^+\pi^-$ 的截面.分析主要基于初态辐射的方法,总的系统误差控制在 0.9%.通过计算得到的形状因子$|F_\pi|^2$与其他两个实验做了比较.两π过程对缪子反常磁矩的贡献为 $a_\mu^{\pi\pi,\mathrm{LO}}(600\sim900\ \mathrm{MeV}/c^2)=(368.2\pm2.5_{\mathrm{stat}}\pm3.3_{\mathrm{sys}})\times10^{-10}$.

关键词:缪子反常磁矩;真空极化;初态辐射

0 Introduction

The hadronic vacuum polarization (VP) plays an important role in the precision test of the Standard Model (SM). One of the cases is the theoretical prediction for the anomalous magnetic moment of muon, $a_\mu\equiv(g-2)_\mu/2$. With dozens of years' efforts, the precision on the a_μ is in the order of 6×10^{-10} for both experiment and theory. The significance of the discrepancy of (28.7±8.0)

Received: 2015-11-30; **Revised**: 2016-04-20

Foundation item: Supported by German Research Foundation DFG under Collaborative Research Center (CRC-1044).

Biography: WANG Yaqian, male, born in 1984, PhD. Research field: particle physics. E-mail: whyaqm@gmail.com

$\times 10^{10}$ between them is 3.6σ[1]. In the following years, a new experiment at Fermilab is expected to reach the precision of 0.14 parts per million[2], which makes the theoretical calculation of a_μ under pressure to improve the precision accordingly.

The largest contribution to a_μ is from quantum electro-dynamics (QED) including all photonic and leptonic loops, and the calculation is performed up to 4-loop level and estimated to 5-loop level. As a result, the error from QED is negligible. The weak part includes Z, $W^{\pm}$ and Higgs loop contributions, and is suppressed due to the heaviness of their masses. Until now, it is not possible to calculate the hadronic contributions from first principles. Generally, there are three parts in the hadronic contribution. In terms of uncertainty, the largest contribution is from the lowest order (LO) hadronic VP, to a less extent, from the hadronic light-by-light scattering contribution and higher order hadronic VP.

By using the experimental measurements, the hadronic VP contribution is obtained via the dispersion integral[3-4],

$$a_\mu^{\mathrm{had,LO}} = \frac{\alpha^2(0)}{3\pi^2}\int_{4m_\pi^2}^{\infty} \mathrm{d}s \frac{K(s)}{s} R(s) \qquad (1)$$

where $K(s)$ is the QED kernel[5], and $R(s)$ denotes the ratio of the bare cross section for e^+e^- annihilation into hadrons to the point-like muon-pair cross section. The integrand decreases monotonically with increasing s. Therefore, precision measurement at low energy is very important. About 91% of the total contribution to $a_\mu^{\mathrm{had,LO}}$ is accumulated at center-of-mass energies $\sqrt{s} < 1.8$ GeV and the two-pion channel contributes more than 70% of $a_\mu^{\mathrm{had,LO}}$.

Two precision measurements of $\sigma_{\pi\pi}$ have been done by the KLOE Collaboration in Frascati[6-9], and the BABAR Collaboration at SLAC[10], both of which claim an accuracy of better than 1% in the energy range below 1 GeV. However, a discrepancy of approximately 3% on the peak of the $\rho(770)$ resonance is observed. The discrepancy is even increasing towards higher energies and has a large impact on the SM prediction of a_μ.

In this paper, I report the two-pion cross section in the mass range between 600 and 900 MeV/c^2. This range includes the important ρ peak, which contributes more than 70% to the two-pion contribution $a_\mu^{\pi\pi}$ and to about 50% of the total hadronic vacuum polarization correction of a_μ. Besides the $\pi^+\pi^-$ channel, perspective on the study of $e^+e^- \to \pi^+\pi^-\pi^0$ is also included.

1 BESIII experiment

Located at the double-ring Beijing Electron-Positron Collider, the cylindrical BESIII detector covers 93% of the full solid angle. As a multi-functional detector, it is described in detail elsewhere[12]. A charged-particle tracking system, Multilayer Drift Chamber (MDC), is immersed in a 1 T magnetic field. A time-of-flight (TOF) system and an electromagnetic calorimeter (EMC) surrounding the tracking system are used to identify charged particles and to measure neutral particle energies, respectively. Located outside the EMC, a muon chamber (MUC) is used to detect muon tracks.

2 Cross section measurement

From the integrand of the dispersion integral, the most important contribution comes from the low energy region. We exploit the initial state radiation (ISR) technique to measure the cross section with data sample taken at the 3.773 GeV.

2.1 ISR technique

The emission of the ISR photon is suppressed by $\frac{\alpha}{\pi}$. This is the reason why it is necessary to have large data sample for the application of the ISR technique. Radiation of a high energy photon from the initial e^+ or e^- allows the production of the hadronic system at an energy point ($\sqrt{s'}$) much below the nominal machine energy ($\sqrt{s}$), which follows $\sqrt{s'} = \sqrt{s - 2\sqrt{s}E_\gamma}$, where E_γ is the energy of the ISR photon. The radiation function, used to

describe this ISR effect, is precisely known. Monte Carlo (MC) samples are available for many channels with PHOKHARA[13]. The ISR photons favor large polar angles, which is beyond the acceptance of the common symmetrical e^+e^- collider. There is only a small fraction of the ISR photons that falls in the coverage of EMC. In the final state of an ISR event, there are particles including the ISR photon and the hadrons, which should be of course reconstructed to measure the hadronic cross sections. Then, according to the angular direction of the ISR photon, different methods can be used.

If the ISR photon is emitted at small polar angle, it is possible to detect (tag) it, and the ISR event can be fully reconstructed together with the hadronic particles. In this case, a wide mass spectrum is available from threshold to the machine energy. The disadvantage is that we suffer from a large background contribution, especially in the higher mass range.

Since the majority of the ISR photons favor the beam direction, the detector loses the power to find it (untag). It is still possible to reconstruct all the hadronic particles in the ISR events when the energy of the ISR photon is not extremely high. With this characteristic, requiring a missing photon along the beam pipe removes quite an amount of continuum backgrounds and keeps the signal almost background free.

2.2 Measurement of $e^+e^-\to\pi^+\pi^-$

There are only two charged tracks in the channel under study. As a result, Bhabha events survive the selections due to a very high cross section. Information from dE/dx, TOF and EMC is used to veto electrons and positrons. A 4-constraint (4C) kinematic fit is performed by exploiting the kinematics. Events with χ^2_{4C} larger than 60 are rejected.

2.2.1　μ-π separation

In terms of background level, the most important one is $e^+e^-\to\gamma\mu^+\mu^-$, in which the kinematics is quite similar to the signal. We utilize a track-based particle identification (PID), which is based on the artificial neural network (ANN) method, as provided by the TMVA package[14]. The following observables are exploited for the separation: the Zernicke moments[15] of the EMC clusters induced by pion or muon tracks, the ratio of the energy E of the charged track deposited in the EMC to its momentum p measured in the MDC, the ionization energy loss dE/dx in the MDC, and the depth of a track in the MUC. The ANN is trained by using MC samples of $\pi^+\pi^-\gamma$ and $\mu^+\mu^-\gamma$. We choose the implementation of a Clermont-Ferrand Multilayer Perceptron (CFMlp) ANN as the method resulting in the best background rejection for a given signal efficiency. The output likelihood yANN is calculated after training the ANN for the signal pion tracks and background muon tracks. The response value yANN is required to be greater than 0.6 for each pion candidate in the event selection, yielding a background rejection of more than 90% and a signal loss of less than 30%.

2.2.2　QED test

Differences between data and MC are taken to correct the efficiency at the track level. The validity of such corrections needs to be proved.

We select $\mu^+\mu^-\gamma$ events from data and compare them after efficiency corrections with the QED prediction, which is scaled to the luminosity of data. The event selections are quite similar to that for $\pi^+\pi^-\gamma$. The only difference is the PID, i.e., we are selecting muons instead of pions. Fig. 1 shows the comparison of the di-muon mass spectrum between data and QED prediction.

The difference between them is $(1.0\pm0.3\pm0.9)\%$ from a linear fit as shown below. The uncertainties of the corrections are taken as the systematics, which is 0.9% in total.

2.2.3　Cross section and form factor

With the QED test in the previous section, all the corrections we made to the efficiency prove to be reliable. The cross section is obtained by dividing the two-pion mass spectrum by the global

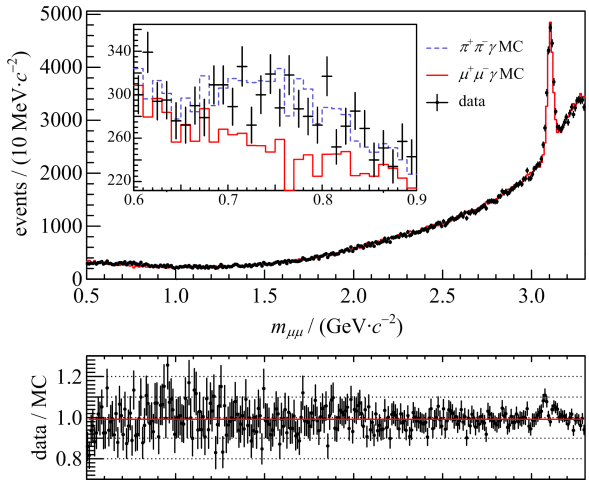

The upper panel presents the event yield found in data and MC. The inlay shows the zoom for invariant masses between 600 and 900 MeV/c^2. The lower panel shows the ratio of these two histograms.

Fig. 1 Invariant $\mu^+\mu^-$ mass spectrum of data and $\mu^+\mu^-\gamma$ MC

efficiency and the effective luminosity including corrections of final state radiation (FSR) and VP. The black dots in Fig. 2 show the cross section from 600 to 900 MeV/c^2.

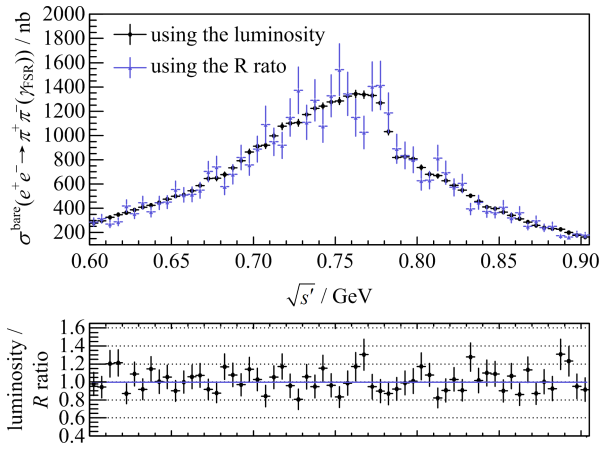

Only the statistical errors are shown.

Fig. 2 The bare $e^+e^-\to\pi^+\pi^-(\gamma_{FSR})$ cross section

Another method to obtain the cross section is to normalize the $\pi^+\pi^-\gamma$ events to the $\mu^+\mu^-\gamma$ events, since the di-muon cross section is precisely known. In this approach, part of the systematics is canceled, for instance, the luminosity, tracking efficiency, photon efficiency, and so on. As shown in Fig. 2, the cross section with this normalization method, represented as blue dots, shows very good consistency with the black one with a difference estimated to be $(0.85\pm1.68)\%$ from a linear fit. Since the precision of the blue dots is limited by the statistics of the $\mu^+\mu^-\gamma$ events, result from the black points is taken as final. The a_μ is calculated in the same mass range to be $a_\mu^{\pi\pi,\mathrm{LO}}(600\sim900\ \mathrm{MeV}/c^2)=(368.2\pm2.5_{\mathrm{stat}}\pm3.3_{\mathrm{sys}})\times10^{-10}$. Fig. 3 shows the comparison between BESIII and other measurements. Obviously, the BESIII result tends to confirm KLOE's result, but we need to keep in mind that the deviation with BaBar is only 1.7σ.

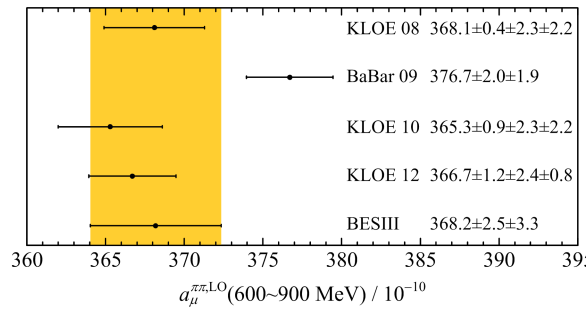

The statistical and systematic errors are added quadratically. The band shows the 1σ range of the BESIII result.

Fig. 3 Our calculation[11] of the LO hadronic vacuum polarization 2π contributions to $(g-2)_\mu$ in the energy range 600~900 MeV/c^2 from BESIII and based on the data from KLOE 08[7], 10[8], 12[9], and BaBar[10], with the statistical and systematic errors

The form factor is also extracted with formula

$$|F_\pi|^2(s')=\frac{3s'}{\pi\alpha\beta_\pi^3(s')}\sigma_{\pi\pi}^{\mathrm{dressed}}(s') \qquad (2)$$

with the pion velocity $\beta(s')=\sqrt{1-4m_\pi^2/s'}$, the charged pion mass m_π, and the dressed cross section dressed $\sigma_{\pi\pi}^{\mathrm{dressed}}(s')=\sigma(e^+e^-\to\pi^+\pi^-)(s')$ including vacuum polarization, but corrected for FSR effects. To make a comparison with other experiments, we fit the form factor with the vector meson dominance model, where the Gunaris-Sakurai parameterization[16] for the ρ resonances is adopted. The fitted result is shown in Fig. 4.

The fit gives $\chi^2/ndf=49.1/56$, and the fitted parameters are listed in Tab. 1, all of which are consistent with the Particle Data Group (PDG)[17]

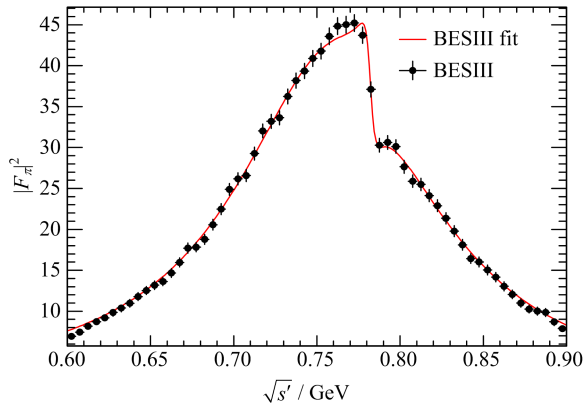

Only statistical errors are shown. The red line represents the fit using the Gounaris-Sakurai parametrization.

Fig. 4　The measured squared pion form factor $|F_\pi|^2$

values except the width of ρ, which shows a 3.4σ difference.

Tab. 1　Parameters and statistical errors in the Gounaris-Sakurai fit of the pion form factor

parameter	BESIII value	PDG[17]
m_ρ/(MeV·c^{-2})	776.0±0.4	775.26±0.25
Γ_ρ/MeV	151.1±0.7	147.8±0.9
m_ω/(MeV·c^{-2})	782.1±0.6	782.65±0.12
Γ_ω/MeV	fixed to PDG[17]	8.49±0.08
$\lvert c_\omega\rvert/10^{-3}$	1.7±0.2	—
$\lvert\phi_\omega\rvert$/rad	0.04±0.13	—

Comparisons with other measurements are illustrated in Figs. 5 and 6. Here, the shaded error band of the fit includes the systematic error only, while the uncertainties of the data points include the sum of the statistical and systematic errors. We observe a very good agreement with the KLOE 08 and KLOE 12 data sets up to the mass range of the ρ—ω interference. In the same mass range, the BaBar and KLOE 10 data sets show a systematic shift; however, the deviation is, within 1 to 2 standard deviations. At higher masses, the statistical error bars in the case of BESIII are relatively large, such that a comparison is not conclusive. There seems to be a good agreement with the BaBar data, while a large deviation with all three KLOE data sets is visible. There are indications that the BESIII data and BESIII fit show some disagreement in the low mass and very high mass tails as well.

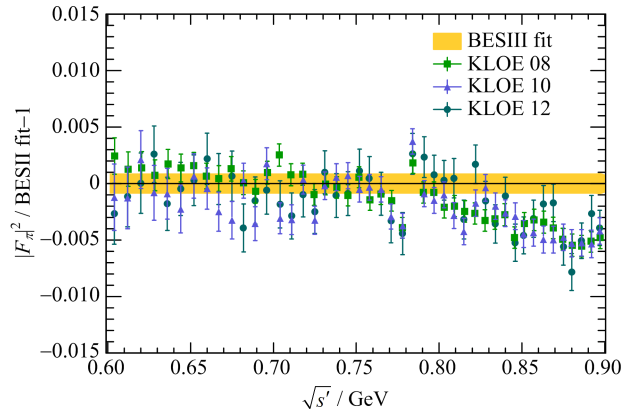

Statistical and systematic uncertainties are included in the data points. The width of the BESIII band shows the systematic uncertainty only

Fig. 5　Relative difference of the form factor squared from KLOE[7-9] and the BESIII fit

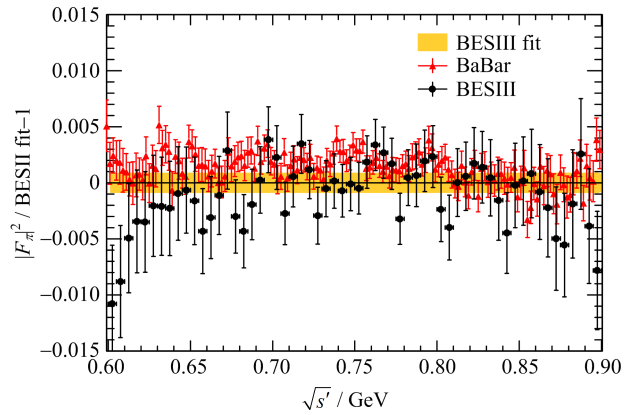

Statistical and systematic uncertainties are included in the data points. The width of the BESIII band shows the systematic uncertainty only

Fig. 6　Relative difference of the form factor squared from BaBar[10] and the BESIII fit

2.3　Perspective of $e^+e^-\to\pi^+\pi^-\pi^0$

Many efforts have been made on the study of $e^+e^-\to\pi^+\pi^-\pi^0$ process, including both energy scan experiments and ISR analysis. Below 1.0 GeV, ω and ϕ dominate the mass spectrum, and the most precise results so far have come from energy scan experiments, like CMD2[18-20] and SND[21-24]. By comparing results from the two, there are still points where the difference between them is as large as 10%. Above the ϕ resonance, BaBar measured the cross section until 3.0 GeV[25]. The discrepancy with DM2[26] is very

large, around 1.6 GeV. All these differences need to be clarified with upcoming new results.

At BESIII, we use the 2.93 fb^{-1} data taken at the ψ'' peak to perform an ISR study. The wide mass spectrum is expected to be measured from ω to J/ψ resonance. Compared to BaBar, the advantage is that we can benefit from both tagged and untagged methods for different mass ranges. Above 1.4 GeV, the statistics is increased significantly due to the untagged method. As a result, measurement of branching fraction $J/\psi\to\pi^+\pi^-\pi^0$ with very high precision is feasible.

3 Conclusion

We perform a cross section measurement of the $\sigma^{\rm bare}(e^+e^-\to\pi^+\pi^-(\gamma_{\rm FSR}))$ with an accuracy of 0.9% in the dominant $\rho(770)$ mass region between 600 and 900 MeV/c^2. The two-pion contribution to the hadronic vacuum polarization part of $(g-2)_\mu$ is determined to be $a_\mu^{\pi\pi,{\rm LO}}(600\sim900\ {\rm MeV}/c^2)=(368.2\pm2.5_{\rm stat}\pm3.3_{\rm sys})\times10^{-10}$. The pion form factor is extracted with vacuum polarization. It is found to be closer to KLOE's result, while the deviation with BaBar is less than 2σ. By exploiting the ISR technique, study on other channels is ongoing.

References

[1] DAVIER M, HOECKER A, MALESCU B, et al. Reevaluation of the hadronic contributions to the muon $g-2$ and to $\alpha(M_Z^2)$[J]. Eur Phys J C, 2011, 71: 1 515.

[2] GRANGE J, GUARINO V, WINTER P, et al. Muon $(g-2)$ Technical Design Report[EB/OL]. (2015-01-27)[2015-11-30]. http://arxiv.org/abs/1501.06858.

[3] BOUCHIAT C, MICHEL L. La résonance dans la diffusion méson π- méson π et le moment magnétique anormal du méson μ[J]. J Phys Radium, 1961 22: 121.

[4] GOURDIN M, DE RAFAEL E. Hadronic contributions to the muon g-factor[J]. Nucl Phys B, 1969, 10(4): 667-674.

[5] BRODSKY S J, DE RAFAEL E. Suggested boson-lepton pair couplings and the anomalous magnetic moment of the muon[J]. Phys Rev, 1968, 168(5): 1 620-1 622.

[6] ALOISIO A, AMBROSINO F, ANTONELLI A, et al. Measurement of $\sigma(e^+e^-\to\pi^+\pi^-\gamma)$ and extraction of $\sigma(e^+e^-\to\pi^+\pi^-)$ below 1 GeV with the KLOE detector[J]. Phys Lett B, 2005, 606(1/2): 12-24

[7] AMBROSIO F, ANTONELLI A, ANTONELLI M, et al. Measurement of $\sigma(e^+e^-\to\pi^+\pi^-\gamma(\gamma))$ and the dipion contribution to the muon anomaly with the KLOE detector[J]. Phys Lett B, 2009, 670(4/5): 285-291.

[8] AMBROSINO F, ARCHILLI F, BELTRAME P, et al. Measurement of $\sigma(e^+e^-\to\pi^+\pi^-)$ from threshold to 0.85 GeV^2 using initial state radiation with the KLOE detector[J]. Phys Lett B, 2011, 700(2): 102-110.

[9] BABUSCI D, BADONI D, BALWIERZ-PYTKO I, et al. Precision measurement of $\sigma(e^+e^-\to\pi^+\pi^-\gamma)/\sigma(e^+e^-\to\mu^+\mu^-\gamma)$ and determination of the $\pi^+\pi^-$ contribution to the muon anomaly with the KLOE detector[J]. Phys Lett B, 2013, 720(4/5): 336-343.

[10] AUBERT B, KARYOTAKIS Y, LEES J P, et al. Precise measurement of the $e^+e^-\to\pi^+\pi^-(\gamma)$ cross section with the initial state radiation method at BABAR[J]. Phys Rev Lett, 2009, 103: 231801.

[11] ABLIKIM M, ACHASOV M N, AI X C, et al. Measurement of the $e^+e^-\to\pi^+\pi^-$ Cross Section between 600 and 900 MeV Using Initial State Radiation [EB/OL]. (2015-11-17)[2015-11-30]. http://arxiv.org/abs/1507.08188.

[12] ABLIKIM M, AN Z H, BAI J Z, et al. Design and construction of the BESIII detector[J]. Nucl Instrum Meth A, 2010, 614(3): 345-399.

[13] CZYŻ H, KÜHN J H, WAPIENIK A. Four-pion production in τ decays and e^+e^- annihilation: An update[J]. Phys Rev D, 2008, 77: 114005.

[14] HOECKER A, SPECKMAYER P, STELZER J, et al. TMVA - Toolkit for Multivariate Data Analysis [EB/OL]. (2007-03-04)[2015-11-30]. http://arxiv.org/abs/physics/0703039.

[15] AGOSTINELLI S, ALLISON J, AMAKO K, et al. GEANT4-a simulation toolkit[J]. Nucl Instrum Meth A, 2003, 506(3): 250-303.

[16] GOUNARIS G J, SAKURAI J J. Finite-width corrections to the vector-meson-dominance prediction for $\rho\to e^+e^-$[J]. Phys Rev Lett, 1968, 21: 244.

[17] OLIVE K A, AGASHE K, AMSLER C, et al. Review of particle physics [J]. Chin Phys C, 2014, 38(09): 090001.

[18] AKHMETSHIN R R, AKSENOV G A, ANASHKIN E V, et al. Measurement of φ meson parameters with CMD-2 detector at VEPP-2M collider[J]. Phys Lett B,

1995, 364(3): 199-206.

[19] AKHMETSHIN R R, AKSENOV G A, ANASHKIN E V, et al. Study of dynamics of $\varphi\to\pi^+\pi^-\pi^0$ decay with CMD-2 detector [J]. Phys Lett B, 1998, 434(3/4): 426-436.

[20] AKHMETSHIN R R, ANASHKIN E V, AULCHENKO V M, et al. Measurement of ω meson parameters in $\pi^+\pi^-\pi^0$ decay mode with CMD-21[J]. Phys Lett B, 2000, 476(1/2): 33-39.

[21] ACHASOV M N, AULCHENKO V M, BARU S E, et al. The process $e^+e^-\to\pi^+\pi^-\pi^0$ in the energy range $2E_0 = 1.04 \sim 1.38$ GeV [J]. Phys Lett B, 1999, 462(3/4): 365-370.

[22] ACHASOV M N, BELOBORODOV K I, BERDYUGIN A V, et al. Measurements of the parameters of the $\varphi(1020)$ resonance through studies of the processes $e^+e^-\to K^+K^-$, K_SK_L, and $\pi^+\pi^-\pi^0$[J]. Phys Rev D, 2001, 63: 072002.

[23] ACHASOV M N, AULCHENKO V M, BELOBORODOV K I, et al. Study of the process $e^+e^-\to\pi^+\pi^-\pi^0$ in the energy region $\sqrt{s}$ from 0.98 to 1.38 GeV[J]. Phys Rev D, 2002, 66: 032001.

[24] ACHASOV M N, BELOBORODOV K I, BERDYUGIN A V, et al. Study of the process $e^+e^-\to\pi^+\pi^-\pi^0$ in the energy region $\sqrt{s}$ below 0.98 GeV[J]. Phys Rev D, 2003, 68:052006.

[25] AUBERT B, BARATE R, BOUTIGNY D, et al. Study of the $e^+e^-\to\pi^+\pi^-\pi^0$ process using initial state radiation with BABAR [J]. Phys Rev D, 2004, 70: 072004.

[26] ANTONELLI A, BALDINI R, BIAGINI M E, et al. Measurement of the $e^+e^-\to\pi^+\pi^-\pi^0$ and $e^+e^-\to\omega\pi^+\pi^-$ reactions in the energy interval 1 350～2 400 MeV [J]. Z Phys C, 1992, 56(1): 15-19.

(上接第 300 页)

[25] 胡海明,祁向荣,黄光顺, 等.北京谱仪 R 值测量中的初态辐射修正[J]. 高能物理与核物理,2001, 25(8): 701-709.
HU Haiming QI Xiangrong, HUANG Guangshun, et al. Initial state radiative correction in R measurement at BES[J]. High Energy Physics and Nuclear Physics, 2001, 25(8): 701-709.

[26] 胡海明,台安,黄光顺,等. LUND 面积定律产生子在 R 值测量中的应用[J]. 高能物理与核物理, 2001, 25(11):1 035-1 043.
HU Haiming, TAI An, HUANG Guangshun, et al. Applications of LUND area law generator in R measurement[J]. High Energy Physics and Nuclear Physics, 2001, 25(11):1 035-1 043.

[27] 胡海明, 戴玉梅, 马凤才. LUND 面积定律对 J/ψ 非微扰强衰变的描述[J]. 高能物理与核物理, 2003, 27(8): 673-677.
HU Haiming, DAI Yumei, MA Fengcai. Descriptionof LUND area law to J/ψ non-perturbative hadronie decay [J]. High Energy Physics and Nuclear Physics, 2003, 27(8): 673-677.

[28] SJÖSTRAND T. PYTHIA 5.7 and JETSET 7.4: Physics and Manual[R]. CERN, 1993: CERN-TH. 7112/93.

第46卷第4期 中国科学技术大学学报 Vol. 46, No. 4
2016年4月 JOURNAL OF UNIVERSITY OF SCIENCE AND TECHNOLOGY OF CHINA Apr. 2016

Article ID: 0253-2778(2016)04-0308-08

Threshold phenomenology of nucleon form factors

BALDINI FERROLI Rinaldo[1], PACETTI Simone[2], TOMASI-GUSTAFSSON Egle[3]

(1. *Laboratori Nazionali di Frascati dell'INFN, Frascati* 00044, *Italy*;
2. *Dipartimento di Fisica e Geologia e Sezione INFN, Perugia* 06123, *Italy*;
3. *CEA, IRFU, SPhN, Saclay, Gif-sur-Yvette Cedex* 91191, *France*)

Abstract: The complete knowledge of nucleon form factors is a mandatory pass to deeply understand the dynamics of strong interaction at regimes where QCD is still non perturbative. Phenomenology, i. e., the description of the data by means models based of first principles and depending on physical quantities, represents one of the most powerful tools to attain such a degree of knowledge.

Key words: Nucleon form factors; analyticity; threshold behavior; asymptotic behavior

CLC number: O572.3 **Document code**: A doi: 10.3969/j.issn.0253-2778.2016.04.008

Citation: BALDINI FERROLI Rinaldo, PACETTI S, TOMASI-GUSTAFSSON E. Threshold phenomenology of nucleon form factors[J]. Journal of University of Science and Technology of China, 2016, 46(4): 308-315.

核子形状因子的阈值效应

BALDINI FERROLI Rinaldo[1], PACETTI Simone[2], TOMASI-GUSTAFSSON Egle[3]

(1. INFN 弗拉斯卡蒂国家实验室,弗拉斯卡蒂 00044,意大利;2. INFN 物理系,佩鲁贾 06123,意大利;
3. 法国原子能委员会萨克莱核研究中心,吉夫伊维特 91191,法国)

摘要:在微扰量子色动力学不再适用的低能区,核子形状因子可以作为一个重要参数来研究其强相互作用.诸如根据第一性原理和某个物理基本量的各种模型来描述数据的唯象物理学可以作为一个有效的工具来研究该领域.

关键词:核子形状因子;解析方法;阈值效应;渐进性

0 Definition and basic properties

0.1 Definitions

The nucleon form factors[1] (FFs) parametrize the factor to be associated to the photon-nucleon-antinucleon vertex, see Fig. 1, $\gamma N\overline{N}$, assuming extended nucleons, i. e., particles with non-pointlike charge and magnetic moment spatial distributions.

The Feynman amplitude of diagram in Fig. 1, in the space-like direction, i. e., for the scattering process, reads

$$\mathcal{M}=\frac{1}{q^2}e\bar{u}(k_2)\gamma_\mu u(k_1)e\overline{U}(p_1)\Gamma^\mu(p_1,p_2)U(p_2),$$

where e is the electron charge, u and U are the spinors of electrons and nucleons respectively, and

Received: 2015-11-30; **Revised**: 2016-04-20

Corresponding author: PACETTI Simone, PhD. Research field: high energy physics. E-mail: simone.pacetti@pg.infn.it

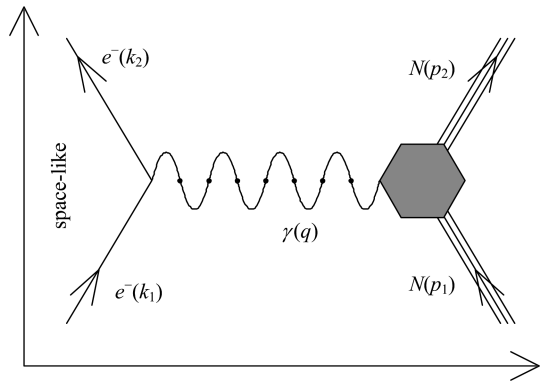

The hexagon represents the non-pointlike nucleon vertex.

Fig. 1 Feynman diagram of the one-photon exchange annihilation and scattering processes $e^+e^-\to N\overline{N}$ and $e^-N\to e^-N$

the four-momenta, in parentheses, are defined as in Fig. 1. The non-constant matrix, $\Gamma^\mu(p_1,p_2)$, which describes the nucleon vertex is

$$\Gamma^\mu(p_1,p_2)=\gamma^\mu F_1^N(q^2)+\frac{i\sigma^{\mu\nu}q_\nu}{2M_N}F_2^N(q^2) \quad (1)$$

where F_1^N and F_2^N are the Dirac and Pauli FFs. Such an expression represents the most general Lorentz four-vector, containing gamma matrices and nucleon four-momenta, that fulfills Lorentz, parity, time-reversal and gauge invariance. Form factors are scalar Lorentz functions of q^2, where q is the photon four-momentum.

0.2 Analyticity

The hexagon in Fig. 1 symbolizes the sum of all the electromagnetic contributions, i. e., all those diagrams having an arbitrary number of loops of all hadrons (computable in scalar quantum electrodynamics), with external lines only be photon, nucleon and antinucleon. The amplitudes of all these diagrams are analytic functions in the whole q^2 complex plane, except for a discontinuity cut, along the positive real axis, starting from $q_0^2=(2M_\pi)^2$. Such a threshold corresponds to the mass of the lightest hadronic state that can couple with the virtual photon. Moreover, the hermiticity of the electromagnetic current operator of the nucleons implies the Schwarz reflection principle for FFs so that, they are real for real q^2 outside the cut, while they have non vanishing imaginary parts for real $q^2>(2M_\pi)^2$.

0.3 Sachs form factors

From the expression of the nucleon electromagnetic four-current in terms of the Dirac and Pauli FFs,

$$J_N^\mu=e\overline{U}(p_1)\Gamma^\mu(p_1,p_2)U(p_2)=e\left(F_1^N+\frac{q^2}{4M_N^2}F_2^N,\overline{U}(p_1)\gamma U(p_2)(F_1^N+F_2^N)\right),$$

another pair of FFs can be defined as

$$\left.\begin{aligned}G_E^N(q^2)&=F_1^N(q^2)+\tau F_2^N(q^2)\\G_M^N(q^2)&=F_1^N(q^2)+F_2^N(q^2)\\\tau&=\frac{q^2}{4M_N^2}\end{aligned}\right\} \quad (2)$$

These are the Sachs electric and magnetic FFs[2], that, in the Breit frame, where the nucleon four-momenta are $p_1=(E,-\boldsymbol{q}/2)$ and $p_2=(E,\boldsymbol{q}/2)$, represent the Fourier transforms of the nucleon charge and magnetization spatial distributions. It follows that their values at $q^2=0$ correspond to the total charge, Q_N, and magnetic moment, μ_N, of the nucleon, i. e., $G_E^N(0)=Q_N$, $G_M^N(0)=\mu_N$.

0.4 Measuring form factors

The differential cross section for the elastic scattering, in Born approximation, Feynman diagram of Fig. 1 in vertical direction, and in the laboratory frame (Lab), also known as Rosenbluth formula[3], reads

$$\frac{d\sigma_{eN}}{d\Omega}=\frac{\alpha^2\omega_2\cos^2\left(\frac{\theta_e}{2}\right)}{4\omega_1^3\sin^4\left(\frac{\theta_e}{2}\right)}\frac{1}{1-\tau}\cdot\left\{G_E^{N^2}(q^2)-\tau\left[1+2(1-\tau)\tan^2\left(\frac{\theta_e}{2}\right)\right]G_M^{N^2}(q^2)\right\} \quad (3)$$

while the annihilation cross section, in the same approximation, but in the e^+e^- center of mass frame (CoM), is[4]

$$\left.\begin{aligned}\frac{d\sigma_{N\overline{N}}}{d\Omega}&=\frac{\alpha^2\beta}{4q^2}\left[\frac{1}{\tau}\sin^2(\theta)\mid G_E^N(q^2)\mid^2+(1+\cos^2(\theta))\mid G_M^N(q^2)\mid^2\right]\\\beta&=\sqrt{1-\frac{1}{\tau}}\end{aligned}\right\} \quad (4)$$

where θ_e, $\omega_{1,2}$ are the scattering angle, the initial

and final energies of the electron in Lab, $\mathscr{C}$ is the Coulomb correction, θ is the scattering angle and β the velocity of the outgoing proton in CoM.

By studying the angular distributions of the scattering and annihilation processes, Sachs FFs can be measured: completely in the space-like region, $q^2 < 0$, where they are real; only in modulus in the time-like region, $q^2 > 0$, above the physical threshold $q_1^2 = (2M_N)^2$, where they are complex. Moreover, by using only cross section data, the time-like complex structure of FFs remains inaccessible, as well as their values below the threshold q_1^2, in the so-called unphysical region, $0 \leqslant q^2 \leqslant q_1^2$.

Besides this procedure, FFs can also be measured by using polarization observables, i. e., by exploiting the so-called Akhiezer-Rekalo polarization method[5-6]. In particular, the polarization transferred to the nucleon, initially unpolarized, by longitudinally polarized electrons in a scattering process, allows to measure space-like FFs. More in detail, by exploiting of the scattering process $e^- \uparrow\ p \to e^-\ p\uparrow$ (the up-arrow stands for polarization), the ratio between the transversal (in the scattering plane) and the longitudinal component of the outgoing proton polarization vector in Lab is proportional to the ratio of FFs[5-6], i. e.,

$$\frac{P_T^p(q^2)}{P_L^p(q^2)} = -\frac{2M_p \cot(\theta_e/2)}{\omega_1 + \omega_2}\frac{G_E^p(q^2)}{G_M^p(q^2)},$$

where the symbols are those of Eq. (3).

In the annihilation process $e^+ e^- \to N\uparrow\ \overline{N}\uparrow$, due to the complex nature of time-like FFs, unpolarized electrons produce polarized nucleons. In particular, the component, orthogonal to the scattering plane, of the nucleon polarization vector in CoM is[7]

$$P_\perp^N(q^2) = \frac{-\sqrt{\tau}\sin(2\theta)\left|\frac{G_E^N(q^2)}{G_M^N(q^2)}\right|}{\tau(1+\cos^2(\theta)) + \sin^2(\theta)\left|\frac{G_E^N(q^2)}{G_M^N(q^2)}\right|^2}\sin(\Phi^N),$$

where symbols follow the labelling of Eq. (4) and Φ^N is the relative phase between electric and magnetic FFs. It follows that, by detecting the polarization of only one of the final nucleons, the phase of the complex ratio G_E^N/G_M^N can be measured.

0.5 Basic properties

The complex nature of the amplitude and hence of FFs, for time-like values of q, which is expressed formally by the optical theorem, lies in the fact that the photon, with such a four-momentum, gets enough virtual mass, $\sqrt{q^2}$, to couple with, and hence produce a series of on-shell hadronic intermediate states. Besides multi hadron ones, light vector meson resonances are the strongest coupled, i. e., the most probable intermediate states. They represent the main contributions to the FFs even though, having masses below the physical threshold $\sqrt{q_1^2}$, their peaks lie in the unphysical region. The complex structure of a prototype FF $F(q^2)$ is sketched in Fig. 2, where the three-dimensional surface (grid) represents the modulus squared $|F(q^2)|^2$ versus the unphysical q^2 complex plane. Indeed, it is in this Riemann sheet, where analyticity can be violated, that a generic resonance, of mass M_j and width Γ_j, manifests itself as a pair of complex conjugate poles z_j and z_j^* (this is due to the Schwarz reflection principle), with① $z_j \backsimeq M_j^2 + i\Gamma_j M_j^*$.

0.6 The asymptotic behavior

The space-like asymptotic behavior of FFs is inferred by means of dimensional counting rules of quantum chromodynamics[8-9]. At high space-like q^2, i. e. $q^2 \ll -\Lambda_{\rm QCD}^2$, the momentum transferred by

① The position of the pole in the q^2 complex plane is strictly connected to the physical mass and width of the resonance, the definition of such quantities depends on the function used to describe the cross section. For instance, by using the relativistic Breit-Wigner formula and that in modulus squared reads $|BW(s)|^2 = [(M_j^2 - s)^2 + \Gamma_j^2 M_j^2]^{-1}$, the poles would be located exactly at $M_j^2 \pm i, \Gamma_j M_j$.

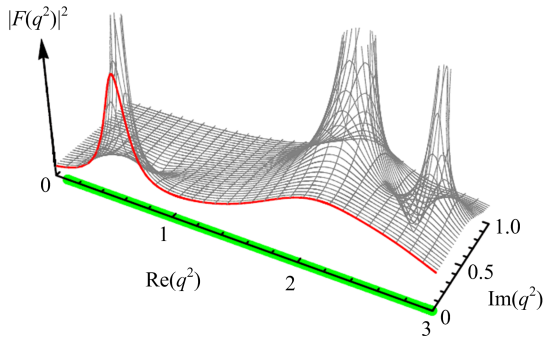

The grid surface represents the modulus squared of a prototype FF $F(q^2)$. The poles are the resonances, the red curve is the $|F(q^2)|^2$ as it appears for real values of q^2, i. e., it is the intersection between the surface and the plane $\mathrm{Im}(q^2)=0$. The green band indicates the discontinuity cut $((2M_\pi)^2,\infty)$.

Fig. 2　Pictorial representation of first quarter of the q^2 unphysical complex plane

the virtual photon to the nucleon must be shared among the constituent quarks, in order for the nucleon to remain intact, by gluon exchanges.

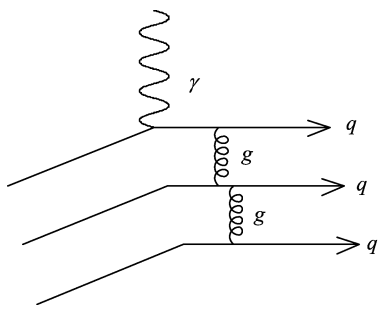

Fig. 3　Gluon (g) exchanges among the constituent quarks (q), to share the momentum transferred to the nucleon by the virtual photon

Following the schematic representation in Fig. 3, for the nucleons, that have three valence quarks, the minimum number of exchanges is two hence

$$F_i^N(q^2)\propto(-q^2)^{-1-i},\ q^2\to-\infty,$$

with $i=1,2$.

The Pauli FF has a further power $(-q^2)^{-1}$ since it is responsible for the spin-flip part of the nucleon electromagnetic current. The Sachs FFs, given in Eq. (2), have the same behavior

$$G_{E,M}^N(q^2)\propto(-q^2)^{-2},\ q^2\to-\infty.$$

The asymptotic behavior in the time-like region can be obtained by taking advantage from the analyticity and boundedness of FFs in the upper half plane, $\mathrm{Im}(q^2)>0$. Such regularities allow to apply the Phragmén-Lindelöf theorem[10] which ensures that FFs have the same vanishing power-law along any straight line from the origin to infinity, i. e.,

$$\lim_{|q^2|\to\infty}\frac{G_{E,M}^N(|q^2|e^{i\pi})}{G_{E,M}^N(|q^2|e^{i\theta})}=1,\ \forall\theta\in[0,\pi].$$

The identity between space-like and time-like asymptotic behavior is verified by taking this limit with $\theta=0$. It follows that

$$G_{E,M}^N(q^2)\propto(q^2)^{-2},\ q^2\to\infty.$$

This result, since time-like FFs are complex, implies that imaginary parts vanish faster than the real ones

$$\lim_{q^2\to\infty}\frac{\mathrm{Im}[G_{E,M}^N(q^2)]}{\mathrm{Re}[G_{E,M}^N(q^2)]}=\lim_{q^2\to\infty}\arctan(\phi_{E,M}^N(q^2))=0,$$

i. e., $\Phi_{E(M)}(q^2)$, the phase of the electric (magnetic) FF, tends to 2π radians as stated by the Levinson theorem[11].

1　The threshold

The threshold region is represented by few hundreds MeV, say δE, interval $(2M_N, 2M_N+\delta E)$, which starts at the time-like $N\overline{N}$ production energy. An e^+e^- collider operating at a CoM energy $E\in(2M_N, 2M_N+\delta E)$ would produce $N\overline{N}$ pairs almost at rest.

It is in this energy interval that charged nucleon and antinucleon experience the strongest electromagnetic interaction that, in the Born differential cross section formula of Eq. (4), is accounted for by the Coulomb factor $\mathscr{C}$. The expression of $\mathscr{C}$ can be obtained in the point-like limit as[12-13]

$$\mathscr{C}=|\psi_{\mathrm{Coul.}}(0)|^2=\frac{\pi\alpha}{\beta}\times\frac{1}{1-e^{-\pi\alpha/\beta}}\equiv\mathscr{E}\times\mathscr{R}\quad(5)$$

where $\psi_{\mathrm{Coul.}}(r)$ is the wave function solution of the Schrödinger equation with the Coulomb potential and β is the nucleon velocity given in Eq. (4). The two terms $\mathscr{E}$ and $\mathscr{R}$, called enhancement and resummation factor[14], account for the single and multi-photon contributions, respectively; $\mathscr{E}$

dominates at threshold where $\mathcal{R}\backsimeq 1$, i. e. ,

$$\mathcal{C}\backsimeq\mathcal{E}=\frac{\pi\alpha}{\beta},\ \beta\to 0^{+}.$$

The enhancement factor compensates for the closing of the phase-space by making the total Born cross section finite and different from zero at threshold, in particular[15]

$$\lim_{q^2\to 4M_N^2}\sigma_{N\bar{N}}(q^2)=\frac{\pi^3\alpha^2}{2M_N^2}\,|\,G^N(4M_N^2)\,|^2 \qquad (6)$$

where $G^N(4M_N^2)$ is the common threshold value of electric and magnetic FFs, that is, from the definitions of Eq. (2), assuming no singularities for the Dirac and Pauli FFs, $G_E^N(4M_N^2)=G_M^N(4M_N^2)\equiv G^N(4M_N^2)$. It follows that, the cross section and modulus of FFs can be measured even exactly at threshold. By taking advantage from the initial state radiation techniques, BaBar Collaboration measured $p\bar{p}$ cross section[16-17], practically reaching the threshold.

Solid and empty black circles in Fig. 4 represent two sets of BaBar data[16-17] on $e^+e^-\to p\bar{p}$ cross section, while the red point at the production threshold, which is indicated by the blue dashed line, is the expected value for the total cross section in case of

$$|\,G_E^p(4M_p^2)\,|=|\,G_M^p(4M_p^2)\,|=|\,G^p(4M_p^2)\,|=1.$$

In other words, assuming a flat cross section in the threshold region, BaBar Collaboration has measured, for the first time and at a percent level, a unit FF at threshold. Such a result seems to suggest that the physical threshold has a special meaning for the FFs, in contrast with their basic theoretical properties. Indeed, by considering an FF as the superposition of intermediate resonances and multi-hadron states, at these time-like four-momenta its value should be the sum of tails of these contributions, hence there is no reason for expecting this sum to be exactly one.

The flat $e^+e^-\to p\bar{p}$ cross section in the threshold region could be explained by considering:

① FFs almost constant and unitary;

② a resummation factor which accounts for multi-gluon exchanges ($\alpha\to\alpha_s$)

$$\mathcal{R}\to\mathcal{R}_s=\frac{1}{1-e^{-\pi\alpha_s/\beta}},\ \alpha_s=0.5.$$

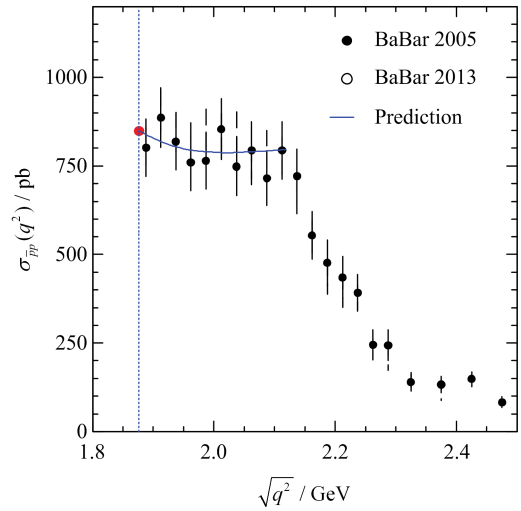

The blue dashed line indicates the physical threshold $\sqrt{q^2}=2M_p$. The solid red point at threshold represents the cross section expected if $|G_E^p(4M_p^2)|=|G_M^p(4M_p^2)|=|G^p(4M_p^2)|=1$. The blue curve is a prediction, see text.

Fig. 4 Total cross section of $e^+e^-\to p\bar{p}$, measured by the BaBar Collaboration in 2005, solid circles, and 2012, empty circles

In fact, in this case, the total cross section, that is obtained from the expression of Eq. (4) where all constants are reported in units of pb, becomes

$$\sigma_{p\bar{p}}(q^2)=[850\ \text{pb}]\frac{1}{\tau}\mathcal{R}_s,$$

and its behavior, shown as a blue curve in Fig. 4, describes the data quite well.

On the other hand, the effective FF

$$G_{\text{eff}}(q^2)=\sqrt{\frac{1}{\mathcal{R}}\frac{\sigma_{p\bar{p}}(q^2)}{\mathcal{E}\frac{4\pi\alpha^2\beta}{3q^2}\left(1+\frac{1}{2\tau}\right)}},$$

extracted from the BaBar cross section data, by considering the usual resummation factor (Eq. (5)) and as reported in Fig. 5, shows a steep decreasing behavior starting from the threshold that, having a flat cross section, turns out to be

$$G_{\text{eff}}(q^2)\backsimeq\frac{1}{\sqrt{\mathcal{R}}}=\sqrt{1-e^{-\pi\alpha/\beta}},$$

$$\sqrt{q^2}\in[2M_p,2M_p+\delta E].$$

The curve $1/\sqrt{\mathcal{R}}$ is shown in red in Fig. 5. It is

in perfect agreement with the BaBar data on $G_{\rm eff}(q^2)$, represented by black circles jointed by lines.

1.1 Isotropy at the $p\bar{p}$ production threshold

The identity of electric and magnetic FFs at the threshold is also interpreted as a consequence of isotropy.

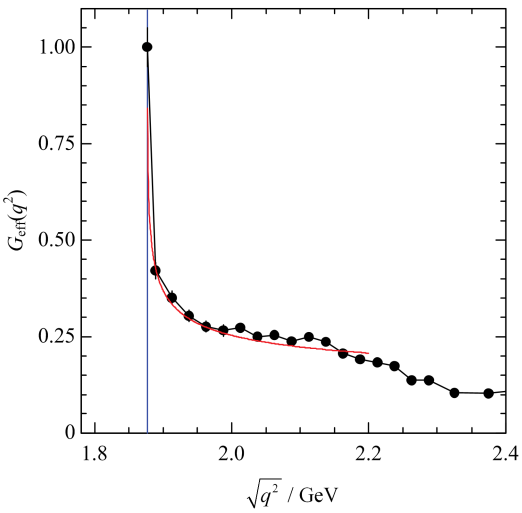

The red solid curve represents the function $1/\sqrt{\mathscr{R}}$, see text.
The dashed blue line indicates the proton physical threshold.

Fig. 5 The black circles, but for the point at the threshold, which has been obtained by extrapolating the cross section, are the data on the effective proton FF measured by the BaBar Collaboration

Besides Sachs, Dirac and Pauli FFs, also partial wave FFs can be defined. From parity and total angular momentum conservation, in Born approximation, $N\overline{N}$ can be produced with only two values of orbital angular momentum, i. e., $L_{N\overline{N}}=0,1$. In fact, the $N\overline{N}$ system has to have parity $P_{N\overline{N}}=P_\gamma=-1$ and total angular momentum $J_{N\overline{N}}=J_\gamma=1$, where P_γ and J_γ are photon quantum numbers. Since, $P_{N\overline{N}}=(-1)^{L_{N\overline{N}}+1}$, -1 is the intrinsic $N\overline{N}$ parity, and the total spin is $S_{N\overline{N}}=0$, 1, it follows that: $L_{N\overline{N}}$ must be even ($L_{N\overline{N}}=0,2,\cdots$) and

$$J_{N\overline{N}}=1\in\{|L_{N\overline{N}}-S_{N\overline{N}}|,\cdots,|L_{N\overline{N}}+S_{N\overline{N}}|\},$$
$$=\begin{cases}\{1\} & (L_{N\overline{N}},S_{N\overline{N}})=(0,1)\\ \{1,2,3\} & (L_{N\overline{N}},S_{N\overline{N}})=(2,1)\end{cases},$$

all the other combinations $(L_{N\overline{N}},S_{N\overline{N}})$ give total angular momenta different from $J_\gamma=1$. Hence only S and D waves are allowed, the corresponding FFs are

$$G_S^N(q^2)=\frac{1}{3}(2\sqrt{\tau}G_M^N(q^2)+G_E^N(q^2)),$$
$$G_D^N(q^2)=\frac{1}{3}(\sqrt{\tau}G_M^N(q^2)-G_E^N(q^2)),$$

while the total annihilation cross section in CoM and in terms of G_S^N and G_D^N reads

$$\sigma_{N\overline{N}}(q^2)=\frac{2\pi\alpha^2\beta}{q^2}\frac{1}{\tau}[\mathscr{C}|G_S^N(q^2)|^2+2|G_D^N(q^2)|^2].$$

where the Coulomb correction acts only on the S-wave term. From the definitions of Eq. (7) follows that the isotropy at threshold, i. e., the presence at threshold of the only S wave and the vanishing of the D-wave contribution, is equivalent to the identity $G_E^N(q_1^2)=G_M^N(q_1^2)$.

Such an identity is experimentally observable, especially for lambda and sigma baryons, in a typical experiment at an e^+e^- collider (e. g. BESIII at BEPCII[18]). In particular, the ratio $|G_E^{\mathscr{B}}(q_1^2)/G_M^{\mathscr{B}}(q_1^2)|$ is measurable, even exactly at the production threshold. This is because all those $\mathscr{B}\overline{\mathscr{B}}$ final states where the (lambda or sigma) baryon, $\mathscr{B}$ (anti-baryon $\overline{\mathscr{B}}$), is at rest in the lab, can decay weakly into a nucleon (anti-nucleon) and a pion which have enough momentum to reach the detector.

Measuring a non-vanishing D-wave contribution, i. e., the inequality $|G_E^{\mathscr{B}}(q_1^2)/G_M^{\mathscr{B}}(q_1^2)|\neq 1$ would be the first observation of the analyticity-violation for the Dirac and Pauli FFs, that must have a simple pole at threshold ($\tau=1$) with opposite residues. In more detail, we define

$$F_1^{\mathscr{B}}(q^2)=\frac{-\Delta G^{\mathscr{B}}}{\tau-1}+F_{1,\rm an}^{\mathscr{B}}(q^2),$$
$$F_2^{\mathscr{B}}(q^2)=\frac{\Delta G^{\mathscr{B}}}{\tau-1}+F_{2,\rm an}^{\mathscr{B}}(q^2),$$

where $\Delta G^{\mathscr{B}}=G_E^{\mathscr{B}}(q_1^2)-G_M^{\mathscr{B}}(q_1^2)$ and $F_{1(2),\rm an}(q^2)$ is the analytic part of the Dirac (Pauli) FF. In this case, i. e., by allowing for different values of Sachs FFs at threshold and assuming $|\Delta G^{\mathscr{B}}|\ll|G_M^{\mathscr{B}}(q_1^2)|$, the annihilation differential cross section of Eq. (4) has the limit

$$\frac{{\rm d}\sigma_{\mathscr{B}\overline{\mathscr{B}}}}{{\rm d}\Omega}\xrightarrow[q^2\to q_1^2]{}$$

$$\frac{\alpha^2\beta}{3M_{\mathscr{B}}^2}[\,|\,G_M^{\mathscr{B}}(q_1^2)\,|^2+\mathrm{Re}(\Delta G^{\mathscr{B}}G_M^{\mathscr{B}^*}(q_1^2))\sin^2(\theta)].$$

It depends on the scattering angle, and hence is not isotropic, even at threshold. This can be also seen by considering the values of the partial wave FFs at $q^2=q_1^2$. They are

$$G_S^{\mathscr{B}}(q^2)\xrightarrow[q^2\to q_1^2]{}G_M^{\mathscr{B}}(q_1^2)+\frac{\Delta G^{\mathscr{B}}}{3}$$

$$G_D^{\mathscr{B}}(q^2)\xrightarrow[q^2\to q_1^2]{}-\frac{V\Delta G^{\mathscr{B}}}{3}.$$

As expected, the anisotropy, which is measured by the threshold value of $G_D^{\mathscr{B}}$, depends on difference between electric and magnetic FFs.

Unique sources of anisotropy are corrections due to $\mathscr{B}\overline{\mathscr{B}}$ final state interaction, that provide an overall power of β^{-2}, which means a simple pole for the FFs. Theoretical calculations give an order-α^2[19] effect in case of only Coulomb final state interaction (charged baryons). On the other hand strong Coulomb-like interaction, computed in case of heavy quarks[20], provides a large effect but is proportional to β^n ($n\in\mathbb{N}$), hence vanishing at threshold.

2 Conclusion

The threshold region for baryon FFs is a rich and unexplored mine of information on low-energy strong dynamics. Recently, in the $p\bar{p}$ final state, an FF oscillatory behavior has been clearly identified[21] and interpreted as a manifestation of $p\bar{p}$ final state interaction. Moreover, the observation of anisotropy, by measuring a value different from one for ratio between the moduli of Sachs FFs, is now suitable for experiments like BESIII[18]. Indeed, in such an experiment the detection efficiency for a $\mathscr{B}\overline{\mathscr{B}}$ pair of lambda or sigma baryons, is different from zero even exactly at threshold, when $\mathscr{B}\overline{\mathscr{B}}$ are produced at rest in Lab, since the decay products have always enough momentum to reach the detector.

From the theoretical point of view shedding light on the threshold behavior would help with understanding not only the nature of possible $\mathscr{B}\overline{\mathscr{B}}$ final state corrections still underestimated or neglected but also the unexpected unitary normalization observed in the case of $p\bar{p}$ and that seems to hold also for other $\mathscr{B}\overline{\mathscr{B}}$ channels[22].

References

[1] PACETTI S, BALDINI FERROLI R, TOMASI-GUSTAFSSON E. Proton electromagnetic form factors: Basic notions, present achievements and future perspectives[J]. Phys Rep, 2015, 550-551: 1-103.

[2] SACHS R G. High-energy behavior of nucleon electromagnetic form factors[J]. Phys Rev, 1962, 126: 2 256-2 260.

[3] ROSENBLUTH M N. High energy elastic scattering of electrons on protons[J]. Phys Rev, 1950, 79: 615-619.

[4] ZICHICHI A, BERMAN S, CABIBBO N, et al. Proton-antiproton annihilation into electrons, muons and vector bosons[J]. Nuovo Cim, 1962, 24: 170-180.

[5] AKHIEZER A, REKALO M. Polarization phenomena in electron scattering by protons in the high-energy region[J]. Sov Phys Dokl, 1968, 13: 572.

[6] AKHIEZER A, REKALO M. Polarization effects in the scattering of leptons by hadrons[J]. Sov J Part Nucl, 1974, 4: 277-278.

[7] DUBNIČKOVÁ A Z, DUBNIČKA S, REKALO M P. Investigation of the baryon electromagnetic structure by polarization effects in $e^+e^-\to B\overline{B}$ processes[J]. Nuovo Cim A, 1996, 109: 241-256.

[8] MATVEEV V, MURADYAN R, TAVKHELIDZE A. Scaling in strong interactions[J]. Teoret Mat Fiz, 1973, 15: 332-329.

[9] BRODSKY S J, FARRAR G R. Scaling laws at large transverse momentum[J]. Phys Rev Lett, 1973, 31: 1 153-1 156.

[10] TITCHMARSH E. The Theory of Functions[M]. Oxford: Oxford University Press, 1939.

[11] LEVINSON N. On the uniqueness of the potential in a Schrodinger equation for a given asymptotic phase[J]. Danske Vid Selsk Mat Fys Medd, 1949, 25(9): 1-29.

[12] SAKHAROV A D. Interaction of the electron and the positron in pair production[J]. Zh Eksp Teor Fiz, 1948, 18: 631-635.

[13] SOMMERFELD A. Atombau und Spektralliniem[M]. Braun-schweig, Germany: Vieweg, 1944, 2: 130.

[14] BALDINI FERROLI R, PACETTI S, ZALLO A. No Sommerfeld resummation factor in $e^+e^-\to p\bar{p}$? [J]. Eur Phys J A, 2012, 48(3):33.

[15] BALDINI R, PACETTI S, ZALLO A, et al.

Unexpected features of $e^+e^- \to p\bar{p}$ and $e^+e^- \to \Lambda\bar{\Lambda}$ cross-sections near threshold[J]. Eur Phys J A, 2009, 39: 315-321.

[16] AUBERT B, BARATE R, BOUTIGNY D, et al. Study of $e^+e^- \to p\bar{p}$ using initial state radiation with BABAR[J]. Phys Rev D, 2006, 73: 012005;

[17] LEES J P, POIREAU V, TISSERAND V, et al. Study of $e^+e^- \to p\bar{p}$ via initial-state radiation at BABAR[J]. Phys Rev D 2013,87:092005.

[18] CHAO K, WANG Y. Physics at BES-III [J/OL]. Int J Mod Phys A, 2009, 24 (supp01) [2015-11-30]. http://www. worldscientific. com/toc/ijmpa/24/supp01.

[19] DMITRIEV V F, MILSTEIN A I. Final state Coulomb interaction and asymmetry of pair production close to threshold in e^+e^- annihilation[J]. Phys Lett B, 2013, 722: 83-85.

[20] BRODSKY S J, HOANG A H, KUHN J H, et al. Angular distributions of massive quarks and leptons close to threshold [J]. Phys Lett B, 1995, 359: 355-361.

[21] BIANCONI A, TOMASI-GUSTAFSSON E. Periodic interference structures in the timelike proton form factor[J]. Phys Rev Lett, 2015, 114: 232301.

[22] BALDINI FERROLI R, PACETTI S. Baryon form factors at threshold[J]. Nucl Phys B(Proc Suppl), 2012, 225-227: 211-215.

(上接第 285 页)

References

[1] ANASHIN VV, AULCHENKO V M, BALDIN E M, et al. Measurement of main parameters of the $\psi(2S)$ resonance[J]. Phys Lett B, 2012,711(3/4):280-291.

[2] ANASHIN V V, AULCHENKO V M, BALDIN E M, et al. Final analysis of KEDR data on J/ψ and $\psi(2S)$ masses[J]. Phys Lett B,2015, 749:50-56.

[3] KURAEV E A, FADIN V S. On radiative corrections to e^+e^- single photon annihilation at high energy[J]. Sov J Nucl Phys, 1985,41:466-472.

[4] ANASHIN VV, AULCHENKO V M, BALDIN E M, et al. Measurement of R_{uds} and R between 3.12 and 3.72 GeV at the KEDR detector[EB/OL]. (2015-11-23)[2015-11-30]. http://arxiv. org/abs/1510. 02667.

[5] AZIMOV Y I, VAINSHTEM A I, LIPATOV L N, et al. Electromagnetic corrections to the production of narrow resonances in colliding e^+e^- beams[J]. JETP Lett,1975, 21: 172.

[6] OLIVE K A, AGASHE K, AMSLER C, et al. Review of particle physics [J]. Chin Phys C, 2014, 38(09): 090001.

第46卷第4期 中国科学技术大学学报 Vol. 46, No. 4
2016年4月 JOURNAL OF UNIVERSITY OF SCIENCE AND TECHNOLOGY OF CHINA Apr. 2016

Article ID:0253-2778(2016)04-0316-07

Experiments on form factors

JOHANSSON Tord

(*Department of Physics and Astronomy, Uppsala University, Uppsala* 75105, *Sweden*)

Abstract: The experimental situation for ground state baryon electromagnetic form factors in the space-like and the time-like regions is reviewed together with an outlook.

Key words: baryon; proton; neutron; hyperon; electromagnetic form factor

CLC number: O572.3 **Document code**: A doi:10.3969/j.issn.0253-2778.2016.04.009

Citation: JOHANSSON Tord. Experiments on form factors[J]. Journal of University of Science and Technology of China, 2016,46(4):316-322.

形状因子的实验现状

JOHANSSON Tord

(乌普萨拉大学物理学和天文学系,乌普萨拉 75105, 瑞典)

摘要:阐述了类空空间和类时空间基态重子电磁形状因子的实验现状及其展望,并进行了展望.

关键词:重子;质子;中子;超子;电磁形状因子

0 Introduction

Electromagnetic form factors (EMFF's) are among the most basic properties that describe the internal structure of hadrons. They give direct access to their spatial charge and magnetisation distributions. The knowledge of these is, however, far from complete and several open questions are awaiting their answer. This review deals with EMFF's of ground state baryons. These are studied in two kinematically different domains: The space-like (SL) region is studied by elastic electron-baryon scattering, whereas the time-like (TL) region is studied in electron-positron annihilation into a baryon-antibaryon pair, or vice versa. The topic of elastic EMFF's has been addressed recently by several review articles and the reader is referred to these (Refs. [1-4]) for a more thorough presentation.

1 Space-like form factors

The most abundant information on EMFF's comes from elastic scattering of electrons on nucleons. This process is visualised in Fig. 1.

It has been assumed that this single virtual photon exchange process gives a good description of the scattering reaction. The upper electromagnetic vertex in Fig. 1 is well known and the baryon electromagnetic properties are contained in the lower non-pointlike baryon vertex. The 4-momentum squared, q^2, is a negative quantity in the SL region and one therefore usually defines Q^2

Received: 2015-11-30; **Revised**: 2016-04-20

Foundation item: Supported by The Swedish Research Council.

Biography: JOHANSSON Tord, PhD/Prof. Research field: high energy physics. E-mail: tord.johansson@physics.uu.se

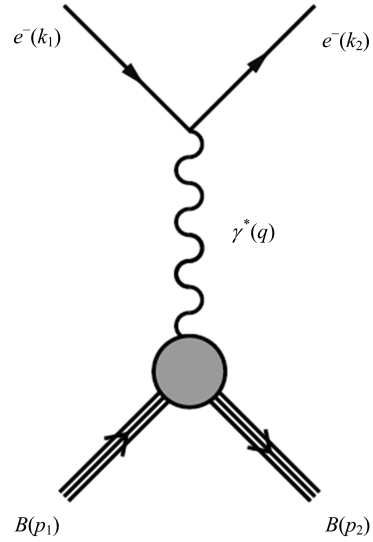

Fig. 1 Feynman diagram of the Born term for elastic electron baryon scattering

$=-q^2$. The baryon vertex matrix element can then be written as

$$\Gamma^\mu = F_1^B(Q^2)\gamma^\mu + \frac{\kappa}{2M_B}F_2^B(Q^2)i\sigma^{\mu\nu}q_\nu \qquad (1)$$

where $F_1^B(Q^2)$ and $F_2^B(Q^2)$ are related to the non-helicity-flip and helicity flip part of the hadronic current and are named Dirac and Pauli EMFF's, respectively. It is convenient to re-write these EMFF's in terms of the Sachs FF's:

$$\left.\begin{aligned} G_E &= F_1 - \tau F_2;\ \tau = \frac{Q^2}{4M_B^2} \\ G_M &= F_1 + F_2 \end{aligned}\right\} \qquad (2)$$

The Sachs FF's correspond, non-relativistically, to the Fourier transformations of the transverse charge and magnetic spatial distributions in the Breit frame. However, the interpretation becomes more complicated as the energy increases (see e. g. Ref. [1]).

The space-like elastic EMFF's have traditionally been obtained in terms of G_E^2 and G_M^2 via the Rosenbluth separation technique as

$$\left.\begin{aligned} \frac{d\sigma}{d\Omega} &= \left(\frac{d\sigma}{d\Omega}\right)_{\text{Mott}} \frac{E_e}{E_{\text{beam}}} \frac{1}{1+\tau}\left(G_E^2 + \frac{\tau}{\varepsilon}G_M^2\right)^2 \\ \varepsilon &= \frac{1}{1+2(1+\tau)\tan^2\theta_e/2} \end{aligned}\right\} \qquad (3)$$

where E_{beam} and E_e are the energy of the incoming and scattered electron, respectively, θ_e the electron scattering angle, and ε is the virtual photon polarisation[1]. The linear dependence on τ and ε of Eq. (3) allows for a definition of a reduced cross section as

$$\sigma_{\text{red}} = \frac{\varepsilon(1+\tau)}{\tau}\frac{E_{\text{beam}}}{E_e}\frac{d\sigma}{d\Omega}\Big/\left(\frac{d\sigma}{d\Omega}\right)_{\text{Mott}} = G_M^2 + \frac{\varepsilon}{\tau}G_E^2 \qquad (4)$$

Hence, σ_{red} has a linear dependence on ε at a given Q^2 with a slope proportional to G_E^2 and an intercept at G_M^2. G_E^2 and G_M^2 are therefore extracted from fits to experimental data by measuring the cross section at a given Q^2 at different energies (ε). It should be noted that the $1/\tau$ factor makes it difficult to determine G_E^2 at higher Q^2 by this method. In turn, corrections to the one-photon approximation can give sizeable impact on the small quantity G_E^2/τ and therefore on the extraction of G_E.

1.1 Proton space-like FF's

Many data have been collected on elastic electron scattering on the proton since the pioneering experiments by Hofstadter[5] in the 50's. In the static limit $G_{M_p} = \mu_p G_{E_p}$ and this is roughly consistent with data. Furthermore, the Q^2 dependence of the proton EMFF's is well characterised by a dipole behaviour: $G_D = (1+Q^2/0.71\ \text{GeV}^2)^2$. This is depicted in Fig. 2 where the G_E and G_M/μ_p are divided by G_D.

A rather coherent picture has emerged from these data. More recently, however, polarisation measurements have brought a new dimension to this topic. Two techniques have evolved:

① Polarisation transfer experiments. Here a longitudinally polarised electron transfers its polarisation to the recoiling proton. The transverse (P_t) and longitudinal (P_l) polarisation of the proton is subsequently measured via a secondary scattering. The G_E/G_M ratio is then determined from

$$\frac{G_E}{G_M} = -\frac{P_t}{P_l}\frac{(E_{\text{beam}}+E_e)}{2M_p}\tan\frac{\theta_e}{2} \qquad (5)$$

② Polarised proton target experiments. Here

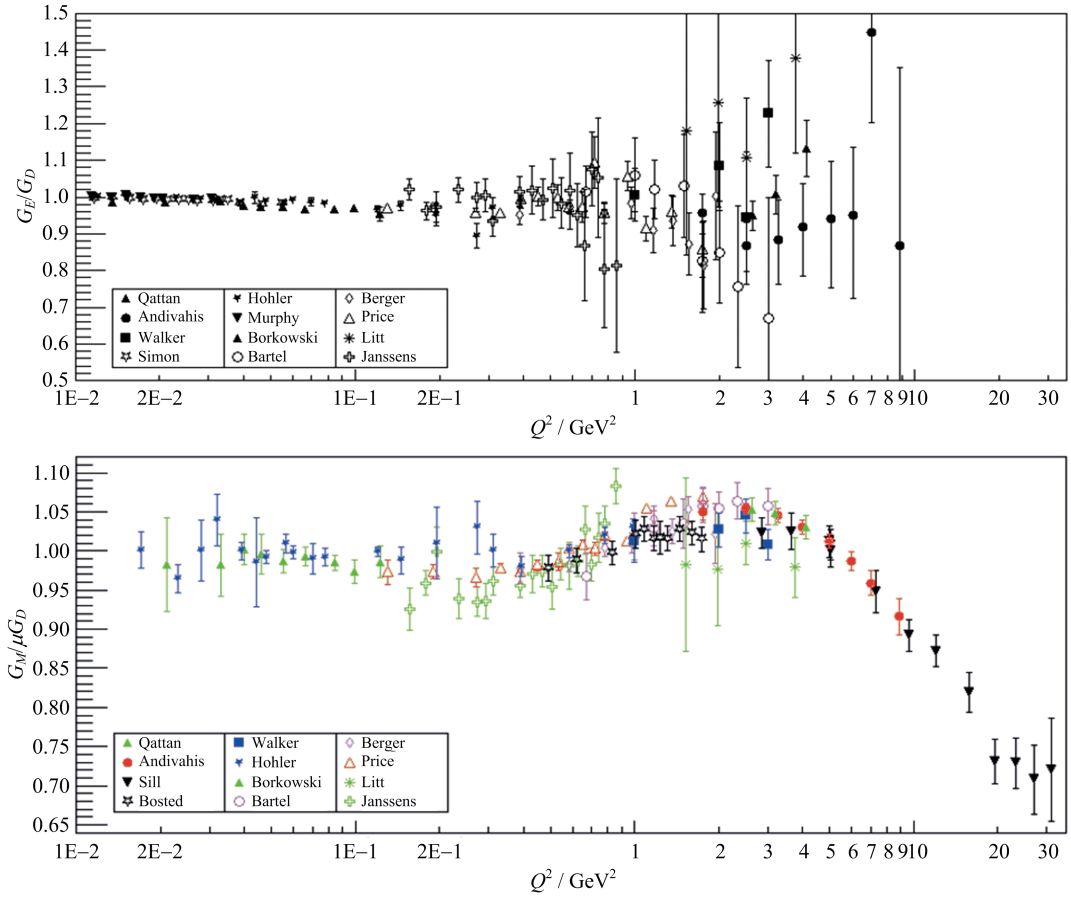

Fig. 2 Experimental data on the proton G_E (upper gure) and G_M/μ_p (lower gure) divided by the dipole function G_D (Refs. [1,3] and references therein)

one measures the asymmetry between the cross sections for the two electron helicity states, $A=(\sigma_+-\sigma_-)/(\sigma_++\sigma_-)$.

Both these methods have the advantage that they do not have the $1/\tau$ suppression of the G_E term and that many systematical effects cancel when taking ratios. See e. g. Ref. [1] for more details. It came as a big surprise when the polarisation measurements of $\mu_p G_{E_p}/G_{M_p}$ from JLab showed a distinct difference from the results obtained from the Rosenbluth separation method as shown in Fig. 3.

Whereas the Rosenbluth separation indicates a constant ratio up to a Q^2 of 10 GeV^2 the polarisation data show a linear decrease of the ratio with Q^2, even indicating a zero-crossing in the region of $Q^2\approx 10$ GeV^2. Why this difference? It is generally believed that the polarisation data are more accurate and one plausible explanation is that the Rosenbluth separation is much more sensitive to contributions from two-photon exchanges. This would then be reflected by this difference. A way to test this hypothesis is to measure the ratio $R=\sigma(e^+p)/\sigma(e^-p)$ since the two-photon contribution enters with different signs for the two cases. It is not straightforward, however, to make precise comparisons of different experiments due to different systematical uncertainties. A way out of this difficulty is offered by the CLAS experiment at JLab by using a beam that simultaneously contains electrons and positrons created by pair-production of high energy photons[6]. The result is not conclusive due to the statistics but points towards the two-photon hypothesis being correct.

Another proton puzzle is the difference in the charge RMS radius extracted from electron

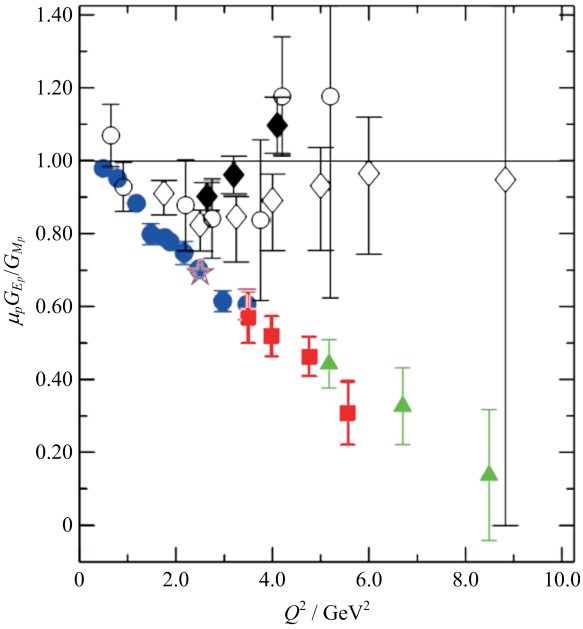

Adapted from Ref. [3]

Fig. 3 Experimental data on the ratio $\mu_p G_{E_p}/G_{M_p}$ extracted using Rosenbluth separation (black symbols) and polarisation measurements (coloured symbols)

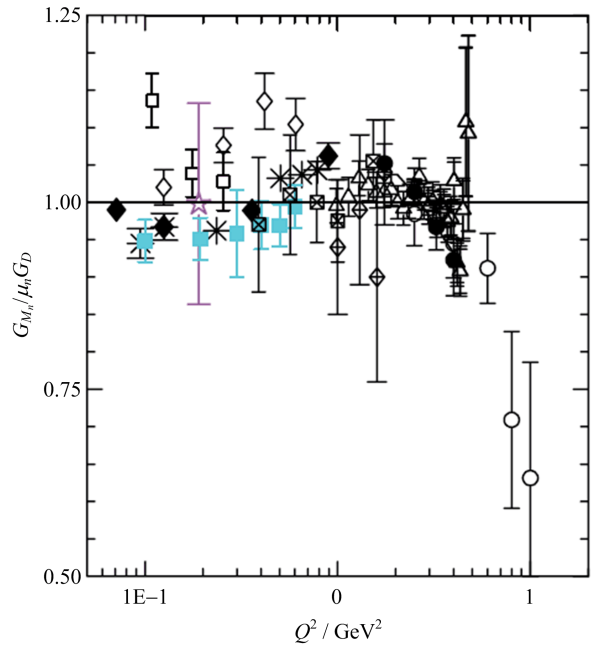

Adapted from Ref. [3]

Fig. 4 Experimental data on the ratio $G_{M_n}/\mu_n G_D$ extracted using Rosenbluth separation (black symbols) and polarisation measurements (coloured symbols)

scattering data at low Q^2 and Lamb-shift measurements in muonic and ordinary hydrogen. This topic is covered in several contributions to these proceedings and the reader is referred to these contributions for more details.

1.2 Neutron space-like FF's

Much less data are available on neutron space-like FF's. G_{E_n} and G_{M_n} have traditionally been extracted from quasi-elastic electron scattering from deuteron targets. The Rosenbluth separation requires large corrections in this case, however. More recent polarisation measurements employ polarised deuteron and ^{3}He targets.

The data on G_{M_n} agree well with the same dipole expression as for the proton, as can be seen in Fig. 4, pointing to the similarity between G_{M_n} and G_{M_p}. See e. g. Refs. [1-2] for more details.

2 Time-like form factors

Baryon form factors in the time-like region are extracted from measurements of the produced particles in $e^-\ e^+ \leftrightarrow B\ \overline{B}$ reactions as depicted in Fig. 5.

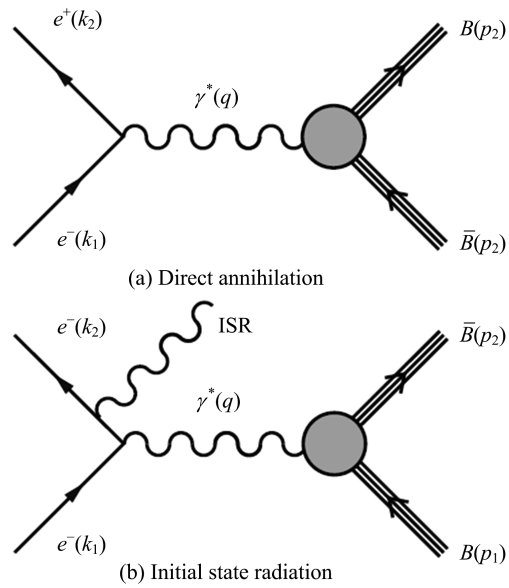

Fig. 5 Feynman diagrams of the Born term for processes used to determine baryon time-like FF's

The FF's in the TL region are complex functions

$$\left.\begin{aligned}\mathrm{Re}[G_E(q^2)G_M^*(q^2)] &= |G_E(q^2)||G_M(q^2)|\cos\phi\\ \mathrm{Im}[G_E(q^2)G_M^*(q^2)] &= |G_E(q^2)||G_M(q^2)|\sin\phi\end{aligned}\right\} \quad (6)$$

where ϕ is the relative phase between G_E and G_M. This relative phase gives polarisation effects on the final state even if the initial state is unpolarised. Assuming one photon exchange (Born term) one can extract information on the TL FF's from the differential cross section according to

$$\left.\begin{aligned}&\frac{\mathrm{d}\sigma}{\mathrm{d}\cos\theta}=\\&\quad\frac{\alpha^2\beta C}{4q^2}\left(|G_M|^2(1+\cos^2\theta)+\frac{1}{\tau}|G_E|^2\sin^2\theta\right)\\&\tau=\frac{q^2}{4M_B^2},\ \beta=\sqrt{1-1/\tau},\\&C=y/(1-\mathrm{e}^{-y}),\ y=\pi\alpha/\beta\end{aligned}\right\}\tag{7}$$

where C is a Coulomb factor. At the kinematical threshold are $\tau=1$ and $G_E=G_M$. It should be noted that the Coulomb factor implies a non-zero cross section at threshold for charged final states, whereas $C=1$ for the neutral case. $\mathrm{Re}[G_E(q^2)G_M^*(q^2)]$ and $\mathrm{Im}[G_E(q^2)G_M^*(q^2)]$ are related to the polarisation P_y and the spin correlation C_{xz} by the relations[7]

$$P_y=-\frac{\sin 2\theta\,\mathrm{Im}[G_EG_M^*]/\sqrt{\tau}}{(|G_E|^2\sin^2\theta)/\tau+|G_M|^2(1+\cos^2\theta)}=-\frac{\sin 2\theta\sin\phi/\tau}{R\sin^2\theta/\sqrt{\tau}+(1+\cos^2\theta)}\tag{8}$$

and

$$C_{xz}=-\frac{\sin 2\theta\,\mathrm{Re}[G_EG_M^*]/\sqrt{\tau}}{(|G_E|^2\sin^2\theta)/\tau+|G_M|^2(1+\cos^2\theta)}=-\frac{\sin 2\theta\cos\phi/\tau}{R\sin^2\theta/\tau+(1+\cos^2\theta)/R}\tag{9}$$

The coordinate system is defined such that y is normal to the scattering plane, z in the direction of the outgoing (anti) baryon and x defines a right handed system.

The TL FF q^2 dependence is either obtained from an energy scan as shown in Fig. 5(a) or by using the initial state radiation (ISR) technique as shown in Fig. 5(b). The latter allows for an energy scan while staying at a fixed energy due to the energy distributions of the ISR photons. This has the advantage that all q^2 are sampled simultaneously, and by these minimising systematic uncertainties. Another advantage is that the final state baryons are not produced at rest at the kinematical threshold using ISR. All this is, however, at the expense of a lower luminosity.

The data from experiments in the TL region are often limited and do not allow for a statistically significant determination of $|G_E|^2$ and $|G_E|^2$ individually. Most experiments quote therefore an effective FF, $|G_{\mathrm{eff}}|^2$, based on the total cross section

$$|G_{eff}|=\left(\frac{\sigma_{\mathrm{tot}}}{\frac{4\pi\alpha^2\beta}{3q^2}C\left(1+\frac{2M_B^2}{q^2}\right)}\right)^{\frac{1}{2}}=\left(\frac{q^2|G_M|^2+2M_B^2|G_E|^2}{q^2+2M_B^2}\right)^{\frac{1}{2}}\tag{10}$$

2.1 Proton time-like FF's

A compilation of proton effective time-like FF is shown in Fig. 6. The most extensive data sets come from the BaBar experiment (Refs. [8-9]) using ISR whereas the other data points are taken at fixed energies (see Ref. [10] and references therein).

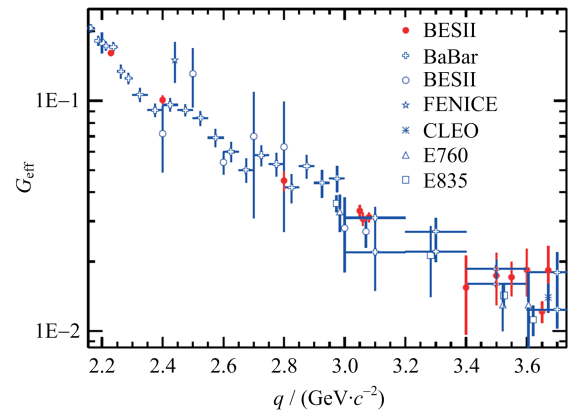

Fig. 6 Plot of the proton effective time-like form factor[10]

There are several open questions concerning proton TL FF's. There is an unexpected increase of $|G_{\mathrm{eff}}|$, i. e. an increase of the cross section with respect to phase space behaviour as one approaches the kinematical threshold in e^+e^- collisions. There are also discrepancies between the experiments that have extracted $|G_E|/|G_M|$ near threshold[8,11]. There are recent results from BESIII that in this region but the statistics are not sufficient to be decisive[10]. Furthermore, there is a structure in

the BaBar data in the region of $q^2<3$ GeV/c as can be seen in Fig. 6. The reason for this structure is not known but it has recently been pointed out in Ref. [12] that the data seem to exhibit an oscillartory pattern, hinting towards some kind of interference effect.

2.2 Neutron time-like FF's

Data are very scarce on the neutron time-like FF's. Few data points on the effective form factor exist from the FENICE experiment at DAϕNE[13] and, more recently, from the SND experiment at VEPP-2000[14]. These data are compatible with the corresponding data on the proton. More details on this topic are given in the contribution from A. Korol in these proceedings.

2.3 Hyperon time-like FF's

Only time-like FF's are accessible for the hyperons due to their short lifetime. Their production in e^+e^- collision is therefore the best way to study their electromagnetic structure. Hyperons also offer a straightforward access to polarisation variables since many of them decay via parity violating weak decays.

Data exist from BaBar[15], CLEO-C[16]. New, preliminary data from BESIII are presented at this workshop by Y. Wang. The BaBar experiment did employ the ISR technique whereas CLEO-C and BESIII use discrete energies. The most complete data set comes from the BaBar experiment which encompasses data on the effective FF of both Λ and Σ^0[15]. These data are displayed in Fig. 7.

One remarkable feature about these data is that there seems to be an enhancement of the cross section as one approaches the kinematical threshold. This is further emphasised in new preliminary data from BESIII presented at this meeting. None of the published data on the hyperon channels have large enough statistics to determine $|G_E|$ and $|G_M|$ or even their ratio with any statistical accuracy. This situation is about to be changed by a recent measurement by BESIII as reported by Y. Wang. There is even the prospect to measure the phase, including the sign, between

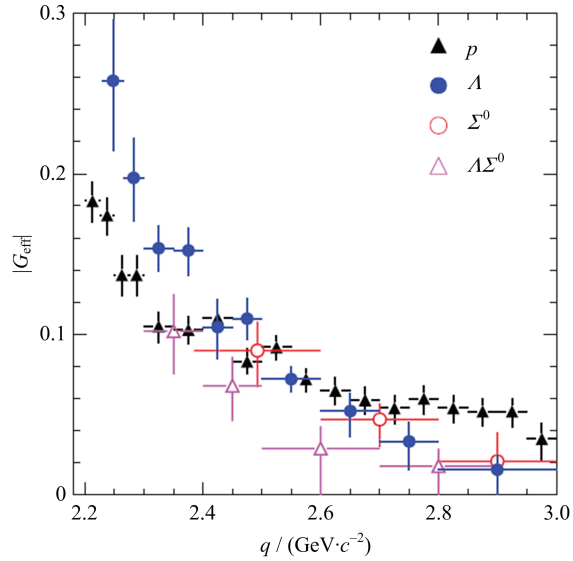

Adapted from Ref. [15]

Fig. 7 Plot of hyperon effective TL FF from the BaBar experiment. The proton effective TL FF is also displayed for comparison

$|G_E|$ and $|G_M|$ for the Λ hyperons.

3 Conclusion and outlook

A lot of progress has been made over the last years on baryon ground state form factors but we still lack a unified understanding of their space-like and time-like form factors. These data have also raised new questions that need to be answered.

① Up to which momentum transfers is the Rosenbluth separation technique valid and how sensitive are different experimental observables?

② Is the proton radius puzzle real?

③ What is the reason for the structure in the proton time-like FF?

④ What is the reason for the threshold enhancement for baryon time-like FF's?

⑤ From what momentum transfer do interpretations based on perturbative QCD for space-like and time-like FF's start to become valid?

New data from JLab 12 GeV, BESIII and the PANDA experiment at FAIR will hopefully be decisive in answering these questions.

References

[1] PERDRISAT C F, PUNJABI V, VANDERHAEGEN

M. Nucleon electromagnetic form factors[J]. Prog Part Nucl Phys, 2007,59(2): 694-764.

[2] DENIG A. AND SALMÈ G. Nucleon electromagnetic form factors in the timelike region[J]. Prog Part Nucl Phys,2013, 68:113-157.

[3] PUNJABI V, PERDRISAT C F, JONES M K, et al. The structure of the nucleon: Elastic electromagnetic form factors[J]. Eur Phys J A, 2015, 51: 79.

[4] PACETTI S, BALDINI FERROLLI R, TOMASI-GUSTAFSSON E. Proton electromagnetic form fators: Basic notions, present achievements and future perspectives[J]. Phys Rep, 2015, 550-551: 1-104.

[5] HOFSTADTER R, MCALLISTER R W. Electron scattering from the proton[J]. Phys Rev, 1955, 98:217.

[6] ADIKARAM D, RIMAL D, WEINSTEIN L B, et al. Towards a resolution of the proton form factor problem: New electron and positron scattering data [J]. Phys Rev Lett, 2015,114: 062003.

[7] DUBNIČKOVÁ A Z, DUBNIČKA S, REKALO M P. Investigation of the baryon electromagnetic structure by polarization effects in $e^+ e^- \to B\overline{B}$ processes[J]. Nuov Cim A,1996, 109(3): 241-256.

[8] LEES J P, POIREAU V, TISSERAND V, et al. Study of $e^+ e^- \to p\bar{p}$ via initial state radiation at BaBar [J]. Phys Rev D, 2013,87: 092005.

[9] LEES J P, POIREAU V, TISSERAND V, et al. Measrement of the $e^+ e^- \to p\bar{p}$ cross section in the energy range from 3.0 to 6.5 GeV[J]. Phys Rev D, 2013, 88: 072009.

[10] ABLIKIM M, ACHASOV M N, Ai X C, et al. Measurment of the proton form factor by studying $e^+e^- \to p\bar{p}$[J]. Phys Rev D, 2015,91:112004.

[11] BARDIN G, BURGUN G, CALABRESE R, et al. Determination of the electric and magnetic form factors of the proton in the time-like region[J]. Nucl Phys B, 1994,411(1):3-32.

[12] Bianconi A, Tomasi-Gustafsson E. Periodic interference structures in the timelike proton form factor[J]. Phys Rev Lett, 2015,114:232301.

[13] ANTONELLI A, BALDINI R, BENASI P, et al. The first measurement of the neutron electromagnetic form factors in the time-like region[J]. Nucle Phys B, 1998,517(1/2/3):3-35.

[14] ACHASOV M N, BARNYAKOV A YU, BELOBORODOV K I, et al. Study of the process $e^+e^- \to n\bar{n}$ at the VEPP-2000 $e^+ e^-$ collider with the SND detector[J]. Phys Rev D, 2014,90:112007.

[15] AUBERT B, BONA M, BOUTIGNY D, et al. Study of $e^+e^- \to \Lambda\bar{\Lambda}$, $\Lambda\bar{\Sigma}^0$, $\Sigma^0\bar{\Sigma}^0$ using initial state radiation with BABAR[J]. Phys Rev D,2007, 76: 092006.

[16] DOBBS S, TOMARADZE A, XIAO T, et al. First measurements of timelike form factors of the hyperons, $\Lambda^0, \Sigma^0, \Sigma^+, \Xi^0, \Xi^-$, and Ω^-, and evidence of diquark correlations[J]. Phys Lett B, 2014,739: 90-94.

第46卷第4期 中国科学技术大学学报 Vol. 46, No. 4
2016年4月 JOURNAL OF UNIVERSITY OF SCIENCE AND TECHNOLOGY OF CHINA Apr. 2016

Article ID:0253-2778(2016)04-0323-08

Preliminary results on pion form factor at CMD-3

AKHMETSHIN R. R.[1,2], AMIRKHANOV A. N.[1,2], ANISENKOV A. V.[1,2], AULCHENKO V. M.[1,2], BANZAROV V. Sh.[1], BASHTOVOY N. S.[1], BERKAEV D. E.[1], BONDAR A. E.[1,2], BRAGIN A. V.[1], FEDOTOVICH G. V.[1,2], EIDELMAN S. I.[1,2], EPIFANOV D. A.[1], EPSHTEYN L. B.[1,2,3], EROFEEV A. L.[1,2], GAYAZOV S. E.[1,2], GREBENUKV A. A.[1,2], GRIBANOVV S. S.[1,2], GRIGORIEV D. N.[1,2,3], IGNATOV F. V.[1], IVANOV V. L.[1,2], KARPOV S. V.[1], KAZANIN V. F.[1,2], KHAZIN B. I.[1,2], KOOP I. A.[1,2], KOROBOV A. A.[1,2], KOVALENKO O. A.[1,2], KOZYREV A. N.[1,2], KOZYREV E. A.[1,2], KROKOVNY P. P.[1,2], KUZMENKO A. E.[1,2], KUZMIN A. S.[1,2], LOGASHENKO I. B.[1,2], LUKIN P. A.[1,2], MIKHAILOV K. Yu.[1,2], OKHAPKIN V. S.[1], PESTOV Yu. N.[1], POPOV A. S.[1,2], RAZUVAEV G. P.[1,2], RUBAN A. A.[1,2], RYSKULOV N. M.[1], RYZHENENKOV A. E.[1,2], SHEBALIN V. E.[1,2], SHWARTZ B. A.[1,2], SHWARTZ D. B.[1,2], SIBIDANOV A. L.[4], SHATUNOV Yu. M.[1], SOLODOV E. P.[1,2], SHEMYAKIN D. N.[1,2], TITOV V. M.[1], TALYSHEV A. A.[1,2], VOROBIOV A. I.[1], YUDIN Yu. V.[1,2]

(1. *Budker Institute of Nuclear Physics, Novosibirsk* 630090, *Russia*;
2. *Novosibirsk State University, Novosibirsk* 630090, *Russia*;
3. *Novosibirsk State Technical University, Novosibirsk* 630092, *Russia*;
4. *Falkiner High Energy Physics, Department, School of Physics, University of Sydney, New South Wales* 2006, *Australia*)

Abstract: The CMD-3 detector has been successfully collecting data at the electron-positron collider VEPP-2000 since December 2010. The first scan below 1 GeV for a $\pi^+\pi^-$ measurement was performed in 2013. The collected data sample corresponds to about 18 pb^{-1} of integrated luminosity in this energy range. Analysis of the $e^+e^- \to \pi^+\pi^-$ cross section is in progress. Preliminary results of this measurement are presented.

Key words: pion form factor; electron positron collider; hadron cross section

CLC number: O572.3 **Document code**: A doi:10.3969/j.issn.0253-2778.2016.04.010

Citation: AKHMETSHIN R R, AMIRKHANOV A N, ANISENKOV A V, et al. Preliminary results on pion form factor at CMD-3 [J]. Journal of University of Science and Technology of China, 2016,46(4):323-330.

CMD-3 实验 π 介子形状因子的初步结果

AKHMETSHIN R. R.[1,2], AMIRKHANOV A. N.[1,2], ANISENKOV A. V.[1,2], AULCHENKO V. M.[1,2], BANZAROV V. Sh.[1], BASHTOVOY N. S.[1], BERKAEV D. E.[1],

Received: 2015-11-30; **Revised**: 2016-04-20

Foundation item: Supported by the Russian Science Foundation (14-50-00080), Russian Foundation for Basic Research (13-02-00215-a, 13-02-01134-a, 14-02-00580-a, 14-02-31275-mol-a, 14-02-00047-a, 14-02-31478-mol-a, 14-02-91332, 15-02-05674).

Corresponding author: IGNATOV F. V., male, PhD. Research field: particle physics. E-mail: ignatov@inp.nsk.su

BONDAR A. E.[1,2], BRAGIN A. V.[1], FEDOTOVICH G. V.[1,2], EIDELMAN S. I.[1,2], EPIFANOV D. A.[1], EPSHTEYN L. B.[1,2,3], EROFEEV A. L.[1,2], GAYAZOV S. E.[1,2], GREBENUKV A. A.[1,2], GRIBANOVV S. S.[1,2], GRIGORIEV D. N.[1,2,3], IGNATOV F. V.[1], IVANOV V. L.[1,2], KARPOV S. V.[1], KAZANIN V. F.[1,2], KHAZIN B. I.[1,2], KOOP I. A.[1,2], KOROBOV A. A.[1,2], KOVALENKO O. A.[1,2], KOZYREV A. N.[1,2], KOZYREV E. A.[1,2], KROKOVNY P. P.[1,2], KUZMENKO A. E.[1,2], KUZMIN A. S.[1,2], LOGASHENKO I. B.[1,2], LUKIN P. A.[1,2], MIKHAILOV K. Yu.[1,2], OKHAPKIN V. S.[1], PESTOV Yu. N.[1], POPOV A. S.[1,2], RAZUVAEV G. P.[1,2], RUBAN A. A.[1,2], RYSKULOV N. M.[1], RYZHENENKOV A. E.[1,2], SHEBALIN V. E.[1,2], SHWARTZ B. A.[1,2], SHWARTZ D. B.[1,2], SIBIDANOV A. L.[4], SHATUNOV Yu. M.[1], SOLODOV E. P.[1,2], SHEMYAKIN D. N.[1,2], TITOV V. M.[1], TALYSHEV A. A.[1,2], VOROBIOV A. I.[1], YUDIN Yu. V.[1,2]

(1. 布德克尔核物理研究所,新西伯利亚 630090,俄罗斯;2. 新西伯利亚州立大学,新西伯利亚 630090,俄罗斯;
3. 新西伯利亚州立理工大学,新西伯利亚 630092,俄罗斯;
4. 悉尼大学物理学院,福基纳高能物理,新南威尔士州 2006, 澳大利亚)

摘要:自 2010 年 12 月起,坐落在正负电子对撞机 VEPP-2000 上的 CMD-3 探测器成功取数. 2013 年首次在对撞能量小于 1 GeV 能区进行扫描,并获取积分亮度为 18 pb^{-1}的数据. 本文给出了 $e^+e^-\to\pi^+\pi^-$ 截面的初步结果.

关键词:π 介子形状因子;正负电子对撞机;强子截面

0 Introduction

The total $e^+e^-\to hadrons$ cross section (or $R(s)$) is important for calculation of various physical quantities: $\alpha_{QED}(M_Z)$ used in precise tests of EW physics, and better precision of this value is required in the case of ILC[1]. Also $R(s)$ is essential for the interpretation of precise measurements of the anomalous magnetic moment of the muon $a_\mu=(g-2)/2$[2]. The comparison of this experimental value to the theoretical prediction provides a powerful test of the Standard Model.

The dominant contribution to production of hadrons in the energy range $\sqrt{s}<1$ GeV comes from the $e^+e^-\to\pi^+\pi^-$ mode. This channel gives the main contribution to the hadronic term and overall theoretical precision of a_μ. And in the light of new $g-2$ experiments at FNAL and J-PARC, which plan to reduce an error by a factor of 4, it is very desirable to improve systematic precision of the $\pi^+\pi^-$ cross section at least by a factor of two.

At CMD-2 this process was measured in the energy range from 0.37 GeV to 1.38 GeV[3-6]. The 0.6% ~ 0.8% systematic uncertainty of this measurement was achieved for $\sqrt{s}<1$ GeV. For energies above 1 GeV it varies from 1.2% to 4.2%. SND measured the $e^+e^-\to\pi^+\pi^-$ cross section in the energy range 0.39~0.97 GeV with the systematic uncertainty of 1.3%[7].

1 VEPP-2000 and CMD-3

The electron-positron collider VEPP-2000[8-9] has been operating at Budker Institute of Nuclear Physics since 2010. The collider is designed to provide luminosity up to 10^{32} cm$^{-2}\cdot$s^{-1} at the maximum center-of-mass energy $\sqrt{s}=2$ GeV. At present two detectors, CMD-3[10-11] and SND[12], are installed in the interaction regions of the collider. In 2010 both experiments started data taking. The physics program[13] includes high precision measurements of the $e^+e^-\to hadrons$ cross sections in the wide energy range up to 2 GeV, studies of known and searches for new vector mesons, studies of $n\bar{n}$ and $p\bar{p}$ production

cross sections near the threshold and searches for exotic hadrons. It requires a detector with high efficiency for multiparticle events and good energy and angular resolution for charged particles as well as for photons.

CMD-3 (Cryogenic Magnetic Detector) is a general-purpose detector, see Fig. 1. Coordinates, angles and momenta of charged particles are measured by the cylindrical drift chamber with a hexagonal cell for uniform reconstruction of tracks.

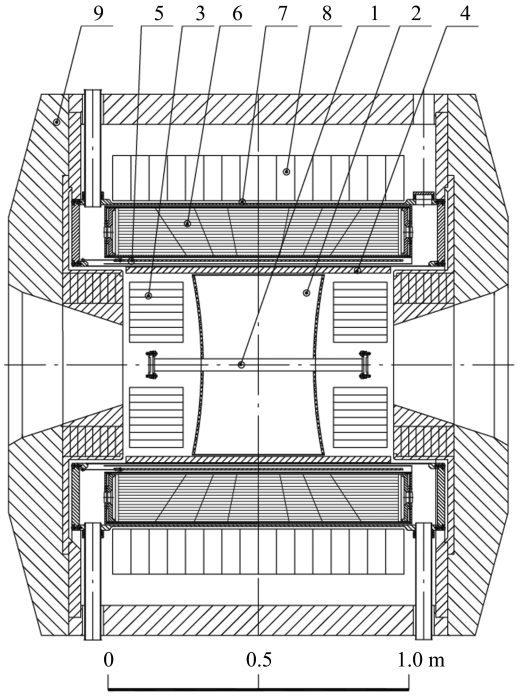

1 - beam pipe, 2 - drift chamber, 3 - BGO calorimeter, 4 - Z—chamber, 5 - SC solenoid (0.13 X_0, 13 kGs), 6 - LXe calorimeter, 7 - TOF system, 8 - CsI electromagnetic calorimeter, 9 - yoke, not shown muon range system

Fig. 1 CMD-3 detector

The calorimetry is performed with the endcap BGO calorimeter and the barrel calorimeter. The barrel calorimeter, placed outside of the superconducting solenoid with 1.3 T magnetic field, consists of two systems: ionization Liquid Xenon calorimeter surrounded by the CsI scintillation calorimeter. The total thickness of the barrel calorimeter is about 13.5 X_0. The LXe calorimeter has seven layers with strip readouts which give information about a shower profile and are also able to measure coordinates of photons with high accuracy of about a millimeter precision.

The 10^{31} $cm^{-2} \cdot s^{-1}$ luminosity was reached by the VEPP-2000 collider. The already collected integrated luminosity is about 60 pb^{-1} per detector in the full energy range, where about 18 pb^{-1} was collected below the ϕ energy. The luminosity at high energy was limited by a deficit of positrons and maximum energy of the booster (825 MeV now), and after upgrade of the accelerator complex we expect the luminosity to gain by a factor of ten. The new positron injection facility and achieved operational experience will also improve luminosity at low energy.

The first energy scan below 1 GeV for a $\pi^+\pi^-$ measurement was performed at VEPP-2000 in 2013. The luminosity of the already collected data sample is higher than that in the previous CMD-2 experiment and is similar to or better than that in the BaBar[14] and KLOE[15-16] experiments (Fig. 2).

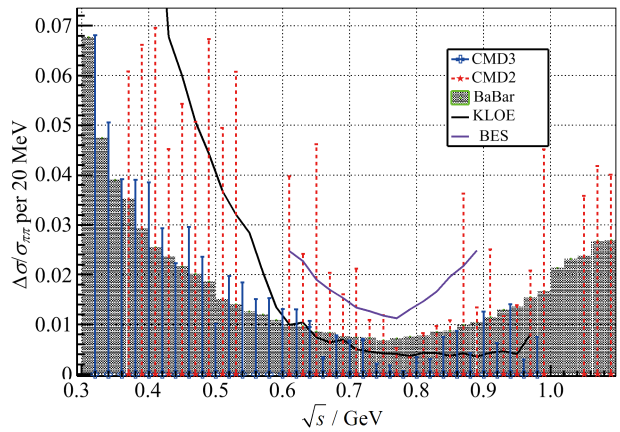

Fig. 2 Statistical precision of $|F_\pi|^2$ from the CMD-3 data in comparison with CMD-2, BaBar, KLOE and BESIII results

2 Data analysis

The $\pi^+\pi^-$ process has a simple event signature with 2 back-to-back charged particles. They can be selected by using the following criteria: two collinear well reconstructed charged tracks are detected, these tracks are close to the interaction point, fiducial volume of event is inside a good

region of the drift chamber. The selected data sample includes events with: e^+e^-, $\mu^+\mu^-$, $\pi^+\pi^-$, cosmic muons, and it practically doesn't contain any other physical background at energies $\sqrt{s} <$ 1 GeV.

These final states can be separated using either the information about energy deposition in the calorimeter or that about particle momenta in the drift chamber, as shown at Fig. 3. At low energies momentum resolution of the drift chamber is sufficient to separate different types of particles. The pion momentum is well aside from the electron one up to energies $E_{\text{beam}} \leqslant 450$ MeV, while the $\mu^+\mu^-$ events are separated from others up to $E_{\text{beam}} \leqslant 330$ MeV, and at higher energies the number of muons should be fixed relative to the number of electrons according to the QED prediction.

At higher energies the peak of electron shower in the calorimeter is far away from the peak of minimal ionization particles. The separation using energy deposition works best at higher energies and becomes less robust at lower energies. In this method the number of muons can be extracted by event separation or fixed according to QED prediction.

Determination of the number of different particles is done by minimization of the binned likelihood function, where two dimensional PDF functions are constructed in different ways for each type of information.

To construct PDF functions in the case of

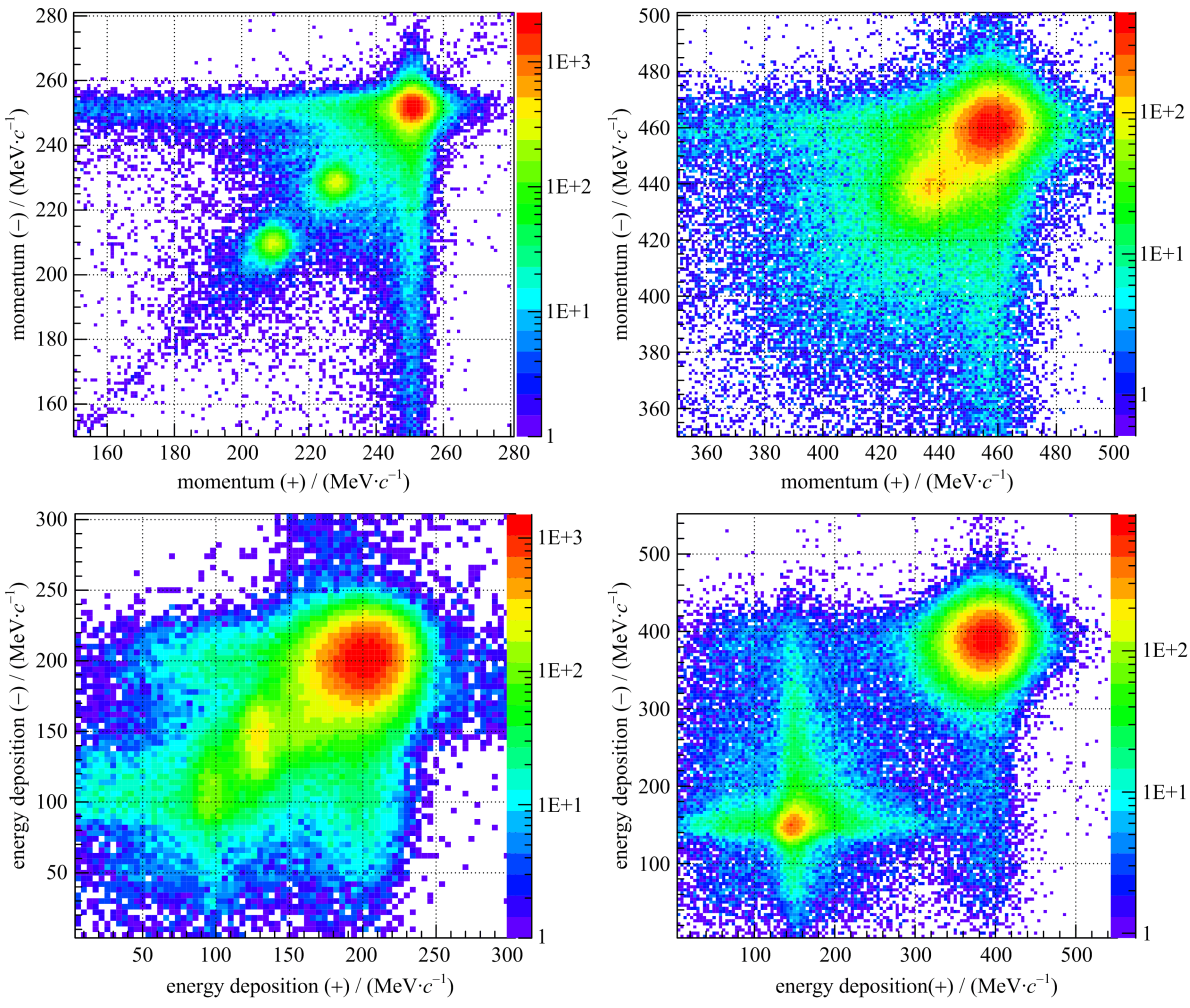

Fig. 3 Distributions of measured momenta in the drift chamber (top row) and energy deposition in the calorimeter (bottom row) of collinear events at energies E_{beam} =250 MeV (left column) and 460 MeV (right column)

event separation by particle momentum we take as an input the ideal momentum spectra for e^+e^-, $\mu^+\mu^-$, $\pi^+\pi^-$ events from the MC generator for applied selection criteria. Then the generated distributions are convolved with the detector response function which includes effects from momentum resolution, bremsstrahlung of electrons at the beampipe, pion decay in flight. The functions themselves are general enough and most of their parameters are free in minimization.

Description of cosmic events is done on the basis of experimental events with impact parameters outside of the beam interaction region.

Distributions of 3π background events (which gives a small contribution) are taken from full MC simulation. The result of minimization at $E_{\text{beam}}=252.8$ MeV is shown in Fig. 4 and for the point at the ω resonance peak $E_{\text{beam}}=391.48$ MeV in Fig. 5.

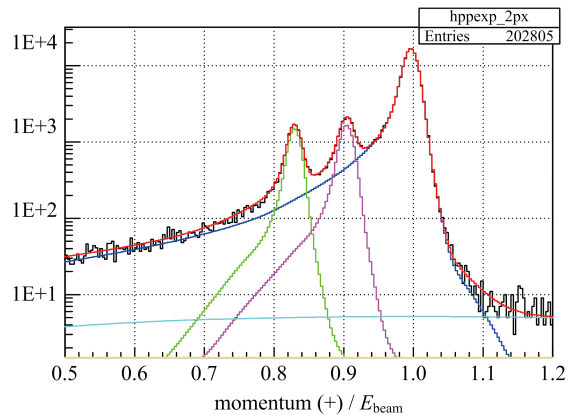

histogram-data, lines-projection of fitted functions after minimization: the peaks from left to right — π^+, μ^+, e^+, cyan line-cosmic events

Fig. 4 Momentum distribution of positive charge particles for $E_{\text{beam}}=252.8$ MeV

In the case of event separation by energy deposition of particles: the PDF distributions of energy deposition are taken from MC or data itself. Each process is fitted by its own analytical function, and then these functions are used during minimization with some free parameters. Electron distributions are described by a function with most of parameters free. Muon description is taken from simulation and convolved with additional smearing

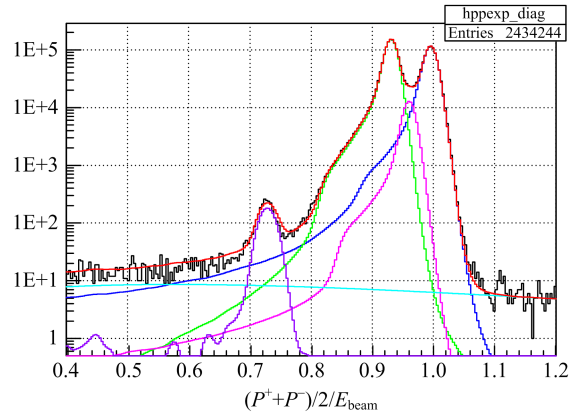

histogram-data, lines-projection of fitted functions after minimization: the peaks from left to right 3π, 2π, 2μ, e^+e^-, cyan line - cosmic events

Fig. 5 Average momentum distribution for events with $|\Delta P|/E_{\text{beam}}<0.038$, $E_{\text{beam}}=391.48$ MeV

as free parameters (it's planned to select muons totally from data). And cosmic events are selected from experimental data by the vertex position. The pion particles can be cleanly selected from huge ω, $\phi\to 3\pi$ data samples. The example of energy deposition of selected pions is shown in Fig. 6.

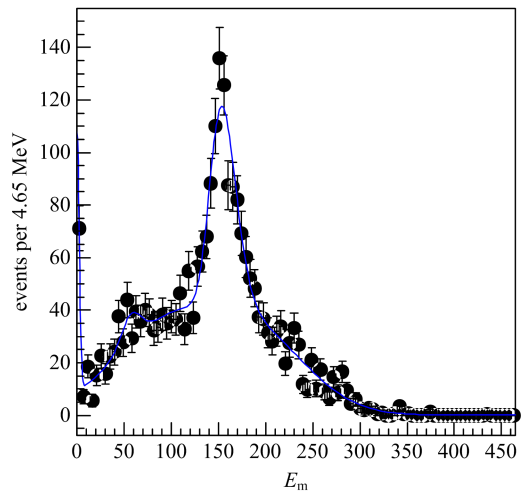

Fig. 6 Energy deposition in the calorimeter of π^- from 3π events with $P_{\pi^-}=387.5$ MeV/c

Full energy deposition in LXe with CsI calorimeters is used at the moment. An example of the minimization result at $E_{\text{beam}}=387.5$ MeV is shown in Fig. 7.

As further development, one can use a neural net for event classification. This can help to exploit information about the showerprofile from 7

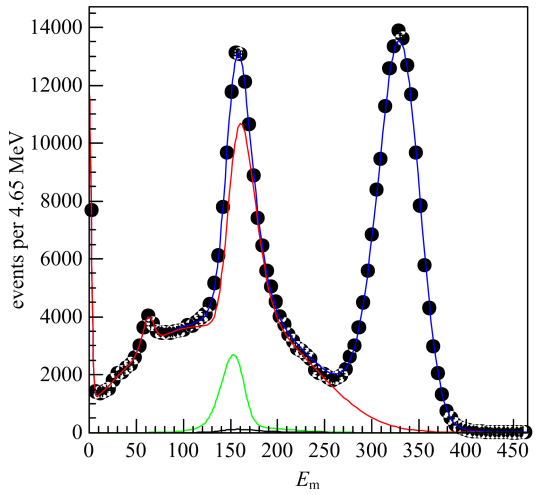

Projection to negative charge particle, where dots - data, blue line is the fit, red line - contribution from $\pi^+\pi^-$, green line — $\mu^+\mu^-$

Fig. 7 Result of event separation based on energy deposition information at E_{beam} =387.5 MeV

strip layers in the LXe and energy deposition in the CsI calorimeter.

The comparison of two approaches with the pion form factor after event separation is shown in Fig. 8, where additional corrections, common to two methods (e. g., the trigger efficiency), are not applied.

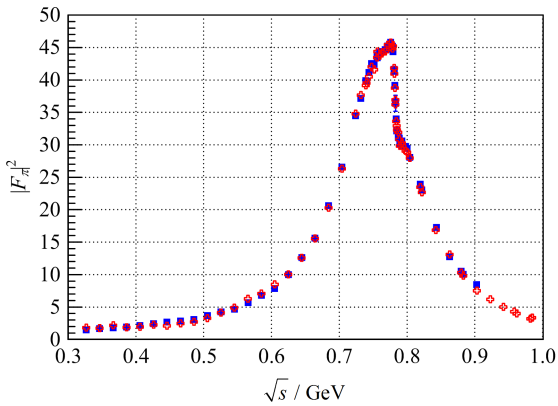

Open crosses — separation done on the calorimeter information, filled squares — on particle momentum. Some additional corrections, common to two methods (e. g., the trigger efficiency), are not applied

Fig. 8 Preliminary results on F_π^2 from CMD-3

These two methods overlap in the wide energy range and provide a cross-check of each other, allowing to reach a systematic error of event separation at the level of 0.2%.

The only significant physical background in the selected data sample is pions from 3π events at the ω energy. The total contribution from these events $N_{3\pi}/N_{ee}<0.85\%$ is small even at the peak of ω. These events are independently identified in particle separation based on momentum distributions. The $\sigma(e^+e^-\to\pi^+\pi^-\pi^0)$ cross section obtained as a by-product of this analysis agrees well with published results by CMD2 and SND experiments. The geometrical acceptance was calculated using Monte-Carlo with 3π in the phase space model, and the reconstruction efficiency is mostly the same as for studied collinear events and will be canceled during $N_{3\pi}/N_{ee}$ normalization.

3 Systematic uncertainty

The systematic error of $\pi^+\pi^-$ channel is expected to be mainly from the following sources: 0.2% — $e/\mu/\pi$ separation, 0.2% — pion specific correction, 0.1% — radiative corrections, 0.1% — fiducial volume, 0.1% — beam energy determination. The final goal of the CMD-3 experiment is to reduce an overall systematic uncertainty in this channel up to 0.35%.

In the CMD-3 detector, a polar angle of tracks is measured by the DC chamber with the help of the charge division method with the z-coordinate resolution of about 2 mm. This measurement is unstable by itself as it depends on calibration and thermal stability of electronic board parameters. An independent calibration should be applied relative to another system, such as the ZC-chamber or the LXe calorimeter. The ZC chamber is a 2-layer multiwire chamber installed at the outer radius of the DC chamber. It has a strip readout along Z coordinate, where the strip size is 6 mm and the z-coordinate resolution is about 0.7 mm for tracks with 1 radian inclination. Also the CMD-3 detector has the unique LXe calorimeter where ionization is collected in 7 layers with a cathode strip readout, where the combined strip size is 10 ~ 15 mm and coordinate resolution is about 2 mm. Both subsystems have precision for

strip position better than 100 μ m, which should give less than a 0.1% systematic contribution to luminosity determination.

Determination of the fiducial volume could be made independently with the help of the LXe and Z-chamber subsystems. It allows an efficient monitoring of detector operation stability during data taking. This monitoring shows compatibility between two subsystems inside the range $|\delta Z/Z| < 6\times10^{-4}$ for the 2013 season, which corresponds to 0.1% systematic error of luminosity determination at $\theta_{\text{track}}=1$ rad. An addition of other crosschecks of Z scale measurement (radiography of detector elements from conversion of particles, momentum versus polar angle correlation and so on) will allow to keep a systematic uncertainty from this source at the 0.1% level.

Measurement of beam energy by Compton backscattering of the laser photons with precision $\sigma_E < 50$ keV[17] will keep a systematic uncertainty from this source below 0.1%.

The reconstruction inefficiency in the CMD-3 detector is about 0.2% ~ 1%, which is 3 ~ 10 times better than was achieved by the CMD-2 experiment. Moreover, we plan to study in more detail pion specific loss because of decay in flight and nuclear interaction using $\phi, \omega \to 3\pi$ experimental data.

Another important source of systematics is theoretical precision of radiative corrections[18]. Additional studies like crosschecks of different calculation approaches and further proof from comparison with experimental data are necessary in this field. Comparison between the MCGPJ[19] and BabaYaga @ NLO[20] generators was performed. The integrated cross-section for applied cuts is well consistent at the level better than 0.1% between both tools, but strong difference in the $P^+ \times P^-$ momentum distributions is observed. Also observed is some discrepancy between experimental data and fitted functions when using event separation by momentum information, where the initial input comes from the MCGPJ generator, while BabaYaga@NLO describes the data better. One of the next steps for improvement of the MCGPJ generator can be an addition to the angular distribution for photon jets. While this discrepancy mostly doesn't affect analysis by energy deposition, it becomes crucial if momentum distribution information is used. We expect that the overall uncertainty from MC tools can be reduced to 0.1%.

One of the tests in this analysis is a measurement of the $e^+e^- \to \mu^+\mu^-$ cross section at low energy, where separation was performed using momentum information. Preliminary results of this test are consistent with the QED prediction with an overall precision of 0.5% as shown in Fig. 9.

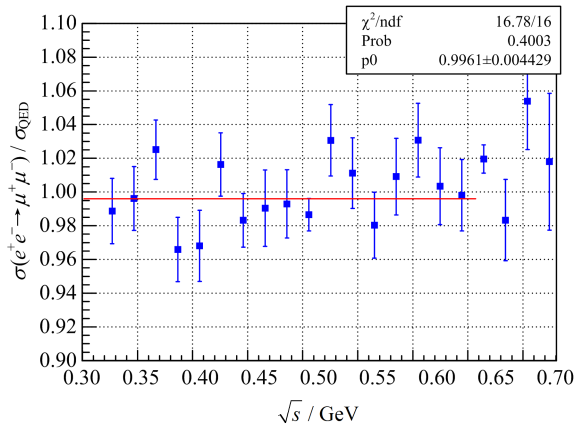

Fig. 9 Preliminary result of the measurement of muon pair production in comparison with the QED prediction

4 Conclusion

VEPP-2000 accelerator successfully operates with a goal to get ~1 fb^{-1} in 5~10 years which should provide new precise results on hadron production. The CMD-3 and SND detectors were upgraded, with significantly improved performance and monitoring capabilities of different detector subsystems. The first scan below 1 GeV for a $\pi^+\pi^-$ measurement was done in 2013. The already collected data sample has the same or better statistical precision of cross sections than was achieved by other experiments. Data analysis is in progress.

A new positron injection complex will be commissioned during this winter. The luminosity will be increased by a factor of 10 up to 10^{32} $cm^{-2} \cdot s^{-1}$ at $2E = 2$ GeV. It is expected that the new positron injection facility and achieved operational experience will also improve the luminosity at low energies for the $\pi^+\pi^-$ scan. High statistics will allow us to study and to better control different systematic contributions, with a final goal of 0.35% precision for the $\sigma(\pi^+\pi^-)$ cross section measurement.

Acknowledgements We thank the VEPP-2000 team for excellent machine operation.

References

[1] JEGERLEHNER F. Precision measurements of σ_{hadronic} for $\alpha_{\text{eff}}(E)$at ILC energies and $(g-2)_\mu$[J]. Nucl Phys B (Proc Suppl), 2006,162: 22-32.

[2] HAGIWARA K, LIAO R, MARTIN A D, et al. $(g-2)_\mu$and $\alpha(M_Z^2)$ re-evaluated using new precise data [J]. J Phys G, 2011, 38(8): 085003.

[3] AKHMETSHIN R R, ANASHKIN E V, ARBUZOV A B, et al. Update: A reanalysis of hadronic cross section measurements at CMD-2[J]. Phys Lett B, 2004,578(3/4):285-289.

[4] AULCHENKO V M, AKHMETSHIN R R, BANZAROV V sh, et al. Measurement of the pion form factor in the energy range 1.04～1.38 GeV with the CMD-2 detector[J]. JETP Lett, 2005,82(12): 743-747.

[5] AULCHENKO V M, AKHMETSHIN R R, BANZAROV V sh, et al. Measurement of the $e^+e^-\to\pi^+\pi^-$ cross section with the CMD-2 detector in the 370-520 MeV cm energy range[J]. JETP Lett, 2006, 84(8): 413-417.

[6] AKHMETSHIN R R, AULCHENKO V M, BANZAROV V Sh, et al. High-statistics measurement of the pion form factor in the rho-meson energy range with the CMD-2 detector[J]. Phys Lett B, 2007, 648(1): 28-38.

[7] ACHASOV M N, BELOBORODOV K I, BERDYUGIN A V,et al. Update of the $e^+e^-\to\pi^+\pi^-$ cross section measured by SND detector in the energy region 400 MeV$<\sqrt{s}<$1 000 MeV[J]. J Exp Theor Phys, 2006,103(3): 380-384.

[8] SHATUNOV Yu M, EVSTIGNEEV A V, GANYUSHIN D I, et al. Project of a new electron positron collider VEPP-2000[C/OL]//Proceedings of EPAC 2000. 2000: 439 [2015-11-30]. http://accelconf.web.cern.ch/accelconf/e00/PAPERS/MOP4A08.pdf.

[9] BERKAEV D, KIRPOTIN A, KOOP I, et al. VEPP-2000 operation with round beams in the energy range from 1 to 2 GeV[J]. Nucl Phys B (Proc Suppl), 2012, 225-227: 303-308.

[10] AULCHENKOV M, BANZAROV V S, AKHMETSHIN R R, et al. CMD-2M Detector Project[R/OL]. 2001:BUDKER-INP-2001-45. http://cds.cern.ch/record/606716/files/sis-2003-102.pdf.

[11] KHAZIN B. Physics and detectors for VEPP-2000[J]. Nucl Phys B (Proc Suppl), 2008,181-182: 376-380.

[12] ACHASOV M N, BERKAEV D E, BOGDANCHIKOV A G, et al. First experience with SND calorimeter at VEPP-2000 collider[J]. Nucl Instrum Meth A,2009, 598(1): 31-32.

[13] EIDELMAN S. Physics at VEPP-2000[J]. Nucl Phys B (Proc Suppl),2006,162: 323-326.

[14] LEES J P, POIREAU V, TISSERAND V, et al. Precise measurement of the $e^+e^-\to\pi^+\pi^-(\gamma)$ cross section with the initial-state radiation method at BABAR[J]. Phys Rev D, 2012,86: 032013.

[15] AMBROSINO F, ANTONELLI A, ANTONELLI M, et al. Measurement of $\sigma(e+e^-\to\pi^+\pi^-\gamma(\gamma))$ and the dipion contribution to the muon anomaly with the KLOE detector[J]. Phys Lett B, 2009, 670(4/5): 285-291.

[16] AMBROSINO F, ARCHILLI F, BELTRAME P, et al. Measurement of $\sigma(e^+e^-\to\pi^+\pi^-)$ from threshold to 0.85 GeV^2 using initial state radiation with the KLOE detector[J]. Phys Lett B,2011, 700(2): 102-110.

[17] ABAKUMOVA E V, ACHASOV M N, BERKAEV D E, et al. Backscattering of laser radiation on ultra-relativistic electrons in transverse magnetic field: evidence MeV-scale photon interference [J]. Phys Rev Lett,2013,110: 140402.

[18] ACTIS S, ARBUZOV A, BALOSSINI G, et al. Quest for precision in hadronic cross sections at low energy: Monte Carlo tools vs. experimental data[J]. Eur Phys J C,2010, 66(3): 585-686.

[19] ARBUZOV A B, FEDOTOVICH G V, IGNATOV F V, et al. Monte-Carlo generator for $e+e^-$ annihilation into lepton and hadron pairs with precise radiative corrections[J]. Eur Phys J C,2006, 46(3): 689-703.

[20] BALOSSINI G, CARLONI CALAME C M, MONTAGNA G, et al. Matching perturbative and parton shower corrections to Bhabha process at avour factories[J]. Nucl Phys B,2006,758 (1/2): 227-253.

第46卷第4期 中国科学技术大学学报 Vol. 46, No. 4
2016年4月 JOURNAL OF UNIVERSITY OF SCIENCE AND TECHNOLOGY OF CHINA Apr. 2016

Article ID:0253-2778(2016)04-0331-06

Measurement of the timelike neutron and proton form factors at VEPP-2000

KOROL A. A.[1,2] (for the CMD-3 and SND Collaborations)

(1. *Budker Institute of Nuclear Physics*, *Novosibirsk* 630090, *Russia*; 2. *Novosibirsk State University*, *Novosibirsk* 630090, *Russia*)

Abstract: Results are presented of the study of the $e^+e^- \to n\bar{n}$ and $e^+e^- \to p\bar{p}$ reactions in the energy range from the nucleons production threshold up to 2 GeV. The measurements have been performed at the VEPP-2000 e^+e^- collider with the SND and CMD-3 detectors using the events collected during the data taking runs of 2011 and 2012. Also discussed here are the obtained electromagnetic form factors of nucleons and future plans of these results improvement.

Key words: proton; neutron; electromagnetic form factor; e^+e^- annihilation; SND; CMD-3

CLC number: O572.3 **Document code**: A doi:10.3969/j.issn.0253-2778.2016.04.011

Citation: KOROL A A. Measurement of the timelike neutron and proton form factors at VEPP-2000[J]. Journal of University of Science and Technology of China, 2016,46(4):331-336.

VEPP-2000 上类时中子和质子形状因子的测量

KOROL A. A.[1,2] (CMD-3 和 SND 合作组)

(1. 布德克尔核物理研究所,新西伯利亚 630090,俄罗斯;2. 新西伯利亚州立大学,新西伯利亚 630090,俄罗斯)

摘要:利用正负电子对撞机 VEPP-2000 上 SND 和 CMD-3 探测器从 2011 至 2012 年获取的对撞数据,给出了从产生阈值到 2 GeV 能区 $e^+e^- n\bar{n}$ 和 $e^+e^- \to p\bar{p}$ 的实验结果. 同时,讨论了核子的电磁形状因子,并对结果的改进进行了展望.

关键词:质子;中子;电磁形状因子;正负电子淹没;SND;CMD-3

0 Introduction

Electromagnetic interaction of the nucleons (neutrons and protons) can be described with two complex functions of transferred momentum, the electric form factor $G_E(s)$ and the magnetic form factor $G_M(s)$. In the timelike region above nucleons production threshold ($s > 4M_N^2$) this functions can be partially extracted from the total cross section and the angle distribution in the annihilation processes $e^+e^- \to p\bar{p}$ and $e^+e^- \to n\bar{n}$.

The early results were obtained by the BaBar[1] and PS170[2] experiments for protons and in the FENICE[3] experiment for neutrons. In this paper we review the results from the CMD-3 and SND detectors for the process $e^+e^- \to p\bar{p}$, and the

Received: 2015-11-30; **Revised**: 2016-04-20

Foundation item: Supported by Russian Science Foundation (14-50-00080).

Biography: KOROL A. A., male, born in 1967, PhD. Research field: high energy physics. E-mail: A. A. Korol@inp. nsk. su

result from the SND detector for process $e^+e^- \to n\bar{n}$. The data were collected at the VEPP-2000 collider[4] during the data taking runs in 2011 and 2012 at the center of mass energy range 1.8～2.0 GeV. The collider allows to study e^+e^- collisions at the center of mass energy range 0.3～2.0 GeV with the luminosity in the studied region (～1.8 GeV) $L \approx 0.7 \times 10^{31}$ cm^{-2} · sec^{-1} and the energy spread $\delta_E \approx 0.6$ MeV. The detectors are located in the opposite sides of the VEPP-2000 collider. The data are being collected in parallel.

The SND[5-9] (Fig. 1) detector includes the drift chamber (DC), the three layer electromagnetic (EMC) NaI(Tl) calorimeter and the muon system.

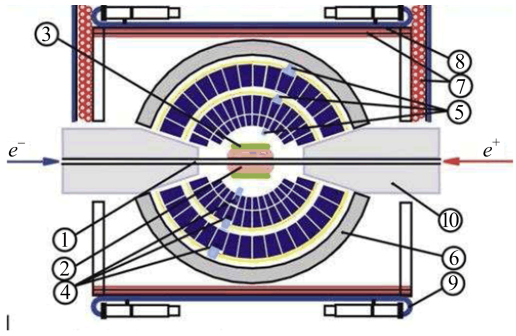

1 – beam pipe, 2 – tracking system, 3 – aerogel cherenkov counter, 4 – NaI(Tl) crystals, 5 – phototriodes, 6 – iron muon absorber, 7～9 – muon system, 10 – VEPP-2000 solenoids

Fig. 1 The SND layout

The CMD-3 detector[10-11] (Fig. 2) includes the drift chamber in the 1.3 T magnetic field, EMC

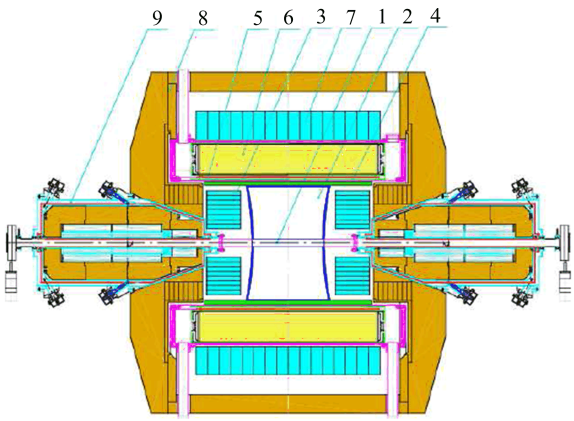

1 – vacuum chamber, 2 – drift chamber, 3 – BGO calorimeter, 4 – Z-chamber, 5 – SC solenoid, 6 – LXe calorimeter, 7 – CsI calorimeter, 8 – yoke, 9 – VEPP-2000 solenoids

Fig. 2 CMD-3 layout

calorimeter consisting of BGO endcap and two barrel layers, LXe and CsI. It also includes the muon system.

The integrated luminosity collected in the region of interest is ～8.7 pb^{-1} and summarized in Tab. 1.

Tab. 1 The integrated luminosity

experiment	IL/pb^{-1}	IL($\sqrt{s}$>1.88 GeV)/pb^{-1}
12.2010～06.2011	25	3.8
01.2012～04.2012	17	4.9
total	43	8.7

The differential cross section of the process $e^+e^- \to N\bar{N}$ can be expressed as a function of transferred momentum squared (s) and polar angle (θ):

$$\frac{d\sigma(s)}{d\Omega} = \frac{\alpha^2\beta C}{4s}\left(|G_M(s)|^2(1+\cos^2\theta) + \frac{4M_N^2}{s}|G_E(s)|^2\sin^2\theta\right) \quad (1)$$

where C is the Coulomb factor[12] taking values $C=1$ for neutron and $C \approx \frac{\pi\alpha}{\beta}\Big/(1-e^{-\frac{\pi\alpha}{\beta}})$ for proton, M_N is the nucleon mass, $G_M(s)$ and $G_E(s)$ are electric and magnetic form factors.

The full cross section then can be written as:

$$\sigma(s) = \frac{4\pi\alpha^2\beta C}{3s}\left(|G_M(s)|^2 + \frac{2M_N^2}{s}|G_E(s)|^2\right) \quad (2)$$

It is convenient to use also "effective form factor" for comparison of the results from the different experiments:

$$F(s) = \frac{|G_M(s)|^2 + \frac{2M_N^2}{s}|G_E(s)|^2}{1+\frac{2M_N^2}{s}} \quad (3)$$

The measured event distribution from cos θ can be used to obtain the ratio of electrical and magnetic form factors $\frac{G_E(s)}{G_M(s)}$.

1 CMD3 and SND $p\bar{p}$ measurements

The selection procedure of $p\bar{p}$ events depends on the proton energy. Close to the kinematic threshold both protons and antinprotons stop in the beam pipe material with loss of the proton,

while the antiproton gives an annihilation star. For the higher proton energy both the proton and the antiproton cross drift chamber, giving high dE/dX tracks. Then antiproton gives an annihilation star in the outer wall of the drift chamber.

The main criteria for selecting $p\bar{p}$ events at CMD-3 and $E_{\text{beam}}<950$ MeV (near the threshold), are the following[13]: 4 or more tracks with a common vertex found in the beam pipe material; no tracks with energy deposition in calorimeter higher than 400 MeV. At $E_{\text{beam}}\geqslant 950$ MeV two opposite-charge collinear central tracks in DC are required; the track momentum values are limited as $\frac{|p_1-p_2|}{|p_1+p_2|}<0.15$ (<0.2 for $E_{\text{beam}}<955$ MeV), and the total energy deposition in the calorimeter is >200 MeV.

The criteria at SND and $E_{\text{beam}}<960$ MeV are the following (preliminary): exactly 3 tracks with a common vertex located in the beam pipe material, and no other tracks (proton is not registered). At $E_{\text{beam}}\geqslant 960$ MeV two collinear central tracks in DC with large dE/dx are required, the total energy deposition in the calorimeter is >650 MeV, one of the tracks should not have any associated calorimeter cluster.

The $p\bar{p}$ cross sections ($\sigma_{p\bar{p}}$) were obtained from the well known expression:

$$N=\varepsilon\delta\sigma_{p\bar{p}}\cdot L \qquad (4)$$

where N is the number of events, L is the integrated luminosity, ε is the detection efficiency, and δ is the radiative correction. The systematic uncertainity is estimated to be 6% for CMD-3 and 7% for SND.

Fit of the cos θ distribution to expract $\frac{G_E}{G_M}$ is also made for both experiments. The results are $\frac{G_E}{G_M}=1.49\pm0.23\pm0.3$ at CMD-3[13] and $\frac{G_E}{G_M}=1.64\pm0.26$ at SND (preliminary result).

The cross sections for the CMD-3[13] and the SND (preliminary) are shown in Fig. 3 and Fig. 4.

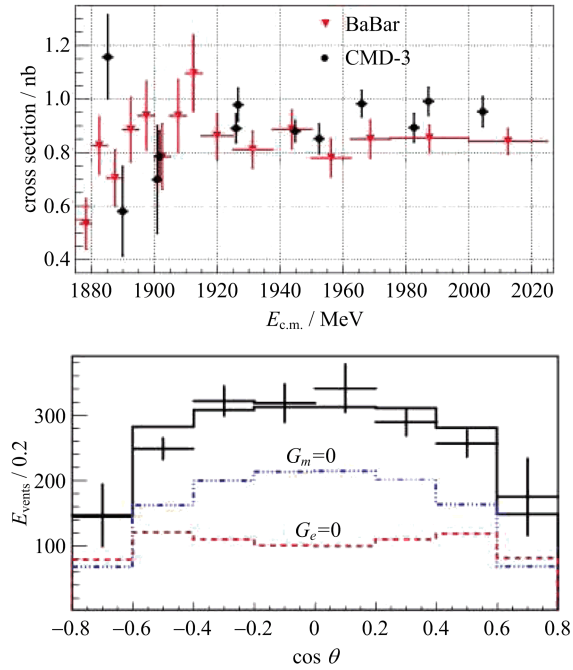

Fig. 3　The CMD-3 $p\bar{p}$ cross section and angle distribution

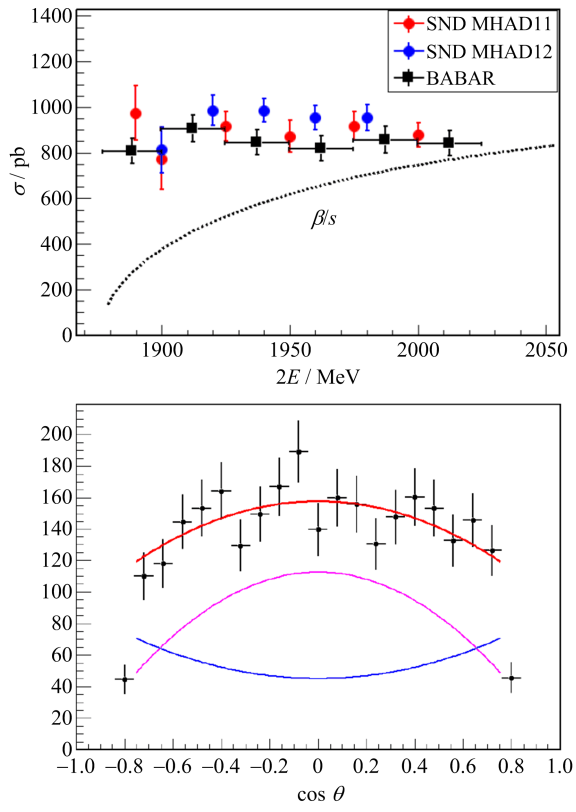

Fig. 4　The SND $p\bar{p}$ cross section and angle distribution (preliminary results)

2 SND $n\bar{n}$ measurement

To select events from the $e^+ e^- \to n\bar{n}$ process[14], all events that meet the criteria for $e^+ e^- \to e^+ e^-$ and $e^+ e^- \to 2\gamma$ are removed explicitly, cosmic background is suppressed with the muon system veto. At least two clusters in the EMC calorimeter are required in the event. Other criteria utilize the energy: 950 MeV$<E_{\rm EMC}<$1 500 MeV and the total event momentum registered in calorimeter: $P_{\rm EMC} > 0.5 \cdot E_{\rm beam}$, $25^\circ < \theta_{P_{\rm EMC}} < 155^\circ$.

To extract the cross section ($\sigma_{n\bar{n}}$) from the number of events (N) the following expression taking into account cosmic background is used:

$$N = \sigma_{\rm TH} \cdot L + \sigma_{p\bar{p},\rm VIS} \cdot L + x \cdot T + \varepsilon\delta\sigma_{n\bar{n}} \cdot L$$

where $\sigma_{p\bar{p},\rm VIS}$ is a visible $p\bar{p}$ cross section satisfying $n\bar{n}$ selection criteria, $\sigma_{\rm TH}$ is a visible cross section of processes with smooth behavior near $n\bar{n}$ pair production threshold, x is the visible cosmic events rate, T is the time of data taking for particular energy, L is the integrated luminosity, ε is the detection efficiency, and δ is the radiative correction. The visible cosmic event rate is obtained with a common fit in all energy points and found to be $(1.40\pm0.07)\times10^{-3}$ Hz. For $\sigma_{\rm TH}$ its direct measurement below $n\bar{n}$ threshold is used, but it is also estimated from possible physical background process contributions and found to be in a good agreement. The obtained cross section separately for two seasons and early data from FENICE[3] are shown in Fig. 5[14].

3 Discussion

The $e^+ e^- \to p\bar{p}$ cross section is almost constant, though it is natural to expect its decrease as $\beta/s=\dfrac{\sqrt{1-\dfrac{4M^2}{s}}}{s}$ when approaching the threshold (Fig. 4). Both SND and CMD-3 results (Fig. 6) confirm the BaBar result, that $\dfrac{G_E}{G_M}$ near threshold strongly differs from unity. This was somewhat unexpected, because of $G_E = G_M$ at threshold.

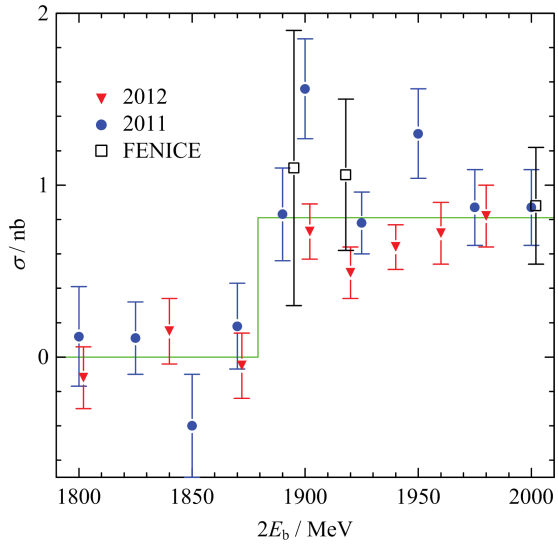

Fig. 5 The SND $n\bar{n}$ cross section

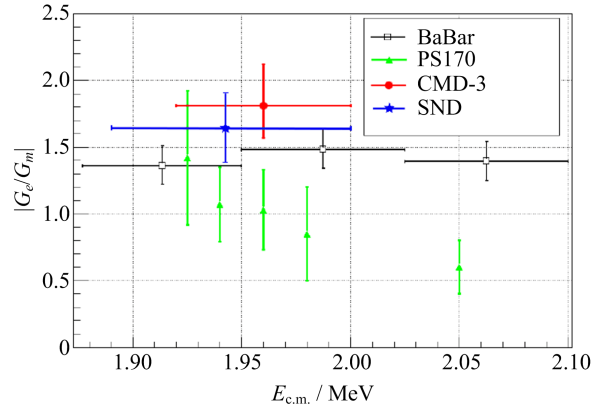

Fig. 6 The p EM form factors ratio

The $e^+ e^- \to n\bar{n}$ cross section is also constant (Fig. 5) and coincides within the errors with for $e^+ e^- \to p\bar{p}$ (Fig. 7). The $\sigma_p = \sigma_n$ relation suggests that either the isoscalar or isovector amplitude dominates in the $e^+ e^- \to n\bar{n}$ process near the threshold. The pQCD asymptotics is $\dfrac{\sigma_p}{\sigma_n}=4$.

Possible explanations of this observation could be:

① sub-threshold resonance;

② final state interaction between nucleons.

The theoretical discussion of the phenomenon on the base of Paris nucleon-antinucleon optical

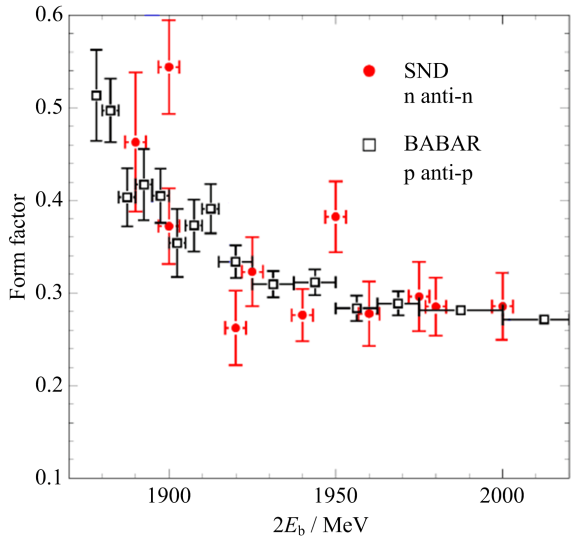

Fig. 7　Nucleon effective form factor

potential[15] suggests that isoscalar channel dominance should lead to attraction while isovector to repulsion. However, it is noted[16] that $e^+e^- \to n\bar{n}$ threshold jump has almost equal value and opposite sign with isovector part of $e^+e^- \to 3(\pi^+\pi^-)+2(\pi^+\pi^-\pi^0)$ processes (Fig. 8). In other multipion channels any features compatible in magnitude are not observed near the nucleon pair production threshold.

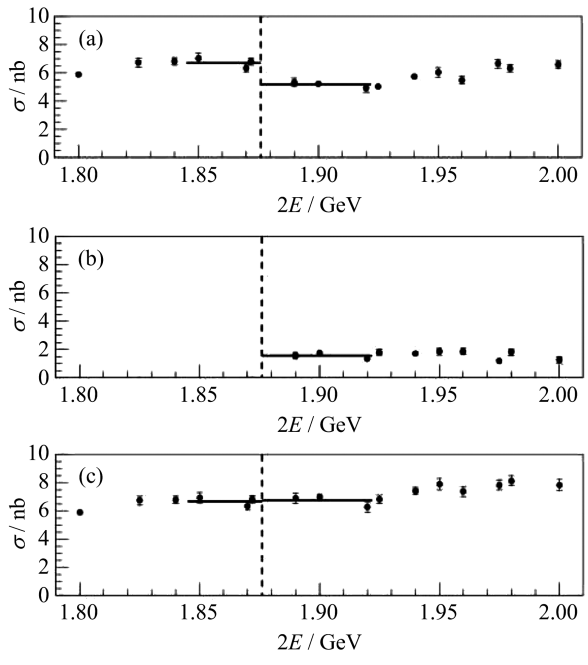

Fig. 8　$e^+e^- \to n\bar{n}$ and isovector $e^+e^- \to 6\pi$ jump compensation

4　Conclusion and plan

The cross section of the $e^+e^- \to p\bar{p}$ is measured independently with the CMD-3 detector and with the SND detector at VEPP-2000 collider. The timelike effective electromagnetic form factor of protons, ratio of electric and magnetic form factors are extracted.

The cross section of the $e^+e^- \to n\bar{n}$ is measured with the SND detector, timelike effective electromagnetic form factor of neutron, ratio of electric and magnetic form factors are extracted.

Results for both the neutron and the proton form factor near the pair production threshold agree well with previous measurements (BaBar, FENICE), but raise some interpretation questions.

Future modernization of collider and both detectors would allow to improve these results. VEPP-2000 is undergoing an upgrade of the electron and positron sources which will allow to increase its luminosity by the order of magnitude. For the new runs the laser Compton backscattering method will be used for the beam energy measurement. An electronics upgrade of the SND detector will allow the time measurement in the calorimeter to better separate antineutron signal from the cosmic background. The new time of flight (TOF) system on the CMD-3 detector will also improve the power of antineutron selection.

References

[1] Lees J P, POIREAU V, TISSERAND V, et al. Measurement of the $e^+e^- \to p\bar{p}$ cross section in the energy range from 3.0 to 6.5 GeV[J]. Phys Rev D, 2013, 88: 072009.

[2] BARDIN G, BURGUN G, CALABRESE R, et al. Determination of the electric and magnetic form factors of the proton in the time-like region[J]. Nucl Phys B, 1994, 411(1): 3-32.

[3] ANTONELLI A, BALDINI R, BENASI P, et al. The first measurement of the neutron electromagnetic form factors in the time-like region [J]. Nucl Phys B, 1998, 517(1/2/3): 3-35.

[4] BERKAEV D E, SHWARTZ D B, SHATUNOV P

Yu, et al. The VEPP-2000 electron-positron collider: First experiments [J]. J Exp Theor Phys, 2011, 113: 213.

[5] ACHASOV M N, AULCHENKO V M, BARU S E, et al. Spherical neutral detector for VEPP-2M collider [J]. Nucl Instrum Meth A, 2000, 449(1/2): 125-139.

[6] ACHASOV M N, BERKAEV D E, BOGDANCHIKOV A G, et al. First experience with SND calorimeter at VEPP-2000 collider [J]. Nucl Instrum Meth A, 2009, 598(1): 31-32.

[7] AULCHENKO V M, BOGDANCHIKOV A G, BOTOV A A, et al. SND tracking system — Tests with cosmic muons [J]. Nucl Instrum Meth A, 2009, 598(1): 102-104.

[8] BARNYAKOV A Yu, BARNYAKOV M Yu, BELOBORODOV K I, et al. High density aerogel for ASHIPH SND — test results[J]. Nucl Instrum Meth A, 2009, 598(1): 163-165.

[9] AULCHENKO V M, BOGDANCHIKOV A G, BOTOV A A, et al. DAQ and electronics for SND at VEPP-2000 — First test results [J]. Nucl Instrum Meth A, 2009, 598(1): 340-341.

[10] AULCHENKO V M, BANZAROV V S, AKHMETSHIN R R, et al. CMD-2M Detector Project[R/OL]. 2001: BUDKER-INP-2001-45. http://cds. cern. ch/record/606716/files/sis-2003-102. pdf.

[11] Fedotovich G V. CMD-3 detector for VEPP-2000[J]. Nucl Phys B (Proc Suppl), 2006, 162: 332-338.

[12] ARBUZOV AB, KOPYLOVA T V, On relativization of the Sommerfeld-Gamow-Sakharov factor[J]. JHEP, 2012, 2012: 9.

[13] AKHMETSHIN R R, AMIRKHANOV A N, ANISENKOV A V, et al. Study of the process $e^+e^- \to p\bar{p}$ in the c. m. energy range from threshold to 2 GeV with the CMD-3 detector[EB/OL]. (2015-07-29) [2015-11-30]. http://arxiv.org/abs/1507.08013.

[14] ACHASOV M N, BARNYAKOV A YU, BELOBORODOV K I, et al. Study of the process $e^+e^- \to n\bar{n}$ at the VEPP-2000 e^+e^- collider with the SND detector [J]. Phys Rev D, 2014, 90: 112007.

[15] DMITRIEV V F, MILSTEIN A I, SALNIKOV S G. Isoscalar amplitude dominance in e^+e^- annihilation to $N\overline{N}$ pair close to the threshold [J]. Phys Atom Nucl, 2014, 77(9): 1 173-1 177.

[16] OBRAZOVSKY AE, SEREDNYAKOV S I. Energy dependence of $e^+e^- \to 6\pi$ and $e^+e^- \to N\overline{N}$ cross sections near the $N\overline{N}$ threshold[J]. JETP Lett, 2014, 99(6), 315-316.

第46卷第4期 中国科学技术大学学报 Vol. 46, No. 4
2016年4月 JOURNAL OF UNIVERSITY OF SCIENCE AND TECHNOLOGY OF CHINA Apr. 2016

Article ID:0253-2778(2016)04-0337-06

Baryon form factors at BESIII

WANG Yadi (for BESIII Collaboration)

(*Helmholtz-Institut Mainz (GSI), Mainz* 55128, *Germany*)

Abstract: With the data collected by the BESIII detector at the BEPCII e^+e^- collider in 2011~2013, the cross section of $e^+e^-\to p\bar{p}$ at 12 center-of-mass energies from 2.232 4 to 3.671 0 GeV was measured. The prospect of new results with the larger e^+e^- scanning data, collected in 2014 and 2015, is reported. The measurement of $p\bar{p}$ form factor with ISR has also been studied using both tagged and untagged methods. With the good performances of BESIII, the feasibility of $n\bar{n}$ form factor measurement in both ISR mode and scan mode is also reported. The preliminary but unexpected result of form factors of $\Lambda\bar{\Lambda}$ measurement is shown, as well as the expectation from the data collected at the threshold of $e^+e^-\to\Lambda_c\bar{\Lambda}_c$. Also expected from these data is a measurement of form factors of all the other hyperons by BESIII.

Key words: Form factors; Baryons; Hyperons; BESIII

CLC number: O572.3 **Document code**: A doi:10.3969/j.issn.0253-2778.2016.04.012

Citation: WANG Yadi. Baryon form factors at BESIII[J]. Journal of University of Science and Technology of China, 2016,46(4):337-342.

BESIII 上的重子形状因子

王雅迪(BESIII 合作组)

(美因茨亥姆霍兹研究所,美因茨 55128,德国)

摘要:利用在2011~2013年BEPCII对撞机上的BESIII探测器收集的数据,测量了 $e^+e^-\to p\bar{p}$ 在2.232 4~3.671 0 GeV之间12个质心系能量点的截面.期待利用在2014年和2015年收集的更大的 e^+e^- 扫描数据样本做更进一步测量.通过标记和不标记初态辐射光子的方法,对 $p\bar{p}$ 形状因子进行了测量.利用BESIII的优良探测器表现,利用标记和不标记初态辐射光子的方法,对 $n\bar{n}$ 形状因子的测量进行了可行性研究.同时也一并报道了 $\Lambda\bar{\Lambda}$ 的形状因子的初步但不符合理论预期的结果,及利用在 $e^+e^-\to\Lambda_c\bar{\Lambda}_c$ 阈值上收集的数据的预期.也期望BESIII能对其他超子的形状因子进行测量.

关键词:形状因子;重子;超子;BESIII

0 Introduction

The measurements of baryon form factors (FFs) in space-like region as well as in the time-like region provide fundamental information on baryon structure, giving crucial tests also to

Received: 2015-11-30; **Revised**: 2016-04-20

Foundation item: Supported by German Research Foundation DFG under Collaborative Research Center (CRC-1044).

Biography: WANG Yadi, female, born in 1984, PhD. Research field: high energy physics. E-mail: wangyd@ihep.ac.cn

models of hadron internal structure in general. Looking back on the history, the experimental results on FFs have driven and renewed models which are trying to explain FFs of Nucleons at low and high q^2, in the space-like region as well as in the time-like region. In a parity, time reversal and gauge invariant theory, the structure of any non-point-like particle of spin S is parametrized in terms of $(2S+1)$ FFs. Hence baryons with $\frac{1}{2}$ spin, which are considered here, are described by two electromagnetic FFs.

In the time-like (TL) region, assuming a metric where the momentum transfer squared q^2 is positive, the FFs have complex values, and their module can be measured by means of cross section and angular distribution measurement. By looking into the polarization of the outgoing baryons, the information on the relative phase can be achieved. The Sachs FFs, electric G_E and magnetic G_M, are introduced as linear combinations of the Dirac and Pauli FFs[1]. The Born cross section, that is the one virtual photon channel, is supposed to be the dominant one in the time-like region. That means the final states have the photon quantum numbers, in particular, the same, negative, charge conjugation. As a consequence there should be a forward/backward symmetry. The two virtual photons would have the opposite one and the interference between these two contributions should produce a forward/backward asymmetry. Indeed a small asymmetry has been found in $e^+e^- \to \gamma_{ISR} p\bar{p}$[9-10]. Conversely, in the space-like region at high q^2 the very different behaviour of G_E and G_M has been assumed to be due to a strong contribution from the two-photon exchange. The Born cross section can be written as a function of G_E and G_M, as in Eq. (1). The differential Born cross section can be written as in Eq. (2), by which the FFs ($|G_E|$ and $|G_M|$ or $R=\left|\frac{G_E}{G_M}\right|$) can be measured.

$$\sigma_{\text{Born}} = \frac{4\pi\alpha^2\beta\mathscr{C}}{3q^2}\left[|G_M|^2+\frac{1}{2\tau}|G_E|^2\right] \quad (1)$$

$$\frac{d\sigma_{\text{Born}}}{d\Omega} = \frac{\alpha^2\beta\mathscr{C}}{4q^2}\left[(1+\cos^2\theta)|G_M|^2+\frac{1}{\tau}\sin^2\theta|G_E|^2\right] \quad (2)$$

The factor $\mathscr{C}$ is a correction to the Born cross section, due to Coulomb interaction between the outgoing charged baryons. Until now $\mathscr{C}$ has been supposed to be the same as for point-like fermions, because of the long range Coulomb interaction. Analiticity of the Dirac and Pauli FF requires $G_E(4M^2)=G_M(4M^2)$. However it might be that some of these assumptions (that have never been under discussion) have to be reviewed, as it seems according to the present data on baryon FFs. For this reason it is worthwhile to collect more data on this topic. BESIII is a detector on a e^+e^- collider with very good performances that provides a good environment for measuring the FFs of baryons.

1 Proton FFs

In the TL region, measurements of proton FFs have been performed by means of $e^+e^- \to p\bar{p}$[2-7], the radiative return $e^+e^- \to \gamma_{ISR} p\bar{p}$[8-10], and also $p\bar{p} \to e^+e^-$[11-14]. While there are many, somewhat consistent, measurements concerning the total cross section, there are few, not consistent, data on the ratio $R=\left|\frac{G_E}{G_M}\right|$, mostly from BABAR[9] and PS170[11].

Recently, based on 157 pb^{-1} collected at 12 scan points between 2.22 and 3.71 GeV in 2011 and 2012, proton FFs have been measured at BESIII[15]. The product of proton and anti-proton selection efficiency times initial-state-radiation (ISR) up to the next-to-leading (NLO) correction factor, $\varepsilon(1+\delta)$, estimated by means of ConExc[16], is about 66% at 2.23 GeV, with a 15% reduction at 4 GeV. After ISR correction, cross section and effective FF are extracted according to Eq. (3) and Eq. (4). The cross section is shown in Fig. 1(a). In Fig. 1(b) R, as extracted from the angular distribution of the proton, is shown, too. The method of moments (MM) (Eq. (5)) has also been used to evaluate R,

see Tab. 1. The cross section has been measured with an accuracy between 6.0% and 18.9% up to $\sqrt{s}<3.08$ GeV, improving the previous results. G_M has also been measured.

$$\sigma_{\text{Born}} = \frac{N_{obs} - N_{bkg}}{\mathscr{L}\varepsilon(1+\delta)} \tag{3}$$

$$|G| = \sqrt{\sigma_{\text{Born}}}\left(1+\frac{1}{2\tau}\right)\left(\frac{4\pi\alpha^2\beta\mathscr{C}}{2E_{CM}^2}\right) \tag{4}$$

$$\langle\cos^2\theta_p\rangle = \frac{1}{N_{\text{norm}}}\int \frac{2\pi\alpha^2\beta C}{4s}\cos^2\theta_p \cdot \left[(1+\cos^2\theta_p)\,|G_M|^2 + \frac{4m_p^2}{s}(1-\cos^2\theta_p)\,|R^2\,|G_M|^2\right]\mathrm{d}\cos\theta_p \tag{5}$$

Tab. 1　Results on R and G_M by fitting the proton angular distribution as well as by the method of moments at different c. m. energies

$\sqrt{s}$/MeV	$\lvert G_E/G_M\rvert$	$\lvert G_M\rvert$ ($\times10^{-2}$)
	Fit on $\cos\theta_p$	
2232.4	0.87±0.24±0.05	18.42±5.09±0.98
2400.0	0.91±0.38±0.12	11.30±4.73±1.53
3050.0～3080.0	0.95±0.45±0.21	3.61±1.71±0.82
	Method of moments	
2232.4	0.83±0.24	18.60±5.38
2400.0	0.85±0.37	11.52±5.01
3050.0～3080.0	0.88±0.46	3.34±1.72

At present, the precision of R is still dominated by statistics. In 2014 and 2015, BESIII has collected more data by means of an energy scan. These data will provide the opportunity to get better results on proton FFs.

The proton FFs have also been measured with the large XYZ dataset collected at BESIII by means of ISR technique, which allows a continuous q^2 measurement from the threshold. Detection efficiency depends slowly on q^2 and it is about 20% with γ_{ISR}-untagged mode, and about 6% with γ_{ISR}-tagged mode. Full angular distribution in hadronic center-of-mass is acquired, and the acceptance at threshold is non-zero, in the untagged mode. BESIII statistics is competitive with BABAR above $M(p\bar{p})\sim2.0$ GeV.

2　Neutron FFs

Up to now, the experimental results on neutron FFs are very few. Only FENICE[5] and SND[17] gave results about neutron effective FFs. This is due to the difficulties in detecting low energy n, when the n does not produce a hadronic shower yet in the electromagnetic calorimeter (EMC). The $\bar{n}$ always annihilates and releases a large amount of hadronic energy, more than twice the nucleon mass. The sources of background in detecting an $\bar{n}$ are other neutral particles, like γ, K_L^0 and mostly beam and neutral cosmic rays.

At BESIII, the depth of the EMC is about 15 electromagnetic radiation lengths, and about 50% of a hadronic interaction length, which is roughtly the probability of detecting high energy n and $\bar{n}$ interacting in the EMC. For a 1 GeV photon the EMC energy resolution is 2.5% in the barrel and 5.0% in the end-caps, which provides a chance to reconstruct at least the $\bar{n}$. The measurements can be performed by means of $e^+e^-\to n\bar{n}$ with the

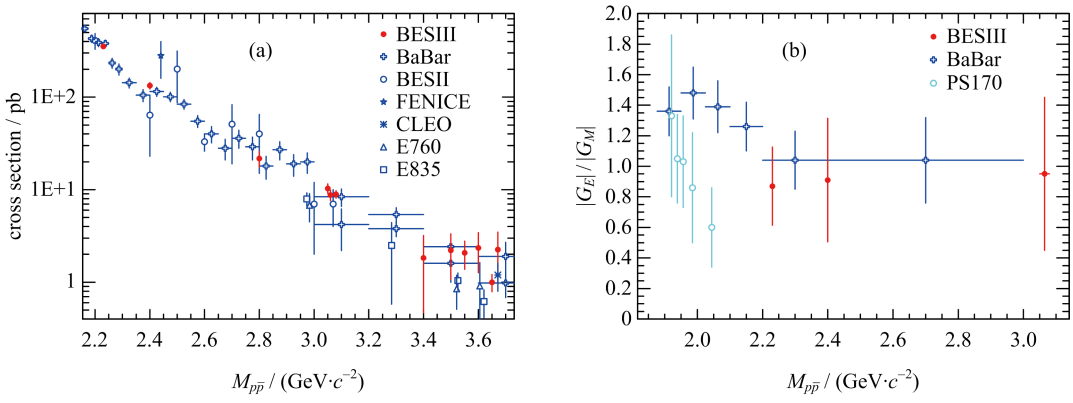

Fig. 1　The Born cross section (a) and R (b) from BESIII compared with other measurements

scanned data and by means of the radiative return $e^+e^-\to\gamma_{ISR}\,n\bar{n}$ using the XYZ data. The detection strategy could be: first identify $\bar{n}$ and γ_{ISR}; then the EMC shower information is used in those cases where n identification is possible; finally event kinematics is used to further veto the remaining backcground. The EMC capability in distinguishing between $\bar{n}$ and photon is comprehensively studied with the Toolkit for Multivariate Data Analysis in the ROOT (TMVA) package. The result is shown in Fig. 2, where one can see that $\bar{n}$ and photon are well seperated.

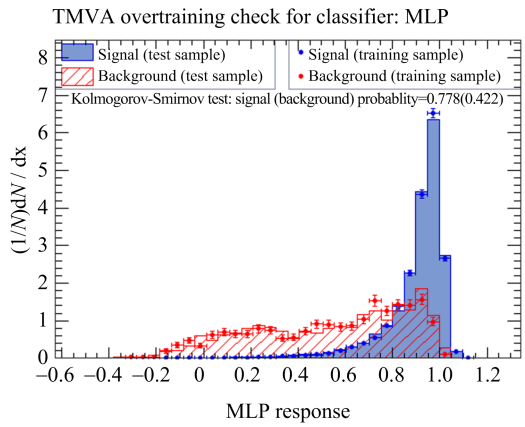

The hatched histogram and dots represent signal.
The other histogram and dots are for background from a photon.

Fig. 2 The EMC capability in distinguishing between $\bar{n}$ and photon studied with TMVA package

To increase the overall detection efficiency, relaxing n identification, the muon counter (MUC) and the TOF counters can be exploited. MUC is made of Resistive Plate Counters interleaved with the yoke iron. The yoke iron is about 54～cm in total, which makes ～96% the probability the $\bar{n}$ interacts in MUC. TOF counters are fired by the $\bar{n}$ annihilation star and the TOF measurement might be enough to get rid of n detection. So these are additional possibilities to detect $\bar{n}$ at BESIII, and their feasibility is under study.

3 Λ FFs

The Coulomb factor should not enter the cross section formula in the case of a neutral baryon pair. Therefore the Born cross section is expected to vanish at threshold, increasing with the velocity of the baryon. The $\Lambda\bar{\Lambda}$ cross section and FFs have been measured by BABAR by means of ISR technique, from threshold to 2.27 GeV, with a non-zero cross section of $(204\pm60\pm20)$ pb at threshold. This result may conflict with the theory prediction but it is integrated on a large energy interval, because of ISR.

With the data collected in 2012, the FFs of $\Lambda\bar{\Lambda}$ have been measured at BESIII preliminarily at four energy points, 2232.4, 2 400.0, 2 800.0, 3 080.0 MeV and a search has been done by looking at $\Lambda\to p\pi^-$ and $\Lambda\to n\pi^0$. At 2 232.4 MeV, very close to the threshold, the momentum of the final proton is too low to leave a message in the detector and the antiproton interacts on the beam pipe. However it is possible to exploit the fact that in the $\Lambda\to\bar{p}\pi^0$ decaying vertex of the secondary particles produced by $\bar{p}$ in the beam pipe is 3～cm displaced, due to the interaction with the beam pipe. For $\Lambda\to n\pi^0$ selection, the TMVA based on Boosted Decision Tree is applied to veto large background. The π^0 in the final state has a monochromatic momentum, about 105 MeV. According to the aforementioned features, 43 ± 7 events have been selected from $\Lambda\to\bar{p}\pi^0$ mode, and 22 ± 6 events from $\Lambda\to n\pi^0$ mode. Surprisingly, a large cross section, about (320 ± 58) pb very close (～1 MeV above) to the threshold has been observed. Cross section and effective FF are listed in Table. 2. Fig. 3 shows $\Lambda\bar{\Lambda}$ cross section, as measured by BESIII, BABAR[18] and DM2[4].

Due to parity violating decay of $\Lambda\to p\pi$, the proton emission depends on Λ polarization in the $\Lambda\bar{\Lambda}$ frame. The imaginary part of FFs leads to a polarization observable, as shown in Eq. (6). θ_Λ is the polar angle of Λ in $\Lambda\bar{\Lambda}$ frame. θ_p is the polar angle of p in Λ frame. According to the data taken in 2014 and 2015, a statistical accuracy between 6% and 17% for P_n can be achieved.

$$P_n=-\frac{\sin2\theta\sin\Delta\phi/\tau}{R\sin^2\theta_\Lambda\tau+(1+\cos^2\theta_\Lambda^2)/R}=\frac{3}{\alpha_\Lambda}\langle\cos\theta_p\rangle \tag{6}$$

Tab. 2 BESIII results on $\Lambda\bar{\Lambda}$ cross section and effective form factor

$\sqrt{s}$/MeV	$\sigma_{\rm Born}$/pb	$\lvert G\rvert$ ($\times 10^{-2}$)
2 232.4		
$\Lambda\to p\pi^-$, $\bar{\Lambda}\to\bar{p}\pi^+$	325±53±46	
$\bar{\Lambda}\to\bar{n}\pi^0$	(3.0±1.0±0.4)×10^2	
combined	320±58	63.4±5.7
2 400.0	133±20±19	12.93±0.97±0.92
2 800.0	15.3±5.4±2.0	4.16±0.73±0.27
3 080.0	3.9±1.1±0.5	2.21±0.31±0.14

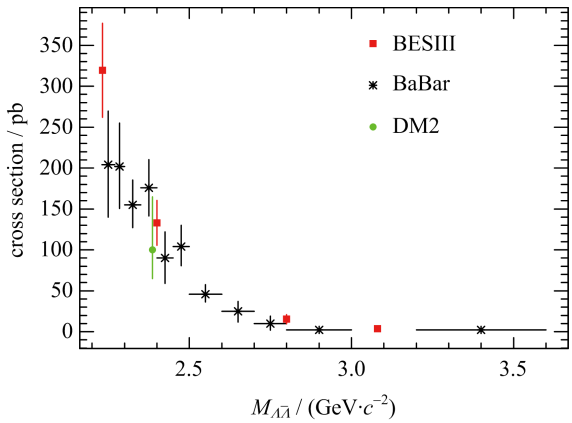

Fig. 3 BESIII, BABAR and DM2 measurements of $\Lambda\bar{\Lambda}$ from 2.0 up to 3.6 GeV

4 FFs of Λ_c and other hyperons

The Coulomb enhancement factor $\mathscr{C}$ at threshold, in the case of $e^+e^-\to\Lambda_c\bar{\Lambda}_c$ predicts $\sigma_{\rm Born}=\frac{\pi^2\alpha^3}{2M^2}\lvert G\rvert^2=0.15\lvert G\rvert^2$ nb. Results from Belle[19] indicate that the cross section near the threshold of $\Lambda_c\bar{\Lambda}_c$ is nearly 0.15 nb, which means $G\sim 1$ at threshold. This strange result is consistent with what has been found by BABAR in $e^+e^-\to p\bar{p}$. Also the ratio R, as measured by BABAR, might be unexpected, being different from 1 (but integrated on an energy interval) as expected according to analiticity. However, the Belle result is affected by a very large uncertainty. To verify this, more integrated luminosity is needed. BESIII collected at 4575 ~ MeV, very close to the threshold, an integrated luminosity of 42 pb^{-1}. Very likely, BESIII will collect more data at high energy. Thus, the cross section measurement will be largely improved, and a 10% precision in the measurement of R is expected with a luminosity of 200 pb^{-1}, assuming an R value similar to the one found in the proton case at BABAR.

Taking the advantage of the large energy range and large data samples at BESIII, the TL-FFs of other hyperons, such as $\Lambda\,\overline{\Sigma^0}$, $\overline{\Sigma^0}\,\Sigma^0$, $\overline{\Sigma^-}\Sigma^+$, $\overline{\Sigma^+}\,\Sigma^-$, $\overline{\Xi^0}\,\Xi^0$, $\overline{\Xi^+}\,\Xi^-$, $\overline{\Omega^+}\,\Omega^-$, together with the measurements of R and relative phase $\Delta\Phi$ at single energy points will be extracted.

5 Conclusion

BESIII is an excellent laboratory for baryon form factor measurements. Both scan and ISR techniques can be used. The proton FFs and the ratio have been measured using 2011~2013 data. With the same data, preliminary results on $\Lambda\bar{\Lambda}$ have been just released. With higher statistics between 2.0 and 3.1 GeV, collected in 2014 and 2015, new significant results will come and improve FFs status for p, n, Λ, Ξ, Ω, Σ, Λ_c. Also the measurements with XYZ datasets by ISR method are worth anticipating.

References

[1] HALZEN F, MARTIN A D. Quarks and Leptons: An Introductory Course in Modern Particle Physics[M]. Canada: John Wiley&Sons, 1984: 172.

[2] DELCOURT B, DERADO I, BERTRAND J L, et al. Study of the reaction $e^+e^-\to pp$ in the total energy range 1925 - 2180 MeV [J]. Phys Lett B, 1982, 86(3/4): 395-398.

[3] BISELLO D, LIMENTANI S, NIGRO M, et al. A measurement of $e^+e^-\to pp$ for ($1975\leqslant\sqrt{s}\leqslant 2250$) MeV[J]. Nucl Phys B, 1983, 224(3): 379-395.

[4] BISELLO D, BUSETTO G, CASTRO A, et al. Baryon pairs production in e^+e^- annihilation at $\sqrt{s}=2.4$ GeV[J]. Z Phys C, 1990, 48(1): 23-28.

[5] ANTONELLI A, BALDINI R, BENASI P, et al. The first measurement of the neutron electromagnetic form factors in the time-like region[J]. Nucl Phys B, 1998, 517(1/2/3): 3-35.

[6] ABLIKIM M, BAI J Z, BAN Y, et al. Measurement of the cross section for image at center-of-mass energies

from 2.0 to 3.07 GeV [J]. Phys Lett B, 2005, 630(1/2): 14-20.

[7] PEDLAR TK, CRONIN-HENNESSY D, GAO K Y, et al. Precision measurements of the timelike electromagnetic form factors of pion, kaon, and proton [J]. Phys Rev Lett, 2005, 95: 261803.

[8] AUBERT B, BARATE R, BOUTIGNY D, et al. Study of $e^+e^- \to p\bar{p}$ using initial state radiation with BABAR[J]. Phys Rev D, 2006, 73: 012005.

[9] LEES J P, POIREAU V, TISSERAND V, et al. Study of $e^+ e^- \to p\bar{p}$ via initial-state radiation at BABAR[J]. Phys Rev D, 2013, 87: 092005.

[10] LEES J P, POIREAU V, TISSERAND V, et al. Measurement of the $e^+ e^- \to p\bar{p}$cross section in the energy range from 3.0 to 6.5 GeV[J]. Phys Rev D, 2013, 88: 072009.

[11] BARDIN G, BURGUN G, CALABRESE R, et al. Determination of the electric and magnetic form factors of the proton in the time-like region[J]. Nucl Phys B, 1994, 411(1): 3-32.

[12] ARMSTRONG T A, BETTONI D, BHARADWAJ V, et al. Proton electromagnetic form factors in the timelike region from 8.9 to 13.0 GeV^2 [J]. Phys Rev Lett, 1993, 70: 1 212.

[13] AMBROGIANI M, BAGNASCO S, BALDINI W, et al. Measurements of the magnetic form factor of the proton in the timelike region at large momentum transfer[J]. Phys Rev D, 1999, 60: 032002.

[14] ANDREOTTI M, BAGNASCO S, BALDINI W, et al. Measurements of the magnetic form factor of the proton for timelike momentum transfers[J]. Phys Lett B, 2003, 559(1/2): 20-25.

[15] ABLIKIM M, ACHASOV M N, AI X C, et al. Measurement of the proton form factor by studying $e^+e^- \to p\bar{p}$[J]. Phys Rev D, 2015, 91: 112004.

[16] Ping R G. An exclusive event generator for e^+e^- scan experiments[J]. Chin Phys C, 2014, 38(8): 083001.

[17] ACHASOV M N, BARNYAKOV A YU, BELOBORODOV K I, et al. Study of the process $e^+e^- \to n\bar{n}$ at the VEPP-2000 $e^+ e^-$ collider with the SND detector[J]. Phys Rev D, 2014, 90: 112007.

[18] AUBERT B, BONA M, BOUTIGNY D, et al. Study of $e^+ e^- \to \Lambda\bar{\Lambda}$, $\Lambda\bar{\Sigma}^0$, $\Sigma^0\bar{\Sigma}^0$ using initial state radiation with BABAR [J]. Phys Rev D, 2007, 76: 092006.

[19] PAKHLOVA G, ADACHI I, AIHARA H, et al. Observation of a near-threshold enhancement in the $e^+e^- \to \Lambda_c^+\Lambda_c^-$ cross section using initial-state radiation [J]. Phys Rev Lett, 2008, 101: 172001.

第46卷第4期 中国科学技术大学学报 Vol. 46, No. 4
2016年4月 JOURNAL OF UNIVERSITY OF SCIENCE AND TECHNOLOGY OF CHINA Apr. 2016

Article ID:0253-2778(2016)04-0343-04

Meson transition form factor studies at WASA-at-COSY

KUPSC A. (for the WASA-at-COSY Collaboration)

(*Uppsala University*, *Uppsala* 75120, *Sweden*)

Abstract: Status of the light neutral meson (π^0, η and ω) studies carried out by the WASA-at-COSY collaboration is presented, with an emphasis is on the processes related to the light meson transition form factors. The recent results on the η meson branching ratios are presented.

Key words: light meson decays; transition form factor; low energy QCD

CLC number: O572.3 **Document code**: A doi:10.3969/j.issn.0253-2778.2016.04.013

Citation: KUPSC A. Meson transition form factor studies at WASA-at-COSY[J]. Journal of University of Science and Technology of China, 2016,46(4):343-346.

WASA-at-COSY 实验介子跃迁形状因子

KUPSC A.（WASA-at-COSY 合作组）

（乌普萨拉大学，乌普萨拉 75105，瑞典）

摘要：介绍了 WASA-at-COSY 实验中对轻中性介子（π^0，η 和 ω）的研究，着重介绍中性介子的跃迁形状因子. 并给出了 η 介子分支比研究的最新进展.

关键词：轻介子衰变；跃迁形状因子；低能 QCD

0 Introduction

Meson transition form factors for the lightest neutral pseudoscalar mesons $P=\pi^0$, η and η' are the scalar functions describing the vertex consisting of the meson and two photons $P\gamma^*\gamma^*$. They are relevant for the description of processes such as radiative decays, $P\to\gamma\gamma$, single and double Dalitz decays, $P\to l^+l^-\gamma$ and $P\to l^+l^-l^+l^-$, meson production processes, $e^+e^-\to P\gamma$ and $e^\pm\gamma\to e^\pm P$[1]. The main features of such processes are relatively well described within approaches based on the Vector Meson Dominance (VMD) model. However, the VMD model does not match QCD predictions for the asymptotic region.

The transition form factors studies are a field of hadronic physics where high-precision measurements are possible and several theoretical calculations are becoming available which could match the experimental precision. Recently they are subject to intensive studies[2] and one of the reasons was their relation to the dark photon searches and to the muon anomalous magnetic moment, a_μ, measurement. The $P\gamma^*\gamma^*$ vertex is the key ingredient of the hadronic light-by-light (HLbL) component for the Standard Model prediction of the a_μ[3-6]. Moreover the precise knowledge of the lepton pair mass spectra is mandatory in searches for the quark-gluon plasma and in studies of hadron properties modifications in

Received: 2015-11-30; **Revised**: 2016-04-30

Biography: KUPSC A., male, born in 1965, PhD. Research field: hadron physics. E-mail: Andrzej.Kupsc@physics.uu.se

heavy ion collisions[7].

The information about transition form factors is obtained from production processes in $e^+ e^-$ colliders or in two photon processes. It could be also studied in decay processes involving lepton antilepton pair (Dalitz decays). The transition form factors are also closely related to the anomalous hadronic process involving odd number of pseudoscalar fields. Two examples of such processes are: $\eta \to \pi^+ \pi^- \gamma$ and $\omega \to \pi^+ \pi^- \pi^0$. The mesons for the decay studies could be produced at many facilities in the world including e. g. photoproduction and hadroproduction experiments.

1 WASA-at-COSY experiment

WASA-at-COSY experiment collected data between 2006 and 2014 at the Cooler Synchrotron (COSY) ring at Forschungszentrum Jülich in Germany. COSY can provide deuteron or proton beams with momentum up to 3.7 GeV/c. The experimental facility includes WASA detector optimized for the study of interactions and decays of the light mesons and a fixed internal target using hydrogen or deuterium 30 μm frozen pellets[8].

The WASA detector consists of a forward part arranged to measure baryonic ejectiles and a central section to detect light mesons or their decay products (leptons and photons). The forward part consists of plastic scintillator layers of various thicknesses and drift chambers covering full azimuthal angle. The central part consisting of a CsI(Na) electromagnetic calorimeter with 1012 elements and a mini drift chamber surrounded by a plastic scintillator barrel is inside a superconducting solenoid. A detailed description of the WASA detector is found in Refs. [8-9].

The mesons for the decay studies are produced using two complementary hadronic reactions in pp or pd collisions. The two reaction types for the production of a neutral meson X are $pd \to {}^3\mathrm{He}X$ or $pp \to ppX$.

The first group of the reactions are characterized by initially fast rising cross sections which reaches plateau. The optimal signal to background ratio is reached at energies close to the reaction threshold. The two body final state includes ^{3}He which enables easy identification of the meson production process by reconstructing very clean signal in the forward part of the WASA detector. It allows to collect a data sample without bias on the decay channel of the studied meson. However, the drawback is large total cross section of the pd interactions which limits the useful luminosities (due to pile-up processes which are most significant for the calorimeter and for the drift chamber). At the same time the maximum cross section of the meson production in the ^{3}He fusion is rather low. For example, for the $pd \to {}^3\mathrm{He}\eta$ it is 0.40(3) μb[10-11], meaning that few η mesons are produced per second at a typical luminosity of 2×10^{31} cm$^{-2}\cdot$s^{-1}. The $pd \to {}^3\mathrm{He}X$ fusion reaction could therefore provide unbiased data sample suitable for determination of the branching ratios and for searches of invisible decay modes. This reaction could be also used for high precision studies of the decay distributions for the more common decays.

The total data set for the η meson decay studies includes 3×10^7 tagged mesons produced in the pd collisions. The $pd \to {}^3\mathrm{He}\eta$ reaction was used with a proton beam of 1 GeV. The published analyses include studies of reaction mechanisms of the common decays such as $\eta \to \pi^+ \pi^- \pi^0$[14] and $\eta \to \pi^+ \pi^- \gamma$[15]. The recently finished measurement of the branching ratios is reported in the next section[16]. $pd \to {}^3\mathrm{He}\omega$ reaction at 1.45 and at 1.5 GeV was used for studies of $\omega \to \pi^+ \pi^- \pi^0$ Dalitz plot and for studies of other hadronic decays of the ω meson. The analysis of the ω decays is ongoing and the status was presented in Ref. [17].

The meson production in the $pp \to ppX$ reaction has larger cross sections. In addition, lower total cross section for the proton-proton interactions allows for larger luminosities to be

used. However, more restrictive trigger conditions have to be used to limit the number of the rates of the collected events. The conditions include information on the decay channel i. e. separate chains for charged and neutral decay channels. For example, η mesons have been produced in protonproton interactions at beam kinetic energy of 1.4 GeV, corresponding to the excess energy of 56 MeV and cross section 9.8 ± 1.0 μb[12]. The collected data sample corresponds to more than 5×10^8 η mesons produced. The ω mesons were produced in proton-proton interactions at beam kinetic energies 2.06 GeV and 2.54 GeV with the corresponding cross sections of 5.7 μb and 35 μb.

The WASA detector was in fact designed and optimized for studies of rare π^0 meson decays produced in $pp \to pp\pi^0$ reaction at CELSIUS storage ring in Uppsala at the kinetic beam energy of 550 MeV. This corresponds to the excess energy of 122 MeV with respect to $pp\pi^0$ threshold (i. e. below two pion production thresholds) with a cross section of 1.12 mb[13]. In the series of runs WASA-at-COSY has collected a few millions of $\pi^0 \to \gamma e^+ e^-$ events for dark photon searches, π^0 transition form factor studies and for measurement of $\pi^0 \to e^+ e^-$ branching ratio. The results based on about 10% of the collected data samples were published in 2013[18].

2 Branching ratios of the η meson decays

The η meson data sample collected from pd collisions was used to determine the branching ratios of the η meson decay modes[16]. The following four decay modes are considered: $\eta \to \pi^+\pi^-\gamma$, $\eta \to e^+e^-\gamma$, $\eta \to \pi^+\pi^-e^+e^-$ and $\eta \to e^+e^-e^+e^-$. The branching ratios are normalized to the $\eta \to \pi^+\pi^-\pi^0$ decay. In addition a CP-violating asymmetry in $\eta \to \pi^+\pi^-e^+e^-$ is measured.

The absolute branching ratios were obtained by using the world average from Ref. [19] for the $BR(\eta \to \pi^+\pi^-\pi^0) = (2.292 \pm 0.028) \times 10^{-1}$. The results are presented in Tab. 1.

Tab. 1　Summary of the η meson branching ratios measured by WASA-at-COSY

Channel	Branching Ratio
$\eta \to \pi^+\pi^-\gamma$	$(4.67 \pm 0.07_{\mathrm{stat/fit}} \pm 0.19_{\mathrm{sys}}) \times 10^{-2}$
$\eta \to e^+e^-\gamma$	$(6.72 \pm 0.07_{\mathrm{stat/fit}} \pm 0.31_{\mathrm{sys}}) \times 10^{-3}$
$\eta \to \pi^+\pi^-e^+e^-$	$(2.7 \pm 0.2_{\mathrm{stat}} \pm 0.2_{\mathrm{sys}}) \times 10^{-4}$
$\eta \to e^+e^-e^+e^-$	$(3.2 \pm 0.9_{\mathrm{stat}} \pm 0.5_{\mathrm{sys}}) \times 10^{-5}$

The value for the $\Gamma(\eta \to \pi^+\pi^-\gamma)/\Gamma(\eta \to \pi^+\pi^-\pi^0)$ is $0.208 \pm 0.003_{\mathrm{stat/fit}} \pm 0.008_{\mathrm{sys}}$. It is in a good agreement with the older experiments[20-21] but is 2.6 and 2.5 standard deviations above the recent values from CLEO[22] and KLOE[23] respectively.

The branching ratio for $\eta \to e^+e^-\gamma$ is consistent with the most recent Particle Data Group fit $(6.9 \pm 0.4) \times 10^{-3}$ but it is more precise. The absolute branching ratios for $\eta \to \pi^+\pi^-e^+e^-$ and $\eta \to e^+e^-e^+e^-$ decays are in good agreement with the values reported by KLOE[24-25].

The uncertainties for $\eta \to \pi^+\pi^-\gamma$ and $\eta \to e^+e^-\gamma$ are dominated by the systematic effects and the largest contribution comes from a comparison of two data sets corresponding to the experimental runs with different luminosities and accelerator settings and which were separated by more than one year.

The CP violating asymmetry, A_ϕ, determined from the distribution of the angle ϕ between the $\pi^+\pi^-$ and e^+e^- decay planes for $\eta \to \pi^+\pi^-e^+e^-$ has been also determined and found to be consistent with zero: $A_\phi = (-1.1 \pm 6.6_{\mathrm{stat}} \pm 0.2_{\mathrm{sys}}) \times 10^{-2}$.

References

[1] LANDSBERG L G. Electromagnetic decays of light mesons[J]. Phys Rep, 1985, 128: 301-376.

[2] CZERWINSKI E, EIDELMAN S, HANHART C, et al. MesonNet workshop on meson transition form factors[EB/OL]. (2013-07-12)[2015-11-30]. http://arxiv.org/abs/1207.6556.

[3] BIJNENS J, PRADES J. The hadronic light-by-light contribution to the muon anomalous magnetic moment: where do we stand? [J]. Mod Phys Lett A, 2007, 22: 767-782.

[4] HAYAKAWA M, KINOSHITA T. Pseudoscalar pole terms in the hadronic light-by-light scattering contribution to muon g-2[J]. Phys Rev D, 1998, 57:

465-477.

[5] COLANGELO G, HOFERICHTER M, KUBIS B, et al. Towards a data-driven analysis of hadronic light-by-light scattering[J]. Phys Lett B, 2014, 738: 6-12.

[6] PAUK V, VANDERHAEGHEN M. Anomalous magnetic moment of the muon in a dispersive approach [J]. Phys Rev D, 2014, 90: 113012.

[7] FRIMAN B, HÖHNE C, KNOLL J, et al. The CBM Physics Book[M]. Heidelberg: Springer, 2011.

[8] HOISTAD B, RITMAN J, et al. Proposal for the Wide Angle Shower Apparatus (WASA) at COSY-Juelich-"WASA at COSY"[EB/OL]. (2004-11-19)[2015-11-30]. http://arxiv.org/abs/nucl-ex/0411038.

[9] BARGHOLTZ C, BASHKANOV M, BERLOWSKIET M, et al. The WASA detector facility at CELSIUS[J]. Nucl Instrum Meth A, 2008, 594: 339-350.

[10] BILGER R, BRODOWSKI W, CALÉN H, et al. Measurement of the $pd\to{}^3\mathrm{He}\,\eta$ cross section between 930 and 1100 MeV [J]. Phys Rev C, 2002, 65: 044608.

[11] RAUSMANN T, KHOUKAZ A, BÜSCHER M, et al. Precision study of the $dp\to{}^3\mathrm{He}\,\eta$ reaction for excess energies between 20 and 60 MeV[J]. Phys Rev C, 2009, 80: 017001.

[12] CHIAVASSA E, DELLACASA G, DE MARCO N, et al. Measurement of the $pp\to pp\eta$ total cross section between 1.265 and 1.50 GeV[J]. Phys Lett B, 1994, 322: 270-274.

[13] RAPPENECKER G, RIGNEYA M, DIDELEZAET J P, et al. Cross sections and asymmetries for the $p(\vec{p},\pi^0)$ reaction from threshold to 1 GeV[J]. Nucl Phys A, 1995, 590: 763-784.

[14] ADLARSON P, AUGUSTYNIAK W, BARDAN W, et al. Measurement of the $\eta\to\pi^+\pi^-\pi^0$ Dalitz plot distribution[J]. Phys Rev C, 2014, 90: 045207.

[15] ADLARSON P, ADOLPH C, AUGUSTYNIAK W, et al. Exclusive measurement of the $\eta\to\pi^+\pi^-\gamma$ decay [J]. Phys Lett B, 2012, 707: 243-249.

[16] ADLARSON P, AUGUSTYNIAK W, BARDAN W, et al. Measurements of branching ratios for η decays into charged particles[EB/OL]. (2015-09-22)[2015-11-30]. http://arxiv.org/abs/1509.06588.

[17] HEIJKENSKJÖLD L. Hadronic decays of the omega meson measured with WASA-at-COSY [C/OL]// Proceedings of the 53rd International Winter Meeting on Nuclear Physics (Bormio2015). 2015: 046[2015-11-30]. http://pos.sissa.it/archive/conferences/238/046/Bormio2015_046.pdf.

[18] ADLARSON P, AUGUSTYNIAKB W, BARDAN W, et al. Search for a dark photon in the $\pi\to e^+e^-\gamma$ decay [J]. Phys Lett B, 2013, 726: 187-193.

[19] OLIVE K A, AGASHE K, AMSLER C, et al. Review of particle physics[J]. Chin Phys C, 2014, 38: 090001.

[20] GORMLEY M, HYMAN E, LEE W, et al. Experimental determination of the Dalitz-plot distribution of the decays $\eta\to\pi^+\pi^-\pi^0$ and $\eta\to\pi^+\pi^-\gamma$, and the branching ratio $(\eta\to\pi^+\pi^-\gamma)/(\eta\to\pi^+\pi^-\pi^0)$ [J]. Phys Rev D, 1970, 2: 501-505.

[21] THALER J J, APPEL J A, KOTLEWSKI A, et al. Relative decay rates of $\eta\to\pi^+\pi^-\pi^0$, $\eta\to\pi^+\pi^-\gamma$, $\eta\to\pi^+\pi^-\pi^0\gamma$ and $\eta\to\pi^+\pi^-$[J]. Phys Rev D, 1973, 7: 2 569-2 571.

[22] LOPEZ A, MEHRABYAN S, MENDEZET H, et al. Measurement of prominent η-Decay branching fractions [J]. Phys Rev Lett, 2007, 99: 122001.

[23] BABUSCI D, BADONI D, BALWIERZ-PYTKO I, et al. Measurement of $\Gamma(\eta\to\pi^+\pi^-\gamma)/\Gamma(\eta\to\pi^+\pi^-\pi^0)$ with the KLOE detector[J]. Phys Lett B, 2013, 718: 910-914.

[24] AMBROSINO F, ANTONELLI A, ANTONELLI M, et al. Measurement of the branching ratio and search for a CP violating asymmetry in the $\eta\to\pi^+\pi^-e^+e^-(\gamma)$ decay at KLOE[J]. Phys Lett B, 2009, 675: 283-288.

[25] AMBROSINO F, ANTONELLI A, ANTONELLI M, et al. Observation of the rare $\eta\to e^+e^-e^+e^-$ decay with the KLOE experiment[J]. Phys Lett B, 2011, 702: 324-328.

List of Talks

Opening Address	Liang Han (USTC, Hefei)
Session 1. R-measurements	Chaired by Xiaoyan Shen (IHEP, Beijing)
Overview of the CMD-3 results	Gennady Fedotovich (BINP)
BaBar ISR measurements	Evgeny Kozyrev (Novosibirsk)
Study of e^+e^- annhilation to hadrons below 2 GeV with SND	Tatyana Dimova (BINP)
Precise measurement of $e^+e^-\to K^+K^-$ at SND	Konstantin Beloborodov (BINP)
Session 2. R-measurements	Chaired by Paolo Gauzzi (INFN)
Recent results from the KEDR detector at the VEPP-4M	Korneliy Todyshev (BINP)
KLOE/KLOE2 results	Veronica De Leo (INFN)
BESIII R scan	Haiming Hu (IHEP, Beijing)
BESIII $2\pi/3\pi$ ISR	Yaqian Wang (JGU Mainz)
Session 3. Form Factors	Chaired by Rinaldo Baldini (IHEP & INFN)
Theory review on form factors	Simone Pacetti (Perugia)
Experimental review on form factors	Tord Johansson (Uppsala)
Preliminary results on $e^+e^-\to\pi^+\pi^-$ form factor at CMD-3	Fedor Ignatov (BINP)
Measurement of the time-like neutron and proton form factors at VEPP-2000	Aleksandr Korol (Novosibirsk)
Session 4. Form Factors	Chaired by Alberto Lusiani (Pisa)
BaBar form factor measurements	Evgeny Kozyrev (Novosibirsk)
BESIII form factor measurements	Yadi Wang (HIM-GSI)
Form factor measurements at WASA	Andrzej Kupsc (Uppsala)
Form factor measurements at JLAB	Bogdan Wojtsekhowsk(remote)
Session 5. Flavor Physics	Chaired by Tatyana Dimova (BINP)
Charm physics at Belle	Longke Li (USTC, Hefei)
Flavour physics at LHCb	Sergey Barsuk (Orsay)
Charm physics at BESIII	Hailong Ma (IHEP, Beijing)
BaBar measurement of the $D^0\to\pi^-\ e^+\nu$	Konrad Griessinger (JGU Mainz)
Session 6. Tau Physics	Chaired by Andrzej Czarnecki (U. Alberta)
A new look at V_{us} from inclusive flavor-breaking hadronic τ decay sum rules	Kim Maltman (York University)
Radiative tauleptonic decays	Matteo Fael (U. Bern)
Five-lepton lepton decays in the SM and beyond	Pablo Roig (Mexico)
Combined analysis of the decays $\tau^-\to K_S\pi^-\nu$ and $\tau^-\to K^-\eta\nu$	Rafel Escribano (U. Barcelona)
Session 7. Muon $g-2$	Chaired by Massimo Passera (Padova)
Theoretical review on $g-2$	Andrzej Czarnecki (U. Alberta)
$g-2$ experiment at FNAL	Seung Cheon Kim (Cornell)
$g-2$ experiment at J-PARC	Boris Shwartz (BINP)
Spacelike measurement for a_μ	Carlo Carloni Calame (Pavia)
Session 8. gamma-gamma/HLbL	Chaired by Achim Denig (JGU Mainz)
gamma-gamma analysis at KLOE/KLOE-2	Paolo Gauzzi (INFN)
Two-photon physics studies at Belle	Qingnian Xu (UCAS, Beijing)

gamma-gamma analysis at BESIII	Christoph Redmer (JGU Mainz)
Hadronic contribution from light by light processes in $(g-2)_\mu$ in nonlocal quark model	Alexey Zhevlakov (Tomsk)
The η transition form factor from space- and time-like experimental data	Rafel Escribano (U. Barcelona)
Session 9. Proton Radius Puzzle	Chaired by Gennady Fedotovich (BINP)
Proton radius QED theory	Savely Karshenboim (MPQ)
New electronic atomic physics measurements	Axel Beyer (MPQ)
New JLab experiment (PRad) on proton charge radius	Haiyan Gao (Duke Kunshan)
Session 10. Electroweak	Chaired by Bradley Lee Roberts (U. Boston)
sin2theta theory and new physics	Hye-Sung Lee (Daejeon)
Perspectives for sin2theta at BelleII	Boris Shwartz (BINP)
P2 measurement at Mainz	Niklaus Berger (JGU Mainz)
Dalitz decay studies at BESIII	Dayong Wang (PKU, Beijing)
Comprehensive study of η/η' physics in chiral effective field theory	Zhihui Guo (HNU, Shijiazhuang)
Poster Session	
$e^+e^-\to\phi\eta$ reaction with CMD-3 detector	Vecheslav Ivanov (BINP)
$e^+e^-\to\overline{K}K$ (K_SK_L, K^+K^-) reactions with CMD-3 Detector	Evgeny Kozyrev (Novosibirsk)
$e^+e^-\to\eta\pi^+\pi^-$, $\omega\pi^+\pi^-$ reactions with CMD-3 Detector	Alexsander Popov (BINP)
$e^+e^-\to VP$ reactions at the VEPP-2000 e^+e^- collider with the SND detector	Alexander Botov (BINP)
Searchfor $\eta'\to e^+e^-$ and $\eta\to e^+e^-$ at the VEPP-2000 e^+e^- collider	Leonid Kardapoltsev (BINP)
Study of interference effects in the decays of ψ mesons into K^+K^-	Alberto Lusiani (Pisa)
Advertising of Chinese Physics C	Caitriana Nicholson (IHEP, Beijing)
Session 11. Spectroscopy	Chaired by Changzheng YUAN (IHEP, Beijing)
Theoretical review of *XYZ*	Xiang Liu (LZU)
XYZ at BESIII	Jingzhi Zhang (IHEP, Beijing)
XYZ at Belle	Chengping Shen (Beihang)
New results on exotic baryon resonances at LHCb	Liming Zhang (TSU)
Session 12. Spectroscopy & Radiative Corrections	Chaired by Savely Karshenboim (MPQ)
BESIII light hadron spectroscopy	Shuangshi Fang (IHEP, Beijing)
Towards nature of the X(3872) resonance	Nikolay Achasov (Sobolev)
Status of MC generators	Henryk Czyz (U. Silesia)
Session 13. Dark Photon	Chaired by Henryk Czyz (U. Silesia)
Dark mediator searches at KLOE/KLOE-2	Elena Perez Del Rio (INFN)
Search for the dark photon in π^0 decays at NA48/NA62	Francesco Gonnella (INFN)
Search for dark photon and long-lived particles at BaBar	Alberto Lusiani (Pisa)
Session 14. Machines and Detectors	Chaired by Zhengguo Zhao (USTC, Hefei)
Facility at JLAB for hadron physics	Haiyan Gao (Duke Kunshan)
MAMI & MESA	Achim Denig (JGU Mainz)
The BelleII experiment and super KEKB upgrade	Boqun Wang (U. Cincinnati)
Status and prospects of e^+e^- colliders at BINP	Pavel Piminov (BINP)
Post BEPCII in China: HIEPA	Jianbei Liu (USTC, Hefei)
Closing Remarks	Guangshun Huang (USTC, Hefei)

List of Participants

Name	E-mail	Institution	City	Country
Prof. ACHASOV, Nikolay	achasov@math. nsc. ru	Sobolev Institute for Mathematics	Novosibirsk	Russian
Prof. AN, Qi	anqi@ustc. edu. cn	USTC	Hefei	China
Dr. BALDINI FERROLI, Rinaldo	baldini@lnf. infn. it	INFN-LNF	Frascati	Italy
Dr. BARSUK, Sergey	sergey. barsuk@cern. ch	Laboratoire de l'Accélérateur Linéaire (FR)	Orsay	France
Mr. BELOBORODOV, Konstantin	K. I. Beloborodov@inp. nsk. su	NSU / BINP	Novosibirsk	Russian
Prof. BERGER, Niklaus	niberger@uni-mainz. de	JGU Mainz	Mainz	Germany
Mr. BEYER, Axel	axel. beyer@mpq. mpg. de	MPQ	Garching	Germany
Mr. BOTOV, Alexander	a. a. botov@inp. nsk. su	BINP	Novosibirsk	Russian
Prof. CAI, Hao	hcai@whu. edu. cn	Wuhan University	Wuhan	China
Mr. CAO, Zheng	caoz@ihep. ac. cn	IHEP	Beijing	China
Dr. CARLONI CALAME, Carlo	carlo. carloni. calame@pv. infn. it	University of Pavia	Pavia	Italy
Mr. CHEN, Rui	chenr2012@lzu. edu. cn	Lan Zhou University	Lanzhou	China
Prof. CHEN, Shenjian	sjchen@nju. edu. cn	Nanjing University	Nanjing	China
Dr. CZARNECKI, Andrzej	andrzejc@ualberta. ca	University of Alberta	Edmonton	Canada
Prof. CZYZ, Henryk	czyz@us. edu. pl	University of Silesia	Katowice	Poland
Dr. DE LEO, Veronica	veronica. deleo@roma3. infn. it	INFN Sezione Roma 3	Roma	Italy
Prof. DENIG, Achim	denig@kph. uni-mainz. de	JGU Mainz	Mainz	Germany
Dr. DIMOVA, Tatyana	baiert@inp. nsk. su	NSU / BINP	Novosibirsk	Russian
Dr. DING, Guijun	dinggj@ustc. edu. cn	USTC	Hefei	China
Prof. DRUZHININ, Vladimir	druzhinin@inp. nsk. su	NSU / BINP	Novosibirsk	Russian
Dr. ESCRIBANO, Rafel	rafel. escribano@ifae. es	U. Barcelona	Barcelona	Spain
Dr. FAEL, Matteo	fael@itp. unibe. ch	University of Bern	Bern	Switzerland
Ms. FANG, Xin	fangx@mail. ustc. edu. cn	USTC	Hefei	China
Mr. FANG, Shuangshi	fangss@ihep. ac. cn	IHEP	Beijing	China
Prof. FEDOTOVICH, Gennady	fedotovich@inp. nsk. su	BINP	Novosibirsk	Russian
Prof. GAO, Daoneng	gaodn@ustc. edu. cn	USTC	Hefei	China
Prof. GAO, Haiyan	yijun. gu@dku. edu. cn	Duke Kunshan University	Kunshan	China
Mr. GAO, Xinlei	gaoxinl@mail. ustc. edu. cn	USTC	Hefei	China
Mr. GAO, Zhen	gaozhen@mail. ustc. edu. cn	USTC	Hefei	China
Dr. GAUZZI, Paolo	paolo. gauzzi@roma1. infn. it	U. Roma / INFN Roma	Rome	Italy
Prof. GOLTERMAN, Maarten	maarten@sfsu. edu	SF State U.	San Francisco	United States
Dr. GONNELLA, Francesco	francesco. gonnella@lnf. infn. it	INFN	Frascati	Italy
Mr. GRIESSINGER, Konrad	griess@slac. stanford. edu	Mainz University	Mainz	Germany
Dr. GUO, Zhihui	dr_guozhihui@163. com	Hebei Normal University	Shijiazhuang	China
Prof. HUANG, Guangshun	hgs@ustc. edu. cn	USTC	Hefei	China
Prof. HU, Haiming	huhm@ihep. ac. cn	IHEP	Beijing	China
Dr. IGNATOV, Fedor	ignatov@inp. nsk. su	BINP	Novosibirsk	Russian
Mr. IVANOV, Vyacheslav	vyacheslav_lvovich_ivanov@mail. ru	BINP	Novosibirsk	Russian
Dr. JIAO, Jianbin	jiaojb@sdu. edu. cn	Shandong University	Jinan	China
Prof. JOHANSSSON, Tord	tord. johansson@physics. uu. se	Uppsala University	Uppsala	Sweden
Mr. KARDAPOLTSEV, Leonid	l. v. kardapoltsev@inp. nsk. su	BINP / NSU	Novosibirsk	Russian
Dr. KARSHENBOIM, Savely	savely. karshenboim@mpq. mpg. de	MPQ	Garching	Germany
Dr. KIM, SeungCheon	sk2528@cornell. edu	Cornell University	Ithaca	United States
Dr. KISELEV, Alexey	kiselev@math. nsc. ru	Sobolev Institute for Mathematics / NSU	Novosibirsk	Russian
Mrs. KONG, HUI	kid007@mail. ustc. edu. cn	USTC	Hefei	China
Dr. KOROL, Aleksandr	a. a. korol@inp. nsk. su	NSU / BINP	Novosibirsk	Russian
Mr. KOZYREV, Evgeny	eakozyrev09@gmail. com	NSU / BINP	Novosibirsk	Russian
Dr. KUPSC, Andrzej	Andrzej. Kupsc@physics. uu. se	Uppsala University	Uppsala	Sweden
Dr. LEE, Hye-Sung	hyesung. lee@cern. ch	IBS CTPU	Daejeon	Republic of Korea
Dr. LI, Cui	cui. li@physics. uu. se	Uppsala University	Uppsala	Sweden
Prof. LI, Haibo	lihb@ihep. ac. cn	IHEP	Beijing	China
Dr. LI, Lei	lilei@ihep. ac. cn	BIPT	Beijing	China
Mr. LI, Longke	lilongke@mail. ustc. edu. cn	USTC	Hefei	China

Ms. LI, Peilian	lipl@mail. ustc. edu. cn	USTC	Hefei	China
Mr. LI, Peirong	lipeirong11@mails. ucas. ac. cn	UCAS	Beijing	China
Mr. LIU, Dong	dliu13@mail. ustc. edu. cn	USTC	Hefei	China
Prof. LIU, Jianbei	liujianb@ustc. edu. cn	USTC	Hefei	China
Dr. LIU, Landiao	liulandiao@gmail. com	Peking University	Beijing	China
Prof. LIU, Shubin	liushb@ustc. edu. cn	USTC	Hefei	China
Prof. LIU, Xiang	xiangliu@lzu. edu. cn	Lanzhou University	Lanzhou	China
Prof. LIU, Yanwen	yanwen@ustc. edu. cn	USTC	Hefei	China
Prof. LU, Caidian	lucd@ihep. ac. cn	IHEP	Beijing	China
Dr. LUSIANI, Alberto	alberto. lusiani@pi. infn. it	ScuolaNormaleSuperiore	Pisa	Italy
Dr. LYU, Xiaorui	xiaorui@ucas. ac. cn	UCAS	Beijing	China
Prof. MAGGIORA, Marco	marco. maggiora@to. infn. it	INFN-TO	Turin	Italy
Dr. MA, Hailong	mahl@ihep. ac. cn	IHEP	Beijing	China
Prof. MALTMAN, Kim	kmaltman@yorku. ca	York University	Toronto	Canada
Dr. MASSRI, Karim	karim. massri@cern. ch	University of Liverpool	Liverpool	UK
Dr. NICHOLSON, Caitriana	c. nicholson@ihep. ac. cn	IHEP	Beijing	China
Mr. NIU, Pengyu	niupengyu14@mails. ucas. ac. cn	IHEP	Beijing	China
Dr. PACETTI, Simone	simone. pacetti@pg. infn. it	U. Perugia / INFN	Perugia	Italy
Dr. PASSERA, Massimo	passera@pd. infn. it	INFN Padova	Padova	Italy
Mr. PENG, Junbo	vortex@mail. ustc. edu. cn	USTC	Hefei	China
Dr. PEREZ DEL RIO, Elena	eperez@lnf. infn. it	INFN Frascati	Frascati	Italy
Dr. PIMINOV, Pavel	piminov@inp. nsk. su	BINP SB RAS	Novosibirsk	Russian
Mr. POPOV, Alexandr	aspopov1@inp. nsk. su	BINP	Novosibirsk	Russian
Prof. QIAO, CONGFENG	qiaocf@ucas. ac. cn	University of CAS	Beijing	China
Dr. REDMER, Christoph Florian	redmer@kph. uni-mainz. de	JGU Mainz	Mainz	Germany
Prof. ROBERTS, B. Lee	roberts@bu. edu	Boston University	Boston	United States
Dr. ROIG, Pablo	proig@fis. cinvestav. mx	Dpto. FisicaCinvestav	Mexico DF	Mexico
Dr. RONGGANG, Ping	pingrg@ihep. ac. cn	IHEP	Beijing	China
Dr. SAVRIE', Mauro	savrie@fe. infn. it	University of Ferrara and INFN	Ferrara	Italy
Prof. SHEN, Chengping	shencp@ihep. ac. cn	Beihang University	Beijing	China
Prof. SHEN, Xiaoyan	shenxy@ihep. ac. cn	IHEP	Beijing	China
Prof. SHWARTZ, Boris	shwartz@inp. nsk. su	BINP / NSU	Novosibirsk	Russian
Dr. SUN, Yanjun	yjsun@mail. ustc. edu. cn	NorthWest Normal University	Lanzhou	China
Mr. TAN, Yaxing	tanyx@mail. ustc. edu. cn	USTC	Hefei	China
Dr. TODYSHEV, Korneliy	todyshev@inp. nsk. su	BINP	Novosibirsk	Russian
Dr. WANG, Boqun	boqunwg@ucmail. uc. edu	U. Cincinnati	Cincinnati	United States
Dr. WANG, Dayong	dayong. wang@pku. edu. cn	Peking University	Beijing	China
Dr. WANG, Ping	wangp@IHEP. ac. cn	IHEP	Beijing	China
Prof. WANG, Qun	qunwang@ustc. edu. cn	USTC	Hefei	China
Mr. WANG, Weiping	cloud13@mail. ustc. edu. cn	USTC	Hefei	China
Prof. WANG, Xiaolian	wangxl@ustc. edu. cn	USTC	Hefei	China
Dr. WANG, Yadi	wangyd@ihep. ac. cn	HIM-GSI	Mainz	Germany
Mr. WANG, Yaqian	whyaqm@gmail. com	KPH	Mainz	Germany
Dr. WANG, Zhihong	wzh1988@mail. ustc. edu. cn	USTC	Hefei	China
Mr. WANG, Zhiyong	wangzy@ihep. ac. cn	IHEP	Beijing	China
Mr. WEI, Yifeng	weiyf@mail. ustc. edu. cn	USTC	Hefei	China
Ms. XUE, Mingxuan	xuemx@mail. ustc. edu. cn	USTC	Hefei	China
Mr. XUE, Sirun	xuesr@ihep. ac. cn	IHEP	Beijing	China
Mr. XU, Qingnian	xuqingnian10@mails. ucas. ac. cn	UCAS	Beijing	China
Dr. XU, Xinping	xuxp@ihep. ac. cn	Soocow Univ.	Suzhou	China
Prof. YAN, Wenbiao	wenbiao@ustc. edu. cn	USTC	Hefei	China
Prof. YUAN, Changzheng	yuancz@ihep. ac. cn	IHEP	Beijing	China
Mr. ZENG, Zhe	zengzhe@mail. ustc. edu. cn	USTC	Hefei	China
Mr. ZHANG, Bingxin	zhangbx@ihep. ac. cn	IHEP	Beijing	China
Dr. ZHANG, Jingzhi	jingzhi@ihep. ac. cn	IHEP	Beijing	China
Dr. ZHANG, Liming	liming_zhang@tsinghua. edu. cn	Tsinghua University	Beijing	China
Mr. ZHANG, Yateng	zyt1988@mail. ustc. edu. cn	USTC	Hefei	China
Dr. ZHANG, Zhenyu	zhangzhenyu@ihep. ac. cn	Wuhan University	Wuhan	China
Prof. ZHANG, Ziping	zpz@ustc. edu. cn	USTC	Hefei	China
Mr. ZHANG, Jielei	zhangjielei@ihep. ac. cn	IHEP	Beijing	China
Prof. ZHAO, Qiang	zhaoq@ihep. ac. cn	IHEP	Beijing	China
Prof. ZHAO, Zhengguo	zhaozg@ustc. edu. cn	USTC	Hefei	China
Dr. ZHEVLAKOV, Alexey	zhevlakov@phys. tsu. ru	Tomsk State University	Tomsk	Russian
Ms. ZHOU, Xiaorong	zxrong@ustc. edu. cn	USTC	Hefei	China
Mr. XIA, Lei	jessemcc@mail. ustc. edu. cn	USTC	Hefei	China
Dr. ZHENG, Bo	zhengb@ihep. ac. cn	University of South China	Hengyang	China